

THESIS ON NATURAL AND EXACT SCIENCES B241

Electrodeposition of Cadmium Chalcogenide Films for Hybrid Solar Cells

JELENA MARICHEVA



TALLINN UNIVERSITY OF TECHNOLOGY

School of Engineering
Department of Materials and Environmental Technology
Laboratory of Photovoltaic Materials

This dissertation was accepted for the defence of the degree of Doctor of Philosophy in Natural and Exact Sciences on November 3rd, 2017.

Supervisors: Dr. Julia Kois, Researcher, Department of Materials and Environmental Technology, Tallinn University of Technology

Dr. Sergei Bereznev, Associate Professor, Department of Materials and Environmental Technology, Tallinn University of Technology

Dr. Natalia Maticiu, Researcher, Department of Materials and Environmental Technology, Tallinn University of Technology

Opponents: Dr. Smagul Karazhanov, Senior Scientist, Institute for Energy Technology, Norway

Dr. Jaak Nerut, Researcher, Institute of Chemistry, University of Tartu, Estonia

Defence of the thesis: December 05, 2017 at 14.00
Lecture hall: U06A-201
Tallinn University of Technology, Ehitajate tee 5,
Tallinn

Declaration:

Hereby I declare that this doctoral thesis, my original investigation and achievement, submitted for the doctoral degree at Tallinn University of Technology has not been submitted for any academic degree.

/Jelena Maricheva/



European Union
European Regional
Development Fund



Investing
in your future

Copyright: Jelena Maricheva, 2017

ISSN 1406-4723

ISBN 978-9949-83-177-7 (publication)

ISBN 978-9949-83-178-4 (PDF)

LOODUS- JA TÄPPISTEADUSED B241

**Kaadmiumkalkogeniidkilede
elektrokeemiline sadestamine
kasutamiseks hübriid-päikesepatareides**

JELENA MARICHEVA

CONTENTS

LIST OF PUBLICATIONS	7
AUTHOR'S CONTRIBUTION TO THE PUBLICATIONS	8
INTRODUCTION	9
LIST OF ABBREVIATIONS	11
1. LITERATURE OVERVIEW	13
1.1. Main properties of Cd-chalcogenides	13
1.2. Three generations of solar cells	14
1.3. Solar cells based on Cd-chalcogenide compounds	15
1.4. Electrodeposition in solar cell technology	16
1.5. Introduction in electrodeposition	17
1.6. Electrodeposition of Cd-chalcogenides	19
1.6.1. Chemistry of CdTe electrodeposition	20
1.6.2. Chemistry of CdSe electrodeposition	22
1.6.3. Chemistry of CdS electrodeposition	24
1.7. Properties and synthesis of conducting polymers	27
1.7.1. Electrodeposition of polypyrrole	27
1.8. Summary of the literature overview and aim of the study	29
2. EXPERIMENTAL	31
2.1. Electrochemical deposition and thermal treatment of CdSe, CdS and CdTe films	31
2.2. Characterization of CdSe, CdS, CdTe films	33
2.3. Fabrication and characterization of hybrid solar cells	34
3. RESULTS AND DISCUSSION	35
3.1. Electrodeposition of CdSe	35
3.1.1. Morphological study of electrodeposited CdSe thin films	36
3.2. Electrodeposition of nanostructured CdSe films	39
3.2.1. Annealing on nanostructured CdSe films	42
3.2.2. Properties of nanostructured CdSe films	43
3.3. Electrodeposition of CdS	47

3.3.1. Influence of H ₂ SeO ₃ microadditive on electrodeposition of CdS	48
3.3.2. Properties of electrodeposited CdS thin film	52
3.3.3. Annealing of CdS films	56
3.4. Nanostructured hybrid solar cells based on electrodeposited CdSe	57
3.4.1. Glass/ITO/CdSe/P3OT:PCBM/graphite structure	57
3.4.2. Glass/ITO/CdSe/CdTe/P3OT:PCBM/graphite structure	58
3.4.3. Glass/ITO/CdS/CdSe/PPy:NSA/graphite structure	60
CONCLUSIONS	62
REFERENCES	64
ACKNOWLEDGEMENTS	75
ABSTRACT	76
KOKKUVÕTE	78
APPENDIX A	81
APPENDIX B	125

LIST OF PUBLICATIONS

The thesis is based on the following publications, which are referred to in the text by the Roman numerals I-VI:

- I. J. Kois, S. Bereznev, O. Volobujeva, **J. Gurevits**, E. Mellikov, Electrocrystallization of CdSe from aqueous electrolytes: Structural arrangement from thin films to self-assembled nanowires, *J. Cryst. Growth* 320 (2011) 9–12.
- II. J. Kois, **J. Gurevits**, S. Bereznev, O. Volobujeva, A. Öpik, E. Mellikov, CdSe nanofiber and nanohorn structures on ITO substrates fabricated by electrochemical deposition, *Appl. Surf. Sci.* 283 (2013) 982–985.
- III. J. Kois, S. Bereznev, **J. Gurevits**, O. Volobujeva, Electrochemically synthesized CdSe nanofibers and pearl-chain nanostructures for photovoltaic applications, *Matter. Lett.* 95 (2013) 110–113.
- IV. **J. Maricheva**, S. Bereznev, R. Naidu, N. Maticiuc, V. Mikli, J. Kois, Improved electrodeposition of CdS layers in presence of activating H₂SeO₃ microadditive, *Mater. Sci. Semicond. Process.* 54 (2016) 14–19.
- V. **J. Maricheva**, S. Bereznev, N. Maticiuc, O. Volobujeva, J. Kois, Influence of selenous acid microadditive on electrochemical formation of CdS thin films, *Electrochim. Acta* 242 (2017) 280–286.
- VI. **J. Gurevits**, J. Kois, S. Bereznev, E. Mellikov, A. Öpik, Electrochemical Synthesis of CdSe/CdTe Nanowires for Hybrid Photovoltaic Structures. *MRS Proceedings* 3 (2014) 1707.

Copies of these articles are included in APPENDIX A.

AUTHOR'S CONTRIBUTION TO THE PUBLICATIONS

The contribution by the author to the papers included in the thesis is as follows:

- I. Electrodeposition of CdSe films from various electrolyte solutions, analysis of the results, and minor part of writing.
- II. Electrodeposition of CdSe films from various electrolyte solutions, linear sweep voltammetry, analysis of the results, and minor part of writing.
- III. Electrodeposition of CdSe films from various electrolyte solutions, UV-Vis characterization of as-deposited and annealed films, analysis of the results, and minor part of writing.
- IV. Electrodeposition of CdS films at various conditions, Raman and UV-Vis characterization, analysis of the results, major part of writing.
- V. Electrodeposition of CdS, cyclic voltammetry of electrochemical systems, photoelectrochemical and Kelvin probe measurements, analysis of the results, and major part of writing.
- VI. Electrodeposition of CdSe and CdTe, fabrication of complete PV, Raman measurements, J-V characterization, analysis of the results, and major part of writing.

INTRODUCTION

During the last 20 years, the global energy consumption increased to ~25 000 TWh in 2016, which is a result of the increasing energy consumption per person in the growing world population. In 2015, the share of the net electricity generated from hydropower, wind turbine and solar power plants in the European Union was 11.9%, 9.7% and 3.5%, respectively [1]. The latter one reached this value in ~10 years from 0.1%. The development of clean energy resources as an alternative to fossil fuels has become one of the most important tasks of researchers engaged in modern science and technology in the 21st century. Among the various renewable energy sources, solar energy is the best choice for meeting the energy demands because of the inexhaustible energy reaching the earth from the sun. In order to promote the use of photovoltaic (PV) devices, it is necessary to develop environment-friendly, low-cost, and high-efficiency solar cells (SCs).

On a large scale, three different generations of SCs can be distinguished. First-generation (1G) cells belong to single-crystal or multi-crystal technology, and they are generally based on monocrystalline silicon (Si) [2]. Second-generation (2G) or thin-film cells were developed to address energy requirements and production costs. Third-generation (3G) technologies were aimed at enhancing poor electrical performance of 2G, while maintaining very low production costs by applying multi-junction (tandem) device architecture and concentrators [3] as well as introducing novel organic materials [4]. Currently, the efficiency of commercial PV wafer-based Si modules is ~17%, whereas that of CdTe module is ~16%. In the laboratory scale, the best performing modules are based on monocrystalline Si with efficiencies of 24.4%. Module efficiencies over 38% have been reached by using the concentrator technology [3]. In 2017, an efficiency over 26% was reported for a large-area amorphous Si SC with an area of ~180 cm² [5]. New 3G technologies will be utilized to produce high-efficiency SCs based on new scientific approaches [6]. The theoretical maximal efficiency of 3G SCs is over 60% [7]. The most effective 3G SC at the laboratory scale is the perovskite SC with an efficiency of ~22%; however, the efficiency of a 16 cm² module reaches only 16% [8]. The advantages of 3G technologies are the wider range of semiconductor materials that can be combined and easier solution-based fabrication processes compared to the 1G and 2G technologies. Materials can be nanoscale structures of solution-processed chalcogenides combined with conducting polymers (CPs) such as poly(3-hexylthiophene) (P3HT), MEH-PPV, and PCPDTBT, which can be applied for hybrid SCs. Both inorganic and organic semiconductors can be synthesized by electrodeposition (ED), which is an economically promising alternative to physical and some other wet chemical processes as it requires low-cost equipment, allows scalability for large-area deposition, and high utilization rate of precursors [9].

There are numerous reports on SCs prepared by various techniques accompanied by electrodeposition (ED) [10–13], whereas the number of reports on all-electrodeposited SCs is much fewer [14–16]. Nevertheless, these SCs have

shown competitive PV properties. The most efficient all-electrodeposited 2G SC has an efficiency of 12%, and it is composed of metal-chalcogenide thin films [14]. The 3G SCs are less efficient because of the issues on electrodeposited self-assembled nanostructures with low growth rates and high-defect densities [17]. When adding a CP for the fabrication of hybrid SCs, other issues may arise in connection with poor e^- mobility, poor adhesion of polymer to the substrate, and structural defects such as inhomogeneities and structural disorders [17]. Although there are studies on ED of self-assembled CdSe films, the fabrication of SCs on its basis is missing. Reports on all-electrodeposited SC structures mainly include 2G technologies, while to our best knowledge, there are none or very few reports on all-electrodeposited 3G SCs. The lack of information on the fabrication of such structures may be due to issues of reproducibility, application of near-boiling temperatures for aqueous solutions, and substrate stability. The target of this study is to achieve a reproducible ED of Cd-chalcogenide films for application in semi- and all-electrodeposited hybrid SCs with conventional and nanostructured device architectures

The aim of the study was electrochemical formation of nanostructured CdSe and nanocrystalline CdS films from acidic aqueous media in order to apply these films as matrix for an electrodeposited nanostructured (glass/indium tin oxide (ITO)/CdS/CdSe/PPy/graphite) 3G SC. Moreover, conditions for self-assembly of CdSe and application of low deposition temperatures of CdS were determined. In addition, the effect of thermal treatment on properties of electrodeposited films was studied.

Introduction provides information on the main properties of Cd-chalcogenides, applications of these compounds, descriptions of SC and 3G PV technology, introduction on electrochemistry of CdS, CdSe, CdTe, and CPs. It is followed by a brief literature review in Chapter 1, which includes a summary of the literature overview and aim of the study. Chapter 2 presents the experimental details on ED and thermal treatment of CdS and CdSe, and describes the characterization methods and fabrication of conventional and nanostructured hybrid SCs. Chapter 3 is divided into three sections and presents the results of the study including the discussions. The results have been published in six peer-reviewed papers included in Appendix A. The thesis concludes with a summary of the main goals and obtained results.

LIST OF ABBREVIATIONS

AFM	Atomic force microscopy
CdS	Cadmium sulfide
CdSe	Cadmium selenide
CdTe	Cadmium telluride
CdX	Cadmium chalcogenide
CP	Conducting polymer
DSSC	Dye sensitized solar cell
e^-	Electron
E	Potential of an electrode
E^0	Standard reduction potential
ED	Electrodeposition
EDTA	Ethylenediaminetetraacetic acid
EDX	Energy dispersive X-ray analysis
E_g	Bandgap
ETA	Extremely thin absorber
FF	Fill factor
FWHM	Full width at half maximum
HR-SEM	High-resolution scanning electron microscopy
h^+	Hole
H_2SeO_3	Selenous acid
ITO	Indium tin oxide
J	Current density
J_{sc}	Short circuit current density
$J-V$	Current-voltage
η	Photoconversion efficiency
Ox	Oxidized form of the standard system
PCBM	(6,6)-phenyl C61 butyric acid methyl ester
PEC	Photoelectrochemical
PEDOT:PSS	Poly(3,4-ethylenedioxythiophene):poly(styrene sulfonate)

PPy	Polypyrrole
PV	Photovoltaic
Py	Pyrrole
P3HT	Poly(3-hexylthiophene)
P3OT	Poly(3-octylthiophene)
QDSSC	Quantum dot sensitized solar cell
R	Reaction
RE	Reference electrode
Red	Reduced form of the standard system
RT	Room temperature
SCE	Saturated calomel electrode
SC	Solar cell
SEM	Scanning electron microscopy
SHE	Standard hydrogen electrode
Si	Silicon
TCO	Transparent conducting oxide
TFSC	Thin film solar cell
UV-Vis	Ultraviolet-visible
V_{oc}	Open circuit voltage
WE	Working electrode
XRD	X-ray diffraction analysis
1G	First-generation
2G	Second-generation
3G	Third-generation
[precursor]	Concentration of a precursor

1. LITERATURE OVERVIEW

1.1. Main properties of Cd-chalcogenides

Chalcogenides are chemical compounds of chalcogens and metals. Cd-chalcogenides belong to a group of II-VI semiconducting materials. Cadmium sulfide (CdS), cadmium selenide (CdSe) and cadmium telluride (CdTe) are the representatives of chalcogenide binary compounds.

There exist two crystalline forms of CdS α - and β - as well as amorphous form. α -CdS corresponds to hexagonal close-packed crystalline structure with the following lattice parameters $a = 4.150 \text{ \AA}$, $c = 6.788 \text{ \AA}$, $z = 2$. β -CdS corresponds to body-centered cubic structure with the lattice parameters as $a = 5.818\text{--}5.83 \text{ \AA}$, $z = 4$. CdS is an n -type semiconductor with a direct band gap of about 2.5 eV for bulk material. Electrical resistivity of CdS changes under illumination and the change is dependent on the wavelength. Ultraviolet illumination, with quantum energy higher than the bandgap (E_g) of CdS, creates additional conductivity, which is dependent on the intensity and wavelength of illumination [18]. Physical and chemical methods as sputtering [19], vacuum evaporation [20], close space sublimation [21] and chemical bath deposition [22], electrodeposition (ED) [23–28] have been applied for the synthesis of CdS.

CdSe has a direct E_g of $\sim 1.75 \text{ eV}$, and it is existing in nature in two crystalline forms: wurtzite and zinc-blend with the lattice parameters equal to $z = 2$, $a = 4.31 \text{ \AA}$, $c = 7.02 \text{ \AA}$ and $z = 4$, $a = 6.05 \text{ \AA}$, respectively. CdSe can exhibit both, n - and p -type conductivity, depending on the synthesis conditions [29]. CdSe crystals are photosensitive in a wide range of illumination from UV to infrared [18]. CdSe for solar cells has been synthesized by hot-injection [30], thermal evaporation [31], sputtering [32], chemical bath deposition [33], and ED [34–36] methods.

CdTe is characterized by zinc-blende crystalline structure with the lattice parameter as $a = 6.464 \text{ \AA}$ and wurtzite structure with the lattice parameters as $a = 4.56 \text{ \AA}$, $c = 4.76 \text{ \AA}$. CdTe exhibits both, n - and p -types of conductivity, direct bandgap of $\sim 1.45 \text{ eV}$ for bulk, and absorption coefficient of $\sim 1.1 \times 10^6 \text{ cm}^{-1}$ [37]. CdTe is also photosensitive with maximum photocurrent in the infrared region [18]. CdTe can be deposited by physical methods, such as close space sublimation [38], vacuum evaporation [39] etc. as wells as chemical [40] and electrochemical (EC) [41, 42] methods.

Owing to their stable properties, Cd-chalcogenides have been applied in a wide range of applications such as solar cells (SC) [14], fuel cells [43], biosensors [44], photodetectors [45], memory devices [46], etc. However, a safety aspect of Cd-containing compounds had been raised in the last decades [47–50]. Generally, Cd exists as a divalent cation, complexed with other elements (e.g., CdCl_2). Studies showed that solid Cd species are nontoxic or low toxic, whereas dissolved Cd-compounds may be toxic [50]. In case of quantum dots and nanoparticles the surface is more reactive, however correctly chosen combinations of compounds

(e.g. CdS/ZnS) and processing help to avoid the radical formation due to electronic properties of the materials eliminating the toxicity [47,49].

1.2. Three generations of solar cells

Currently, the development of SCs can be classified into three generations [51]. The first-generation (1G) is represented by the single-crystal or multi-crystal SCs [2]. Up to the year 2016, the most efficient single-junction terrestrial SC was the crystalline-Si (c-Si) cell with an efficiency of 26.3% and a fill factor (FF) of 83.8% [8]. The drawbacks of the c-Si SC production are high material utilization and costly fabrication methods owing to the relatively low absorption coefficient of c-Si.

The second-generation (2G) is represented by the thin film technology. This technology provides alternative absorber materials, such as amorphous silicon, CdTe, CuInS₂ or Cu(In,Ga)S₂, and other III–V materials. The thickness of the absorber layer in a thin film SC is up to a few micrometers, which has a lower cost but a lower SC efficiency and requires the application of rare elements (e.g., In and Ga) [52]. *n*-type chalcogenide thin films such as CdS and CdZnS with no rare elements have been widely applied for *p-n* heterojunction formation in inorganic thin film SCs [37]. Up to the year 2016, the most effective chalcogenide thin film SCs based on Cu(In,Ga)S₂ and CdTe have efficiencies of ~22.6% and 22.1%, respectively [53,54].

Owing to new emerging technologies, the third-generation (3G) SCs appeared. Examples are organic, dye-sensitized, quantum-sized, and perovskite SCs, which remain the subject of extensive research [4]. The aims of 3G PVs are (a) the use of semiconductors with high absorption coefficient but low diffusion length of photo-generated charge carriers, (b) efficient light trapping to reduce the materials, (c) and reduction of processing costs and energy demands. However, there are several aspects of 3G SCs such as stability, flexibility, and environment-friendly components that need to be improved. Concepts such as extremely thin absorbers (ETAs), nanocomposite absorbers, and quantum dot absorbers (Fig. 1.1) tend to fulfill such requirements. Nanocomposite absorbers are used to increase the diffusion length to an effective one, leading to a reduction of recombination. The ETA, which is placed between the transparent electron (e^-) and hole (h^+) conducting layers, should have a thickness larger than the tunneling length in order to avoid shunts. Finally, in the case of SCs based on quantum dot absorbers, the distance between particles is critical as it should maintain an effective transport of separated charge carriers and at the same time preserve specific electronic states of quantum dots [55]. Currently, the maximal efficiency achieved by 3G SCs is 22.1% for perovskite SCs [53], whereas dye-sensitized solar cells (DSSCs) have a record efficiency of approximately 13% [56]. In general, DSSCs are based on nanostructured TiO₂ and a thin layer of dye. Quantum dot sensitized solar cell (QDSSC) is a variation of the DSSC design in which colloidal quantum dots are used instead of organic dyes [57].

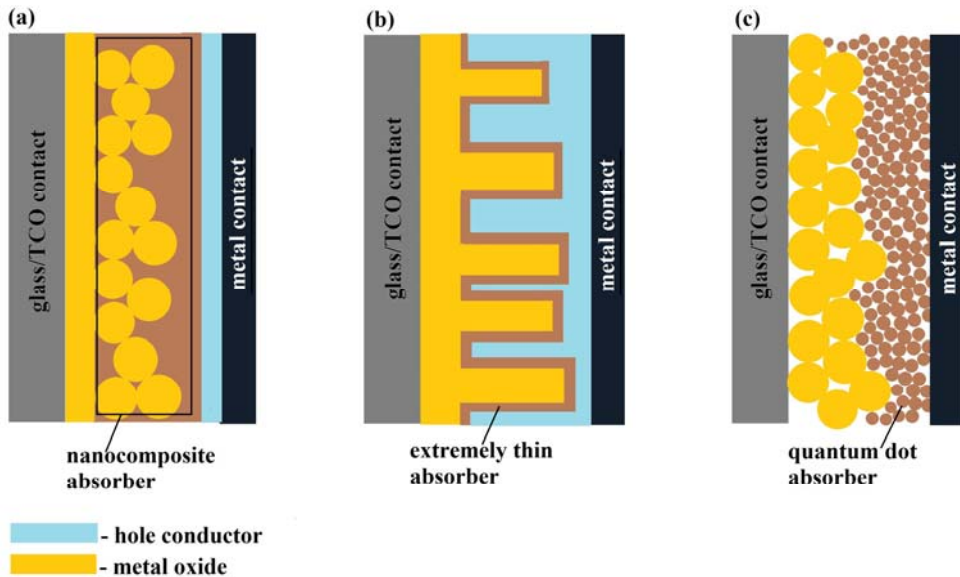


Fig. 1.1. A schematic illustration of nanostructured SCs with (a) ultra-thin nanocomposite absorber, (b) extremely thin absorber and (c) quantum dot absorber, where TCO is transparent conducting oxide [55]

1.3. Solar cells based on Cd-chalcogenide compounds

Cd-chalcogenide compounds have been also intensively applied in 3G SCs owing to their ease of fabrication, size-controlled tunable bandgap, and possible multiple exciton generation [58]. Core/shell quantum dots including CdSe, CdTe, and CdS were investigated by McElroy et al. [57], who found that the recombination rate is significantly more rapid for quantum dots with a CdSe core than with a CdTe core. The application of a CdS shell onto core-shell quantum dots promotes surface passivation and protection from corrosion. In addition, CdS reduces the charge injection from CdSe [57]. QDSSC fabricated with ternary CdS/CdSSe/CdSe quantum dots showed an efficiency of $\sim 5.06\%$ [59]. Xie et al. [60] developed an ITO/ZnO/CdSe/CdTe:CdSe/CdTe/Au device based on solution processed CdTe and CdSe nanocrystals with an efficiency of $\sim 6.25\%$. The nanocomposite In/G3-CdS/*p*-InP/Au:Zn SC including CdS showed an efficiency of $\sim 6.73\%$ [61]. Cd-chalcogenide compounds have been applied in ETA SCs based on TiO₂ and ZnO with recorded efficiencies of up to 3.16% [62–64]. Although the research is intensively running and makes them promising devices for future solar energy conversion, there is no absolute understanding on the effects and mechanisms taking place in 3G SCs.

In order to make 3G SCs more advantageous, inorganic acceptor materials are combined with organic donor materials e.g. conducting polymers (CPs). Such hybrid SC devices represent a combination of easy-to-process and relatively cheap CPs with high absorption coefficient and inorganic materials with higher

stability and size-dependent tunable optical and electrical properties [65]. Common *n*-type materials for such applications are nanoporous TiO₂, and nanoparticles of ZnO, CdSe, CdS, PbS, and CuInS₂, which generate an inorganic part of the device. Al₂O₃ and In₂S₃ are used as buffer layers in ETA SCs [66]. CPs and CP/fullerene mixtures are generally used as *p*-type materials. The most studied polymers are poly(3-hexylthiophene) (P3HT), poly(3,4-ethylenedioxythiophene):poly(styrene sulfonic acid) (PEDOT:PSS), and a blend of P3HT and (6,6)-phenyl C61 butyric acid methyl ester (PCBM) [66].

1.4. Electrodeposition in solar cell technology

One of the most commonly used chemical methods for the preparation of hybrid SCs is ED owing to the variety of electrolyte solutions, conveniently low temperatures (< 100 °C), and possibility for large-scale production. ED has been applied for several components in SCs and for the fabrication of electrodeposited SCs. The most effective devices are thin film solar cells (TFSC) with efficiencies of up to 12% (Table 1.1) [14]. They are 2G SCs based on chalcogenide compounds and metal oxides. 3G SCs including electrodeposited layers show lower efficiencies of up to ~7%. On all-electrodeposited 3G SCs, there are very few reports [11–13].

Table 1.1. Efficiencies of SCs based on electrodeposited layers

SC structure	Type of SC	ED layers	η , %	Ref.
glass/FTO/ZnS/CdS/CdTe/Au	TFSC	ZnS, CdS, CdTe	10.4	[15]
glass/FTO/CdS/CdTe/Au	TFSC	CdS, CdTe	8.0	[15]
glass/ITO/CdS/CdTe/PPy	TFSC	<i>p</i> -PPy	10.4	[10]
glass/FTO/ <i>n</i> -ZnS/ <i>n</i> -CdTe/Au	TFSC	ZnS, CdTe	12.0	[14]
glass/FTO/ZnO/Cu ₂ O/Au	TFSC	ZnO, Cu ₂ O	1.43	[16]
glass/FTO/PPy/MWCNT/back-contact	DSSC	PPy	7.15	[12]
glass/FTO/TiO ₂ /CdSe/ZnS/back-contact	QDSSC	CdSe quantum dots	2.72	[11]
glass/SnO ₂ :F/ZnOsp/ZnOed/CdSe/CuSCN/Au	ETA SC	<i>n</i> -ZnO, CdSe	2.3	[13]

One of the issues on electrodeposited SCs is the low value of the photocurrent. A higher value of photocurrent would result in an improvement of the PV parameters, namely, the open circuit voltage (V_{oc}), fill factor (FF), and efficiency (η). Low values of PV parameters are caused by pinholes or voids in the layers (created during annealing) that act as shunts across the *p-n* junction [15]. Both V_{oc} and short circuit current (J_{sc}) can be improved by an appropriate ED time so that a sufficiently thick layer can maintain its integrity. Pre-treatment may also lead to a higher and more stable V_{oc} value and suppress interdiffusion at the

interface during the final annealing step [15,67]. Finally, synthesized layers should be protected against degradation during succeeding steps of the ED.

In QDSSCs, the V_{oc} and FF are strongly influenced by recombination losses at the photoanode/electrolyte interface, which is indicated by a relatively large recombination resistance [68]; thus, pre-deposited layers should be protected during the succeeding ED steps. A large area of interface can increase the J_{sc} , as it increases the fraction of generated e^-h^+ pairs. It is generally observed that the diffusion length of minority charge carriers in an electrodeposited polycrystalline film is relatively short; hence, for a satisfactory performance, the photocurrent needs to be primarily generated in the space-charge region [69]. The issues of ETA SCs are connected with optimization of the absorber thickness and reduction of the high recombination losses due to the larger interface area. Moreover, ETA SCs suffer from more extreme voltage-dependent collection than planar cells, which is an evidence of a higher conductance at short circuit under an illumination than in the dark.

Alternatively, engineering of the nanostructures such as nanofibers or nanopillars could help to improve the charge collection for this type of SCs [62].

1.5. Introduction in electrodeposition

The electrodeposition (ED) is a chemical method which is held by means of an electrolytic cell and is controlled by properties of the electrode (material, surface area, geometry, surface condition), mass transfer (mode, surface concentration, adsorption), solution (bulk concentration of electroactive species, concentration of other species, solvent), electrical (potential, current, quantity of electricity) and external (temperature, pressure, time) variables [71]. The ED can be applied for the synthesis of inorganic materials as oxides, semiconductors, metals and metal alloys as well as organic materials on the surface of a conducting electrode in an electrolyte solution (aqueous, non-aqueous, organic, inorganic, ionic liquids and fused salts) [70].

According to the type of adsorbed species, the ED may be a faradaic or non-faradaic process. The faradaic ED is governed by Faraday's law (i.e., the amount of chemical reaction caused by the flow of current is proportional to the amount of electricity passed). If this process occurs with specific adsorption of species at the electrode/solution interface causing changes of a potential and solution composition, it is called a non-faradaic process [71].

When the system is set up and the electrode is immersed into a solution, a double-layer forms at the interface. The double layer is composed of a Helmholtz layer and a diffusion layer. The Helmholtz layer contains solvent molecules, and in the case of a non-faradaic process, specifically adsorbed ions or molecules. The location of the electrical centers of the specifically adsorbed species is called the inner Helmholtz plane, and location of the nearest solvated ions (non-specifically adsorbed species) centers is called the outer Helmholtz plane [71]. The overall electrode reaction on the cathode is as follows:



By this reaction, the dissolved oxidized species (Ox) are converted to a reduced form (Red). This reaction is generally influenced by the rate of mass transfer, e^- transfer at the electrode surface, homogeneous or heterogeneous chemical reactions on the electrode surface before or after the e^- transfer, and other surface reactions.

The electrolytic cell may contain two or three electrodes, although a working electrode (WE) is the place where the synthesis occurs. The relations of the cell potential to the standard potential and to the activities of the electroactive species are represented by the Nernst equation (Eq. 1.2).

$$E = E^0 + \frac{RT}{nF} \ln \frac{C_O}{C_R} \quad (\text{Eq. 1.2})$$

where E^0 is the standard reduction potential, R is the universal gas constant equal to $8.314 \text{ J}\cdot\text{K}^{-1}\cdot\text{mol}^{-1}$, T is the temperature in Kelvin, F is the Faraday's constant equal to $9.649 \times 10^4 \text{ C}\cdot\text{mol}^{-1}$, and C_O and C_R are the concentrations of Ox and Red, respectively.

The reduction/oxidation potentials and reversibility of the process can be evaluated by cyclic voltammetry in a certain electrochemical system. Cyclic voltammetry is a type of a linear scan voltammetry carried out by switching the direction of the scan at specific time. A cyclic voltammogram allows analysis of the reduction and oxidation processes as a function of the current and potential. A cathodic slope characterizes a reduction reaction, while an anodic slope corresponds to an oxidation reaction. In the case of a reversible process, the cathodic and anodic peaks are symmetric [71].

Potential–time or current–time transients obtained during ED provide direct and indirect data on the electrode processes. The shape of the transients provides information on polarization and incubation time for nucleation, and usually corresponds to a certain morphology of the synthesized film [42,71].

In general, thin film growth is defined by the relative surface energies [72], and involves heterogeneous nucleation and growth including heterogeneous chemical reactions, adsorption, and desorption on the electrode surface [73]. In the early stages of film formation, highly mobile atomic clusters are distributed on the substrate (Fig. 1.2). A change in the Gibbs free energy (ΔG) defines the initial size of nuclei. Surface defects such as edge and screw dislocations play a crucial role in the film formation, and serve as nucleation centers [74,75]. Their arrangement has an influence on the morphology, particularly on the early stages of growth. Island growth follows the nucleation stage until the coalesce stage resulting in a continuous film (Fig. 1.2). These stages correspond to the basic mechanisms of film formation, which are identified as the Volmer–Weber, Frank–van der Merwe and Stranski–Krastanow growth (Fig. 1.2) [73, p. 20]. Surface energy is a growth-defining parameter, while a change in the Gibbs free energy defines the nuclei size.

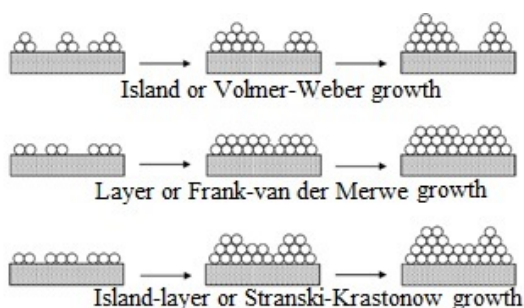


Fig. 1.2. Schematic representation of thin film growth mechanisms [73]

1.6. Electrodeposition of Cd-chalcogenides

A basic knowledge of electrochemistry and its application may help to understand the processes taking place during the ED of Cd-chalcogenide compounds [76]. Numerous research groups [77,78] have electrochemically synthesized Cd-chalcogenide semiconductors in the form of thin films and self-assembled nanostructured films [9,23,79]. Nanostructures have attracted attention owing to their high surface to volume ratio, size-related effects, and size-controlled tunable properties [94].

There are various modes (pulsed, potentiostatic, galvanostatic, cyclic voltammetry, and linear sweep ED) that allow the ED of chalcogenide thin films. In addition, deposition at certain frequencies helps to improve the composition of deposits. In the case when a direct ED of a metal chalcogenide (In_2S_3) is not possible, the metal is electroplated onto the substrate and further post-deposition chalcogenization (sulfurization) is applied to obtain the desired compound [77]. Another parameter influencing the deposition process is illumination, which increases the surface potential of the working electrode (WE), causing changes in the properties of the resulting film. The methods that have been reported comprise a cathodic co-reduction of a metal ion and a chalcogen oxyanion in an aqueous solution onto an inert substrate, cathodic deposition from a solvent containing metal ions and chalcogen in elemental form, or anodic oxidation of the metal in an aqueous electrolyte containing a chalcogenide [95]. Another possible solvent is ionic liquid, which possesses wide electrochemical stability windows, high chemical and thermal stability, and low volatility [95].

Conventionally, ED is carried out in aqueous electrolytes, which can hinder the deposition of electropositive metals and metal chalcogenides whose reduction potential lies outside the electrochemical window of stability for water. The pH of the electrolyte solution plays a crucial role during the process. CdSe and CdTe have been deposited from both alkaline [34,85,86] and acidic [42,87,88] media. CdS is generally electrodeposited in the pH range from 2 to 4 [24,66,89]; however, alkaline solutions have been also used [90]. The drawback of the acidic pH is possible degradation of some templates or substrates [91, p. 380], whereas, previous studies on the effect of pH on ED showed that using acidic solutions

produces films with superior properties, e.g., better stoichiometry and adhesion and improved crystallinity [92,93]. An acidic pH for CdTe ED is determined by the solubility of Te at pH values less than 7 [90]. In the case of CdS, ED is a competitive method to the widely used chemical bath deposition, which allows thin film deposition from both alkaline as well as acidic media.

Besides the pH and temperature of electrolyte, the elemental composition, morphology, crystalline structure, and electrical properties of Cd-chalcogenide deposits may be controlled by using complexing agents such as trisodium citrate, ethylenediaminetetraacetic acid (EDTA), or tartaric acid in the solution, which shift the reduction potential [80–82]. Another chemical, selenous acid (H_2SeO_3), is used as a microadditive for ED of metals and metal alloys [83,84], as it shifts the reduction potential and influences the polarization of the electrode, affecting the current efficiency and energy consumption of the ED process.

As the ED from an aqueous acidic medium is more beneficial in terms of films quality, the mechanisms of CdTe, CdSe and CdS formation in this medium are discussed further in Sections 1.4.1, 1.4.2, and 1.4.3.

1.6.1. Chemistry of CdTe electrodeposition

According to the potential–pH diagram (Fig. 1.3), elemental Cd^0 and Te^0 can be obtained at the potential range from 0.1 V to -1.35 V. Equilibrium reactions marked in numbers in Fig. 1.3 are presented in Table 1.2 [96]. Considering the growth mechanism of CdTe, its formation is also probable at more negative potential values than -1.35 V at a pH lower than 2.8. Owing to the low solubility of TeO_2 , CdTe can be deposited at more positive potentials than the reduction potential (underpotential) of Cd [96]. Water-soluble Na_2TeO_3 is an alternative to weakly soluble TeO_2 and can be used as a precursor of Te [97].

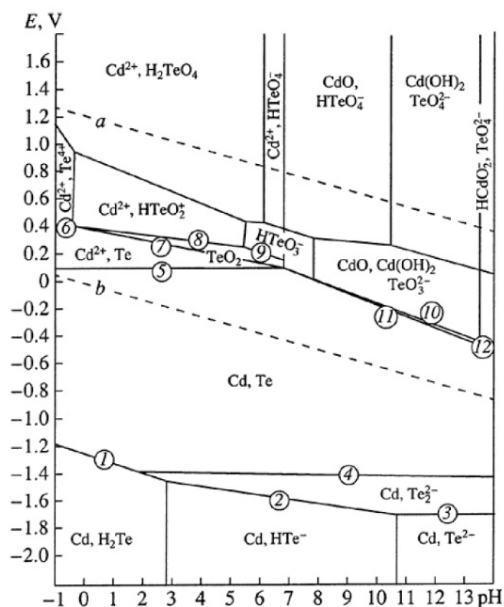


Fig. 1.3. Potential vs. pH diagram for the CdTe-H₂O system at 25 °C [96]

Table 1.2. Reactions describing equilibrium reactions in Fig. 1.3 [96]

Nr.	Reaction
1	$\text{CdTe} + 2\text{H}^+ + 2e^- \leftrightarrow \text{Cd} + \text{H}_2\text{Te}$
2	$\text{CdTe} + \text{H}^+ + 2e^- \leftrightarrow \text{Cd} + \text{HTe}^-$
3	$\text{CdTe} + 2e^- \leftrightarrow \text{Cd} + \text{Te}^{2-}$
4	$2 \text{CdTe} + 2e^- \leftrightarrow 2\text{Cd} + \text{Te}_2^{2-}$
5	$\text{CdTe} \leftrightarrow \text{Cd}^{2+} + \text{Te} + 2e^-$
6	$\text{CdTe} \leftrightarrow \text{Cd}^{2+} + \text{Te}^{4+} + 6e^-$
7	$\text{CdTe} + 2\text{H}_2\text{O} \leftrightarrow \text{Cd}^{2+} + \text{TeO}_2 + 4\text{H}^+ + 6e^-$
8	$\text{CdTe} + 2\text{H}_2\text{O} \leftrightarrow \text{Cd}^{2+} + \text{HTeO}_2^+ + 3\text{H}^+ + 6e^-$
9	$\text{CdTe} + 3\text{H}_2\text{O} \leftrightarrow \text{Cd}^{2+} + \text{HTeO}_3^- + 5\text{H}^+ + 6e^-$
10	$\text{CdTe} + 3\text{H}_2\text{O} \leftrightarrow \text{Cd} + \text{TeO}_3^{2-} + 6\text{H}^+ + 4e^-$
11	$\text{CdTe} + 5\text{H}_2\text{O} \leftrightarrow \text{Cd}(\text{OH})_2 + \text{TeO}_3^{2-} + 8\text{H}^+ + 6e^-$
12	$\text{CdTe} + 5\text{H}_2\text{O} \leftrightarrow \text{HCdO}_2^- + \text{TeO}_3^{2-} + 9\text{H}^+ + 6e^-$

There are numerous reports on ED of CdTe in an aqueous acidic medium [41,42,97] onto various substrates, e.g., ITO [97], CdS [41,98], and *n*-type Si [42]. It was found that stoichiometric CdTe films can be deposited at higher concentration of Cd species and low concentration of Te species. Applied current densities during the ED process influence the conductivity of CdTe: at higher current densities, *p*-type CdTe can be deposited while *n*-type CdTe is obtained at lower current densities [88]. CdTe films electrodeposited at higher temperatures exhibit more crystalline structure [41]. According to Osial et al. [97], CdTe thin films can be electrodeposited in the potential range of -0.45 V to -0.65 V

(vs. saturated calomel electrode (SCE)) at the pH 2 on ITO/glass substrates. In this potential range, the formation of CdTe on ITO takes place according to the interaction between reduced Te^0 (R 1.1) and Cd^{2+} cations (R 1.2), which is called Kröger reaction [44].



When the potential value is more negative than -0.8 V , Cd^{2+} is reduced to metallic Cd (R 1.3) and may react with H_2Te , reduced from Te^0 (R 1.4), forming CdTe by the reaction (R 1.5) [99].



There are also reports suggesting the formation of CdTe from reduced Cd^0 and oxidized Te^0 species (R. 1.6) on the surface of the WE [43].



The use of acidic solutions is determined by the low solubility of the TeO_2 precursor. The drawbacks of the ED of CdTe are high processing temperatures ($> 80 \text{ }^\circ\text{C}$) and the required CdCl_2 post-deposition treatment at temperatures of $\sim 400 \text{ }^\circ\text{C}$ [100,101].

1.6.2. Chemistry of CdSe electrodeposition

Fig. 1.4 shows the potential–pH diagrams for Cd–O–H (left) and Se–O–H (right) systems at standard conditions with 10^{-10} mol/kg total concentration of elements. Such a low concentration allows assuming the activity coefficient to be unity and prevents precipitation of the solid phases which hide the area of dominant aqueous species in the Eh–pH diagram [102]. As observed from Fig. 1.4, only the Cd^{2+} species, Cd(s) species, and a higher number of Se species are present in the acidic medium. For example, at pH values less than 4 HSeO_4 , SeO_4^{2-} , H_2SeO_3 (aq), Se(s), H_2Se (aq), and HSe^- are present.

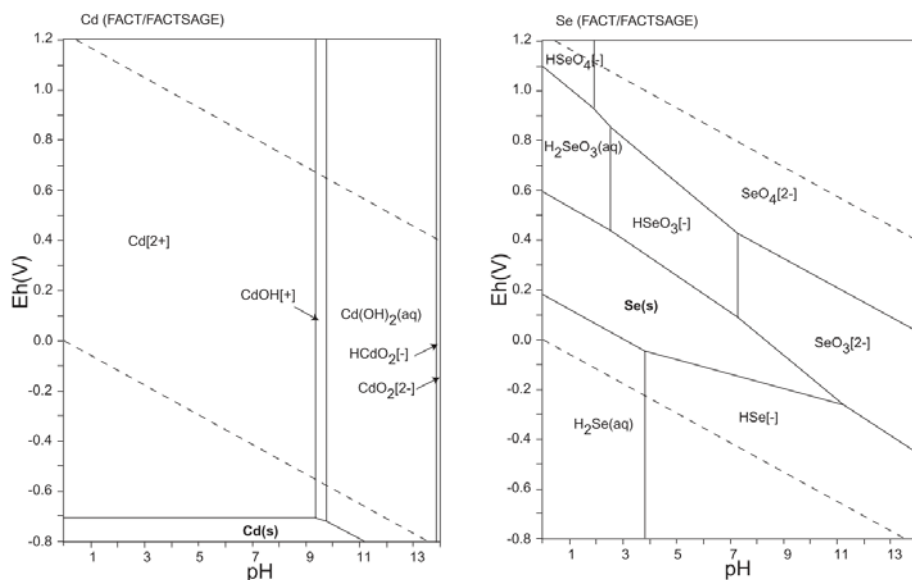


Fig. 1.4. (left) Potential–pH diagram of the system Cd-O-H (1); $\Sigma \text{Cd} = 10^{-10}$, 298.15 K, 105 Pa.; (right) potential–pH diagram of the system Se-O-H; $\Sigma \text{Se} = 10^{-10}$, 298.15 K, 105 Pa [102]

The diffusion-limited nature of the deposition of Se was indicated by steady-state polarization characteristics of the acidic system for the ED of CdSe [90]. It was determined that addition of EDTA into the deposition bath forms complexes with impurities, decreasing the impurity content in the film [90, p. 217]. Skyllas-Kazacos showed that addition of EDTA into aqueous cyanide solution causes a shift of Cd^{2+} ion reduction potential and promote formation of selenide ions, which are reduced from SeCN^- at more negative potentials than Cd^{2+} [35]. When H_2SeO_3 is used as a Se precursor in addition to the reduction reaction (R 1.8), a subsequent chemical reaction (R 1.7) provides formation of more elemental Se [36,90].



Studies on H_2SeO_3 reduction in an acidic medium showed that the reduction potential differs for various substrates, and Se reduction takes place when four electrons are involved in reaction (R 1.8) [36]. The process of the Se formation depends also on the diffusion rate and concentration of H_2SeO_3 , if both reactions (R 1.7) and (R 1.8) occur. Se^0 may be reduced further to H_2Se (R 1.9).



A six-electron reaction takes place on “noble” electrodes. As H₂Se reduces at more negative potential values than metal-selenide [36], the reaction of H₂SeO₃ reduction is not reversible and Se (IV) cannot be oxidized to Se (VI) (R 1.10).



There are several mechanisms proposed for the electrochemical formation of CdSe. Kazacos et al. proposed a CdSe formation through reaction (R 1.11) when Cd²⁺ precipitates to the WE at its high concentration in the working solution [36]. In this case, the process proceeds according to the following reaction:



Considering a six-electron reaction of the H₂SeO₃ reduction (R 1.9), CdSe formation occurs via reaction (R 1.12) as described by Kazacos et al. [36,95].



Overall, the formation mechanism of CdSe can be described as a complex process including chemical and electrochemical reactions where the main components are H₂SeO₃, Se⁰, H₂Se, and Cd²⁺.

The as-electrodeposited CdSe films are amorphous or of poor crystallinity; thus, post-deposition thermal treatment is required to improve the film properties. Annealing temperatures over 300 °C transforms a polymorphic or cubic phase to a hexagonal one and increases the crystallite size [103]. It was also found that annealing influences interestingly the shape of the CdSe nanoparticles, converting the nanodots into nanorods at 450 °C in a N₂ atmosphere [104].

1.6.3. Chemistry of CdS electrodeposition

CdS has been electrodeposited by anodic [24,28], cathodic [24–26] and pulsed [23] ED methods from aqueous [24,26] and non-aqueous [28] solutions and ionic liquids [105].

The ED of CdS from polysulfide solutions is the most widely used. The variation of the sulfur species depending on the pH of the aqueous solution and potential are shown in the metastable potential–pH diagram (Fig. 1.5). At pH values less than 7, polysulfide anions and H₂S(aq) species exist at negative potential values. SO₃²⁻, S₂O₃²⁻, HS⁻, and S²⁻ species exist at pH values above 7.

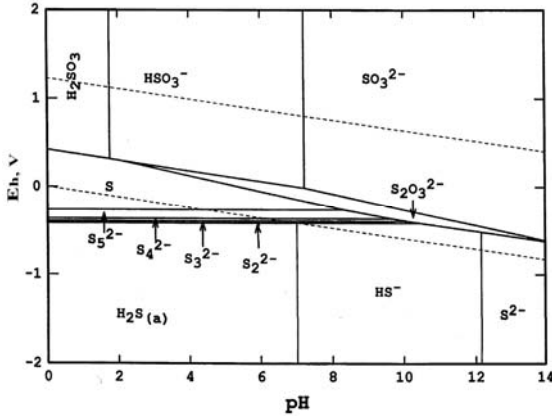


Fig. 1.5. Metastable potential-pH (Eh-pH) diagram for sulfur [105]

According to Morris et al. [89], CdS is formed as a result of Cd^{2+} cation and elemental S^0 reaction (R 1.13), while Dennison et al. [107] proposed that it takes place through Cd^{2+} and $\text{S}_2\text{O}_3^{2-}$ reactions (R 1.14) and (R 1.15). The latter one is more favorable at a lower pH as it requires additional protons. This reaction (R 1.15) includes electrochemical reduction reactions of $\text{S}_2\text{O}_3^{2-}$ (R 1.16) and Cd^{2+} (R 1.3).



In addition, sulfur can be reduced to sulfide (R 1.17) as well as polysulfide can be reduced to polysulfide anions (R 1.18).



In acidic media, $\text{S}_2\text{O}_3^{2-}$ decomposes to S^0 and SO_3^{2-} (R 1.19) [107], but it is also reported that $\text{S}_2\text{O}_3^{2-}$ disproportionates to S^0 and SO_2 [89]. These processes occur faster at a higher temperature of the electrolyte solution [107] and in a more acidic medium. Morris et al. showed [89] that an excess concentration of $\text{S}_2\text{O}_3^{2-}$ in the electrolyte promotes faster film growth, whereas an increased precipitation of S will include secondary phases into the CdS film.



A changing cathodic/anodic process may help to optimize the resulting CdS film by removing the Cd excess in Cd-rich parts of the film [89]. In the anodic process, a reaction of the Cd oxidation takes place following the left direction reaction of (R 1.3).

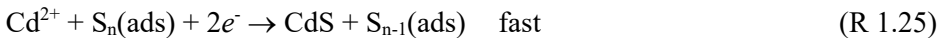
For the galvanostatic deposition technique, McCandles et al. [108] proposed a mechanism of the CdS formation (R 1.20) by including reactions (R 1.15) and (R 1.3).



Tahakashi et al. [27] suggested that CdS forms on a Ti WE through the Cd^{2+} reaction with polysulfide (R 1.21) as a result of the $\text{S}_2\text{O}_3^{2-}$ ion decomposition at pH values less than 4 (R 1.18). They also suggested that stoichiometric CdS films can be formed when the ratio of Cd^{2+} to $\text{S}_2\text{O}_3^{2-}$ is less than 1.



In the above mentioned process, elemental sulfur serves as a nucleus for crystal growth. Elemental sulfur can be specifically adsorbed and form a negatively charged sulfur colloid on the surface of the WE leading to favorable conditions for Cd^{2+} adsorption. The mechanism of CdS formation in a gelatin solution including polysulfides was suggested to proceed by the reactions (R 1.22–R 1.25) [27,109].



Nishino et al. [24] suggested another mechanism of CdS formation in an acidic aqueous electrolyte solution through H_2S adsorbed on the surface of the WE formed by the reduction reaction of S^0 (R 1.26). They deposited CdS films at room temperature (RT) in the presence of $(\text{NH}_4)_2\text{SO}_4$, glycerol, and NaCl, in addition to CdSO_4 and $\text{Na}_2\text{S}_2\text{O}_3$. According to their suggestion, formed H_2S (R 1.26) reacts with Cd^{2+} (R 1.27) producing CdS. Adsorbed H_2S , which did not react, oxidizes back to S^0 (R 1.28).



Owing to the specific properties of S and higher number of chemical and electrochemical reactions, the mechanism of the ED of CdS appears to be more complicated than that of CdSe or CdTe.

As in the case of CdSe, various studies report on the annealing of as-electrodeposited CdS in the temperature range of 200–600 °C in air, N₂, and H₂ atmospheres [110–112,15]. An increase in the annealing temperature leads to an improvement in crystallinity; however, at 500 °C Cd–S bonds start to break and the sulfur atoms evaporate from the CdS film [110]. Such a loss of stoichiometry and increased population of S vacancies reduce the lattice constant [111]. Fatas et al. [111] detected a mixed-phase transition into a hexagonal structure starting from 300 °C as well as recrystallization, agglomeration, and increase in grain size. Air annealing promotes formation of CdO, while no oxides are formed in a H₂ atmosphere at 400 °C [112]. Removal of oxides from grain boundaries can have a negative effect leading to the formation of shortcuts through the CdS film. Thus, the presence of an appropriate concentration of CdO is considered beneficial as it creates a barrier to subsequent interdiffusion between CdS and other layers in a device [112].

1.7. Properties and synthesis of conducting polymers

Conducting polymers (CP) have received much attention as their electrical and electrochemical properties are similar to both traditional semiconductors and metals. CPs have mild synthesis conditions, tunable conductivity, and structural flexibility and can be synthesized by solution-based methods as spin-casting [113], drop-casting [114] and electrodeposition [115–120]. The conductivity of CPs can be improved by incorporation of small concentrations of dopants into the polymer network [121], however the doping mechanism is completely different to that of inorganic materials. Conductivity of CPs is in range of 10⁻¹⁰ to 10⁻⁵ S·cm⁻¹ [122], but it can be increased by doping. Electrochemical oxidation (*p*-doping) or reduction (*n*-doping) allows synthesis of polymers with conductivity varying from 1 to 10⁵ S·cm⁻¹ depending on the doping concentration [122]. The conductivity of the CPs also increases with increasing temperature, however at high doping levels this dependence becomes weaker [123]. The redox processes of the CPs are stable and reversible, however at high potentials and overoxidation conditions a rapid structural degradation and loss of electroactivity (irreversible oxidation) take place in the CP [123].

1.7.1. Electrodeposition of polypyrrole

One of the CPs is the electroactive polypyrrole (PPy) [71, p. 585]. PPy can be electrodeposited by cyclic voltammetry [115,116], galvanostatically [115,117], and potentiostatically [118,116] from aqueous [116] and non-aqueous [115] solutions. Doping occurs during electropolymerization of pyrrole (Py) by the incorporation of anions, which modify electrochemical activity of the polymer [125]. As dopants, unsaturated organic sulfonates [119], heteropolyanions [120] are usually used. The microstructure of a resulting polymer film is dependent on the size of incorporated anions as they induce pores formation [115]. Beleen et al.

[124] showed that a PPy membrane has a memory effect, and it may extract and preconcentrate hydrophobic organic anion from an aqueous phase.

PPy chains are planar and linear; however, structural and conformational defects can appear during the polymerization process [121]. Py oxidizes at the potential values equal or more positive than 0.6 V vs. SCE, while the active films can be electrodeposited in the range of 0.65 to 0.8 V vs. SCE. Too high potentials are harmful to polymers as nucleophilic attack of water or anions may lead to loss of conjugation or opening of Py rings [118]. When Py oxidizes on the surface of the WE, a release of protons causes acidification of the solution area close to the anode [118] influencing negatively the electrical properties of the PPy films.

In case of pores or nanostructures, the ED of CPs with assistance of light is more beneficial as it allows deposition only on the exposed photoactivated semiconductor surface at lower potential values and lower current density (J), which is preferable in terms of higher level of polymer crystallinity and conjugation [125,126]. Photoelectrochemical (PEC) polymerization occurs at the irradiated SC/electrolyte interface. When light is incident on the semiconductor electrode, electrons from the valence band are promoted to the conduction band. These electrons are drained into the external circuit by the applied external bias potential, while the photogenerated h^+ react with species in the solution (solvent, electrolyte anion, or monomer) [127].

It was shown that a UV light illumination improves the ED process of PPy. A higher concentration of Py in the solution results in thicker PPy films [128]. PPy films have been also deposited onto CdTe. The most efficient SCs were obtained with PPy films deposited at 0.5 V and 0.6 V vs. SCE under Xe lamp illumination [129].

After synthesis, CPs are annealed at temperatures lower than those of inorganic materials [130–132]. Annealing causes restructuring of polymers and weight loss due to evaporation of residual solvent [130,131]. With increasing annealing time voids and pores may appear and hinder the path of conducting channels causing a decrease of conductivity [130]. At 150 °C in dry air PPy film dehydrates and its glass transition takes place [132]. Saxena et al. [133] also showed that a 4 h annealing at 200 °C decreases the E_g from 2.64 eV to 2.30 eV.

1.8. Summary of the literature overview and aim of the study

The studies reported in the literature on the electrodeposition of Cd-chalcogenide films and solar cells based on electrodeposited films can be summarized as follows:

1. Binary Cd-chalcogenides are II-VI semiconductors represented by CdX, where X is S, Se or Te. These compounds exhibit photosensitivity and cubic and hexagonal crystalline structure. CdSe and CdTe exhibit both *n*- and *p*-type conductivity, while CdS is an *n*-type semiconductor. Due to optical and electrical properties, these binary compounds are suitable materials for the photovoltaic applications and can be synthesized by both, physical and chemical methods including the electrodeposition.
2. CdS, CdSe and CdTe have been applied in the third-generation solar cell technology as quantum dot sensitized solar cell, dye sensitized solar cell and extremely thin absorber solar cell. Due to quantum confinement effect taking place at a nano-scale size a small amount of material is capable to absorb light efficiently. The higher interface area helps to increase the short circuit current by increasing the fraction of the generated e^-h^+ pairs, however recombination losses may affect the photovoltaic properties dramatically.
3. One of the most suitable solution-processing methods for their synthesis of Cd-chalcogenides is the electrodeposition. The electrodeposition of Cd-chalcogenides allows synthesizing compounds with various conductivities depending on the experimental conditions.
4. Stoichiometric and crystalline Cd-chalcogenides can be electrodeposited from the acidic medium, nevertheless the post-deposition thermal treatment is needed for gaining higher films quality. CdSe and CdS can form self-assembled nanostructures during the electrodeposition process.
5. Due to the complexity of the electrochemical systems the reduction of Cd-chalcogenides is described differently, however there is a common mechanism in the acidic medium represented as $Cd^{2+} + X^0 + 2e^- \rightarrow CdX$. The most complex mechanism takes place during the electrodeposition of CdS, due to the $S_2O_3^{2-}$ ion disproportionation reaction and S property to form polysulfides. CdS and CdTe are usually deposited at temperatures over 80 °C.
6. Conducting polymers are suitable materials for the photovoltaic applications. Electrical properties of the polymers can be tuned by the type and concentration of a dopant or applied potential during the electrodeposition (ED) process. The ED performed with assistance of light is more suitable for the monomer oxidation on porous or nanostructured electrodes as polymerization occurs only on photoactivated area. In addition, assistance of light promotes the formation of a polymer with higher level of crystallinity and conjugation. The post-deposition thermal treatment should be applied for the

evaporation of a residual solvent from the polymer, and for its restructuration.

7. Currently electrodeposited solar cells fabricated with thin film solar cell architecture show the maximal efficiency of 12%. There are very few reports on the fabrication of all-electrodeposited third-generation chalcogenide based solar cell.

On the basis of studies made on the electrodeposition of the Cd-chalcogenide and polymer films and from an application point of view, the aim of the doctoral thesis was set. The aim is to study the electrochemical formation of thin films of CdS at temperature lower than 80 °C, and of nanostructured CdSe films from acidic aqueous media, with a purpose of these films application as a matrix for electrodeposited nanostructured (glass/ITO/CdS/CdSe/PPy/graphite) solar cell.

In order to reach the aim following tasks were set:

1. to study the electrodeposition of stoichiometric Cd-chalcogenide films;
2. to study the electrochemical formation mechanisms of nanostructured CdSe and nanocrystalline CdS films;
3. to synthesize stoichiometric CdS films in the presence of microadditives at deposition temperature lower than 80 °C;
4. to study the effect of thermal treatments of electrodeposited nanostructured and nanocrystalline Cd-chalcogenide films on structural, morphological, optical and electrical properties;
5. to use annealed nanostructured CdSe films as a matrix for nanostructured hybrid SC fabrication with implementation of *p*-type CdTe layer or CdS buffer layer, and to characterize the photovoltaic parameters of obtained nanostructured hybrid SCs.

2. EXPERIMENTAL

This section gives an overview of the experimental details of the processes discussed in the current thesis. Section 2.1 describes methods, electrolytes and ED conditions for the synthesis of CdSe, CdS, and CdTe. Following treatment of the films are also discussed. Section 2.2 describes characterization techniques applied in this study. In section 2.3, fabrication of CPs for the formation of hybrid SCs based on electrodeposited Cd-chalcogenide films and following characterization are described. More details on the experimental part can be found in the publications [I–VI].

2.1. Electrochemical deposition and thermal treatment of CdSe, CdS and CdTe films

All electrochemical experiments were held in a standard three-electrode electrolytic cell using potentiostat/galvanostat Voltalab PGZ100 (Software Voltmaster 4) on commercially available ITO/glass substrates. These substrates were used as working electrodes (WEs). Mercury-mercurous sulfate ($\text{Hg}/\text{Hg}_2\text{SO}_4/\text{SO}_4^{2-}$), silver/silver chloride (Ag/AgCl) or saturated calomel (SCE, $\text{Hg}/\text{Hg}_2\text{Cl}_2/\text{Cl}^-$) electrodes were used as a reference electrode (RE) and Pt-wire or -plate was used as a counter electrode. The ITO/glass substrates were cleaned in concentrated sulphuric acid for 1 hour at room temperature (RT) ($21 \pm 1^\circ\text{C}$) prior the electrodeposition (ED). In order to determine the reduction/oxidation potentials of the compounds all the EC systems were studied by the cyclic voltammetry in acidic media at the scan rate of $20 \text{ mV}\cdot\text{s}^{-1}$. After the ED procedure the electrodeposited films were rinsed with deionised water and dried in air flow.

CdSe was electrodeposited at cathodic potential onto ITO/glass or CdS/ITO/glass at RT from aqueous solutions in the pH range 2–2.5, adjusted with HCl [I–III]. Details on composition of aqueous electrolyte solutions for the ED of CdSe are represented in Table 2.1. In all the studies [I–III] CdCl_2 was used as a precursor of Cd and H_2SeO_3 as a precursor of Se. ED time varied from 3.5 to 25 min in order to tune the thickness and/or to obtain a film with desired structure. The deposition potential value of -0.7 V (Ag/AgCl) was found experimentally as the most appropriate value for the ED of stoichiometric CdSe films.

Table 2.1. Solutions composition for ED of CdSe [I–III]

Solution	Concentration in ED solution (mol/l)		Cd:Se ratio
	CdCl ₂	H ₂ SeO ₃	
S1	0.01	2.5×10^{-4}	40:1
S2		5×10^{-4}	20:1
S3		10^{-3}	10:1
S4		3×10^{-3}	10:3
S5		10^{-2}	1:1
S6	0.025	2.5×10^{-4}	100:1
A		5×10^{-4}	50:1
B		10^{-3}	25:1
C		5×10^{-3}	5:1
D		10^{-2}	5:2
S11	0.1	2.5×10^{-4}	400:1
S12		5×10^{-4}	200:1
S13		10^{-3}	100:1
S14		3×10^{-3}	100:3
S15		10^{-2}	10:1

The ED of CdS films was performed on ITO/glass WEs at 21, 50, and 80 °C, the pH values of 2.5, 3.5, and 4.5 adjusted with HCl [IV,V]. The applied potential value was chosen based on the cyclic voltammetry study as -1.2 V vs. Hg/Hg₂SO₄/SO₄²⁻ (-0.8 V vs. SCE). To the initial solution labeled as B1 various micromolar concentrations of H₂SeO₃ were added. Compositions of the aqueous electrolyte solutions are presented in Table 2.2.

Table 2.2. Solutions composition for CdS ED [IV–V]

Solution	Concentration in ED solution (mol/l)			
	CdCl ₂	Edta-Na ₂	Na ₂ S ₂ O ₃	H ₂ SeO ₃
B1	0.01	0.02	0.05	–
B2	0.01	0.02	0.05	10^{-5}
B3	0.01	0.02	0.05	5×10^{-5}
B4	0.01	0.02	0.05	10^{-4}
B5	0.01	0.02	0.05	5×10^{-4}

CdTe films were synthesized by photo-assisted ED on the annealed CdSe/ITO/glass WE, which was illuminated from the glass side with a lamp ($100 \text{ mW} \cdot \text{cm}^{-2}$). The photo-assisted ED was performed potentiostatically at -0.6 V (SCE) for 0.5 h at RT in an aqueous solution of H₂TeO₃ and CdCl₂ with concentrations of 10^{-3} M and 0.05 M, respectively. The pH was adjusted with HCl to the value of 1.8.

As-electrodeposited films were thermally treated. CdSe nanohorn films were annealed in air at 200 °C for 1 h [II] and CdSe nanofibrous films at 250, 350, and 410 °C for 0.5 h [III]. Electrodeposited CdS films were annealed in vacuum in a closed quartz tube at 120 °C for 1 h [V]. Obtained CdTe/CdSe/ITO/glass structures were secondary annealed in air at 200 °C for 0.5 h. Detailed description of annealing of Cd-chalcogenide films is reported in papers [II, III, V, VI].

2.2. Characterization of CdSe, CdS, CdTe films

Morphology, coverage and grain size of the obtained films and structures were studied by the high-resolution scanning electron microscopy (HR-SEM). In order to determine the chemical composition of the deposits, an energy dispersive X-ray analysis (EDX) was carried out by using a microscope Zeiss ULTRA 55 encoupled with a system of Röntex. In case of the CdS thin films a minimal acceptable accelerating voltage of 7 kV was used. For determination of the presence of Se in the CdS films an accelerating voltage of 4 kV was used. Quantification of the EDX results was performed by the help of interactive PB-ZAF standardless method. The surface topography of the prepared CdS thin films, surface roughness and average grain size were investigated by atomic force microscopy (AFM) using a Bruker Multimode 8.0 instrument with application module based on Nanoscope V controller).

The phase composition, crystallographic properties of the films were determined by X-ray diffraction analysis (XRD) and Raman spectroscopy using Bruker AXSD 5005 diffractometer with CuK α radiation and a Horiba LabRam HR spectrometer, respectively. The average crystallite size was calculated from the full width at half maximum (FWHM) intensity of the preferred XRD peak using the Scherrer equation (2.1), where D is the average crystallite size, K is the constant related to crystallite shape (normally taken as 0.9), λ is the X-ray wavelength, β is the FWHM, and θ is the angle of the diffraction.

$$D = (K \cdot \lambda) / (\beta \cdot \cos\theta) \quad (\text{Eq. 2.1})$$

The optical spectra were measured with the SHIMADZU UV-1800 UV-Vis spectrophotometer. The optical transmission and reflection data were used to determine the absorption coefficient of the films. Based on Tauc's relation (2.2), the E_g values were estimated by extrapolating the linear portion of $(\alpha h\nu)^2$ to zero absorption at a $h\nu$ axis.

$$h\nu = A(h\nu - E_g)^r \quad (\text{Eq. 2.2})$$

$h\nu$ is the photon energy in electronvolts (eV), A is the absorption coefficient, given by $\log(T/d)$ (here d is film thickness in μm and T is transmission), and the exponent r denotes nature of the transition ($r = 1/2$ for allowed direct transition).

2.3. Fabrication and characterization of hybrid solar cells

In order to fabricate hybrid SCs, CPs were deposited by spin-casting or by photo-assisted ED onto electrodeposited inorganic CdSe/ITO/glass, CdTe/CdSe/ITO/glass, and CdSe/CdS/ITO/glass structures.

Thin films of P3OT doped with PCBM were deposited by double-speed spin-casting technique (first rotating speed of 800 rpm; second rotating speed of 3000 rpm). The mass concentration of P3OT and PCBM dissolved in chlorobenzene was 1.5%. The working solution was prepared using a Vortex Genie 2 shaker for 24 h with subsequent treatment in a VWR Ultrasonic bath for 2 h. Hybrid structures with spin-cast CP layers were annealed in an argon atmosphere at 150 °C for 10 min in an Omni Lab glovebox.

PPy was electrodeposited on the CdSe/CdS/ITO/glass structure under a xenon lamp illumination from the aqueous solution containing Py and NaNSA in concentrations of 0.3 M and 0.1 M, respectively. Cyclic voltammetry was performed prior to the ED in order to determine the potential of additional oxidation (Fig. 2.1). The ED was accomplished at an anodic potential 0.2 V vs. SCE in 10, 20, and 60 min. After ED, the obtained hybrid structure was rinsed with deionized water and dried under a nitrogen flow.

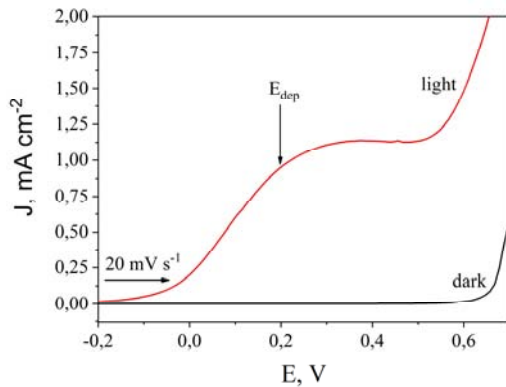


Fig. 2.1. Cyclic voltammograms in Py:NaNSA ($[\text{Py}] = 0.3 \text{ M}$, $[\text{NaNSA}] = 0.1 \text{ M}$) solution on annealed nanostructured CdSe/CdS/ITO/glass electrode

Finally, back-contacts were painted with a graphite suspension from Alfa Aesar on the top of the CP layer and dried at 60 °C for 10 min. The PV parameters of the hybrid structures were obtained from current–voltage (J – V) measurements under a calibrated tungsten-halogen lamp with an intensity of $100 \text{ mW} \cdot \text{cm}^{-2}$.

3. RESULTS AND DISCUSSION

Sections 3.1, 3.2, and 3.3 represent studies of ED and characterization of CdSe and CdS thin films. Taking into account the advantages of the ED in the acidic medium, all CdSe, CdS and CdTe films discussed in this work were electrodeposited in acidic aqueous electrolyte solutions. Section 3.4 discusses preparation of multilayer structures and fabrication as well as characterization of hybrid SCs. Results have been published in the papers [I–VI].

3.1. Electrodeposition of CdSe

The electrochemical formation of CdSe is controlled by the diffusion of Se-containing species such as H_2SeO_3 , HSeO_4^- , and HSeO_3^- (Fig. 1.4) towards the cathode/electrolyte interface and by the speed of the reduction of species at the surface of the WE. Neutral H_2SeO_3 species are present in the solution at pH values lower than 2.4 and they reduce rapidly at the surface of the cathode. With increase in pH, negatively charged HSeO_3^- species become prevalent and the speed of the reduction process decreases. First, Se nuclei form at the WE by the reduction of H_2SeO_3 (*R 1.8*), which is further reduced to H_2Se (*R 1.9*). Then the formation of CdSe takes place preferably by the reaction of Cd^{2+} with adsorbed H_2Se (*R 1.12*) at the surface of the cathode when the Cd^{2+} ions content is sufficient. CdSe can be deposited at potential values more negative than that of the reduction of Se^0 (0.496 V, SCE) and more positive than that of the reduction of metallic Cd. Se^0 species define the nucleation stages, while H_2Se species define the formation of CdSe.

In order to optimize the electrochemical conditions for the growth of stoichiometric CdSe films, the concentrations of the reactants in the deposition solution were varied. The dependence of the composition of deposited films on the concentrations of the precursors is shown in Fig. 3.1. No dependence of composition of electrodeposited CdSe films on low concentrations of H_2SeO_3 (0.025 M and 5×10^{-4} M) nor CdCl_2 was observed. We suppose that with an excess of Cd species the formation of CdSe at the surface of the WE is determined by the rate of H_2SeO_3 reduction to Se^0 (*R 1.8*) and by the rate of Se^0 reduction to H_2Se (*R 1.9*). The reaction of Se^0 formation (*R 1.8*) is determined mostly by the diffusion of H_2SeO_3 towards the cathode, while its reduction to H_2Se (*R 1.9*) is determined by the applied potential value. When there is no excess Se in the deposits, reaction (*R 1.9*) takes place at a higher rate than reaction (*R 1.8*). However, an increase in the concentration values of H_2SeO_3 equal to or greater than 0.01 M in the solution causes deposition of Se-rich films. The excess Se increases at low concentrations of CdCl_2 . At the concentration of CdCl_2 greater than 0.025 M, the Se to Cd ratio in the deposits does not exceed 2. This observation confirms the importance of exceeding the concentration of Cd species for a more stoichiometric ED of CdSe films. At the above-mentioned

conditions (Fig. 3.1), the maximal concentration of H_2SeO_3 for the ED of stoichiometric films appears to be 10^{-3} M.

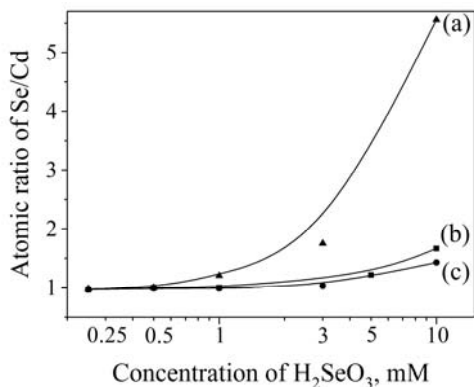


Fig. 3.1. Composition of CdSe films deposited for 15 min vs. various concentrations of H_2SeO_3 in solutions where $[\text{CdCl}_2]$ was (a) 0.01 M, (b) 0.025 M and (c) 0.1 M (Fig. 1 from [1])

3.1.1. Morphological study of electrodeposited CdSe thin films

The morphology of CdSe films electrodeposited at a high concentration of CdCl_2 (0.1 M) and various concentrations of H_2SeO_3 in the solution changes from uniform films to those covered with crystals (Fig. 3.2). CdSe thin films deposited at -0.7 V (Ag/AgCl) at an excess of Cd species and 5×10^{-4} M H_2SeO_3 are compact with plate-like grains having a size of ~ 20 nm that form a thin film with a thickness of 100–120 nm. With the increase in the concentration of H_2SeO_3 of up to 10^{-3} M, round shape particles and multi-rod crystals form on the top of the polycrystalline film (Fig. 3.2(b)). The round shape particles contain ~ 70 at.% of Se [1], and their formation could be attributed to the H_2SeO_3 reduction reaction with formation of elemental Se (R 1.8). When the concentration of H_2SeO_3 is increased up to 3×10^{-3} M, films covered with Se-rich crystals form (Fig. 3.2(c)). It occurs when the rate of deposition of Se (R 1.8) exceeds the rate of reduction of Se (R 1.9).

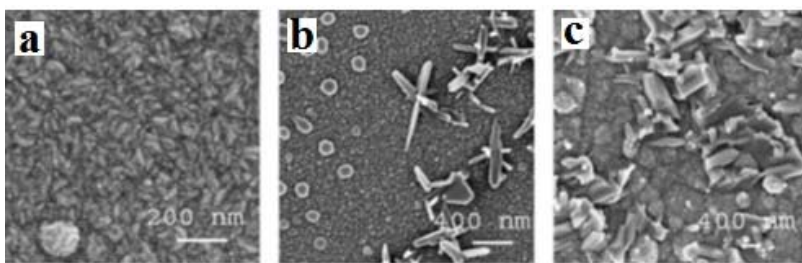


Fig. 3.2. SEM images of CdSe films deposited for 15 min from solutions containing 0.1 M CdCl₂ and different concentrations of H₂SeO₃ (a) 5×10^{-4} M, (b) 10^{-3} M, (c) 3×10^{-3} M (A modified version of Fig. 3 from [I])

Films electrodeposited from solutions with lower concentrations of CdCl₂, that is, 0.025 M and 0.01 M, are slightly Se-rich and show less crystalline morphology (Fig. 3.3). However, CdSe films electrodeposited from a solution with the concentration of CdCl₂ of 0.025 M with various concentrations of H₂SeO₃ are uniform without any large particles or crystals on the surface. The most uniform film is obtained at the lowest H₂SeO₃ concentration. When the concentration of CdCl₂ is decreased to 0.01 M, all the films exhibit a polycrystalline film structure covered with large grains. With an increase of the H₂SeO₃ concentration in the solution, Se-rich round-shaped particles have a tendency to grow into islands. The size and density of the Se-rich particles depend on the concentration of precursors in the electrolyte solution.

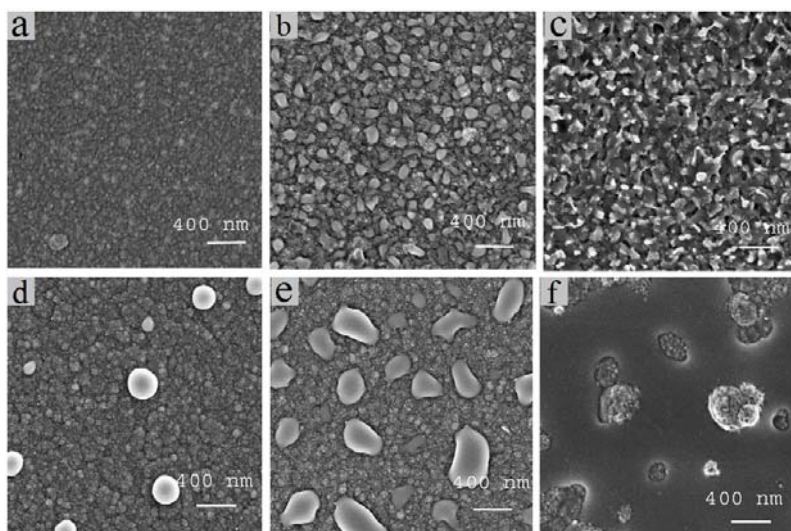


Fig. 3.3. SEM images of CdSe films electrodeposited for 15 min from solutions with 0.025 M [CdCl₂] and [H₂SeO₃] of (a) 5×10^{-4} M, (b) 10^{-3} M and (c) 5×10^{-3} M; and from solutions with 0.01 M [CdCl₂] and [H₂SeO₃] of (d) 2.5×10^{-4} M, (e) 5×10^{-4} M, (f) 10^{-3} M (A modified version of Fig. 5 and Fig. 6 from [I])

XRD patterns of the as-electrodeposited CdSe thin films (Fig. 3.4) obtained from a solution with 0.1 M concentration of CdCl₂ shown an improvement of the crystallinity with increasing H₂SeO₃ concentrations in the electrolytic bath. The film obtained from the solution containing 10⁻³ M H₂SeO₃ is exhibiting (002), (101), and (110) planes corresponding to the hexagonal structure [134]. With the increase in H₂SeO₃ concentration in the ED solution, additional (100) and (110) planes are observed and attributed to the hexagonal structure [134]. The (110) plane at 41.74° can be also attributed to the hexagonal Se [135], which may form in the solution when the concentration of H₂SeO₃ is high enough (0.01 M and 0.02 M) and the rate of Se reduction (*R 1.9*) is suppressed by the exceeding rate of H₂SeO₃ reduction reaction (*R 1.8*). At the highest concentration of H₂SeO₃, one can observe a shift of the (111) peak from 25.65° towards 25.47°, which is a position that corresponds to the cubic structure of CdSe [136]. This shift may be caused by the formation of Se-rich crystals on the film surface as depicted by the SEM analysis (Fig. 3.2).

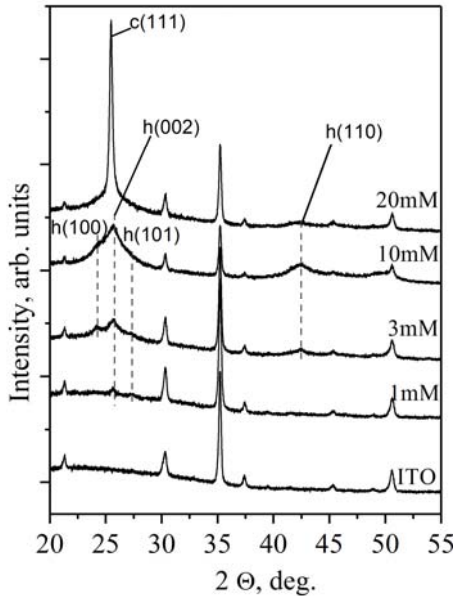


Fig. 3.4. XRD patterns of CdSe films electrodeposited on ITO/glass for 15 min from solution of 0.1 M CdCl₂ and various concentrations of H₂SeO₃ (A modified version of Fig. 4 from [1])

Low concentrations of H₂SeO₃ at excess Cd²⁺ allow the growth of CdSe films with better uniformity but poor crystallinity. Increasing the concentration of H₂SeO₃ promotes the formation of Se-rich particles and crystals on the top of the electrodeposited CdSe layer. Films grown at high concentrations of H₂SeO₃ have improved crystallinity, but also exhibit a secondary phase of Se. At low concentrations of H₂SeO₃ in the solution, we observed the precondition for the formation of a 3D structure of CdSe.

3.2. Electrodeposition of nanostructured CdSe films

Further study shows the stages of formation of nanostructured CdSe films. During the first minutes of ED, a uniform film grows with clearly distinguishable grains having a diameter of up to 50 nm (Fig. 3.5). The secondary electron imaging method identified these particles as Se clusters. After 15 min of ED, the top of the CdSe film is covered with islands, which can be defined as 3D nucleation clusters. Finally, the longest ED time (25 min) shows the formation of a nanofibrous structure (Fig. 3.5(d)).

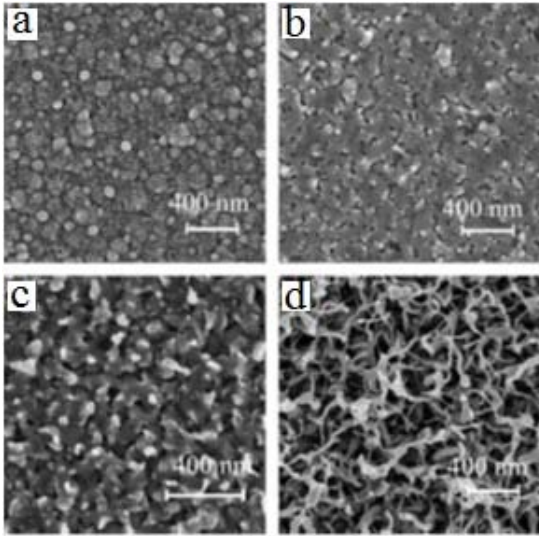


Fig. 3.5. SEM images of CdSe films deposited for (a) 7 min, (b) 10 min, (c) 15 min and (d) 25 min at -0.7 V (Ag/AgCl) from solution C ($[\text{CdCl}_2] = 0.025$ M, $[\text{H}_2\text{SeO}_3] = 5 \times 10^{-3}$ M) (Fig. 7 from [I])

To better understand the growth of CdSe film we analyzed the ED transients (Fig. 3.6). The first sharp drop in the initial current density (J) is charging of the formed double layer. Following the rapid decrease of J is an induction time corresponding to the period of the formation of nucleation centers [137]. The deposition transient obtained in solution A with 5×10^{-4} M concentration of H_2SeO_3 (Table 2.1) shows a different behavior from the other curve. This indicates a steep growth of a continuous and uniform thin film that may correspond to a morphology similar to that shown in Fig. 3.3(a). The shape of the transient obtained during ED in solution C ($[\text{H}_2\text{SeO}_3] = 5 \times 10^{-3}$ M) with a precursor ratio of (Cd:Se) 5:1 indicates the formation of a film with a highly developed surface area [138]. After 600 s of ED, the observed increase in J may correlate with the transition of Se clusters from 2D to 3D. The final decrease in J indicates the formation of nanostructures on the surface of the CdSe film as shown in Fig. 3.5(d).

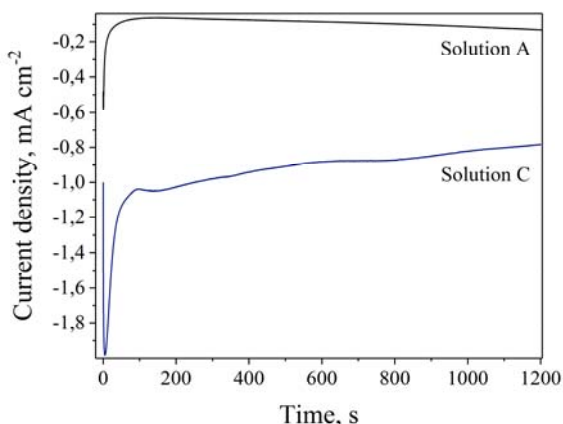


Fig. 3.6. Current density vs time transients of ED of CdSe onto ITO/glass at -0.7 V (Ag/AgCl), RT, pH 2.5 and at 5×10^{-4} M $[\text{H}_2\text{SeO}_3]$ (solution A) and 5×10^{-3} M $[\text{H}_2\text{SeO}_3]$ (solution C) (A modified version of Fig. 3 [II])

According to the analysis of the formation mechanism of CdSe thin films and of the deposition transients (Fig. 3.6) that correspond to the morphological study (Fig. 3.5) we propose a formation mechanism of self-assembled nanostructured CdSe films (Fig. 3.7). First, Se^0 species deposit on the WE and serve as the primary nucleation centers. The nucleation process is followed by the formation of CdSe by reaction *R 1.12*: $\text{Cd}^{2+} + \text{H}_2\text{Se} \rightarrow \text{CdSe} + 2\text{H}^+$. If there is no excess of Se species in the solution, a thin film forms (Fig. 3.7(c)). At higher concentrations of Se species in the solution, a secondary nucleation takes place on the underlying CdSe thin film (Fig. 3.7(d/g)). The excess of Se^0 species in the solution and strong affinity of Se atoms to each other promote the formation of Se-rich particles. This stage of CdSe film growth is characterized by the secondary nucleation, which is required for the growth of nanostructures. The size and distance between these secondary Se nuclei depend on the rate of the Se^0 reduction. The formation of CdSe nanostructures is characterized by an anisotropic asymmetric growth, and this process is defined by surface unsaturation and valence e^- counts [139].

The formation of core/shell Se/CdSe nanohorns (Fig. 3.7(d-f)) from Se islands is determined by the larger diameter of Se nuclei and by Se-terminated facets. On the other hand, the formation of nanohorns is characterized by a radial growth occurring when species diffuse and incorporate on the sidewalls. The initial diameter of a nanohorn is determined by the diameter of a Se nucleus and decreases in the vertical direction during the ED process. The nanofibrous CdSe structure forms owing to the general reaction *R 1.12* on the top of the growing fibers. The growth of the nanofibers (Fig. 3.7(g-i)) is defined by the small diameter of Se nuclei, which determines the top growth.

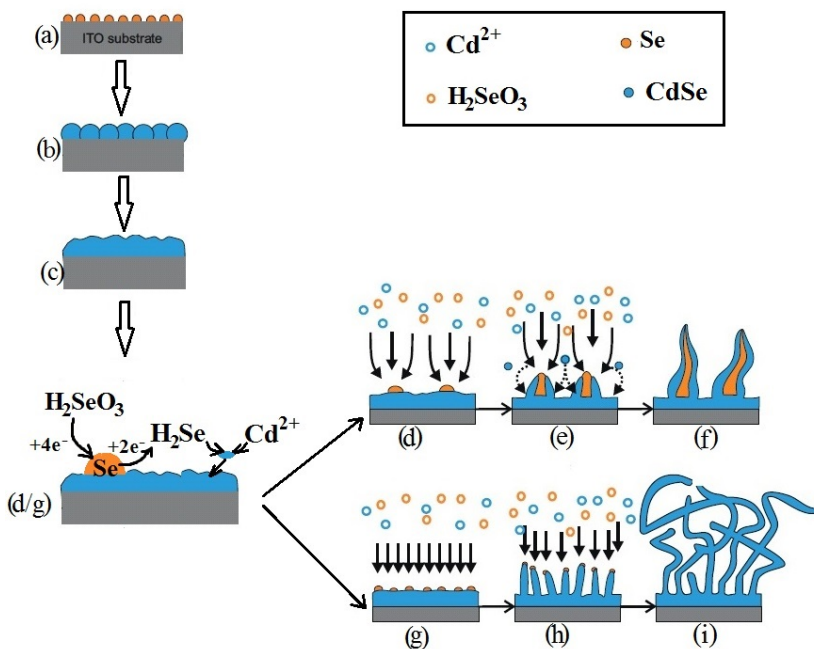


Fig. 3.7. Schematic representation of self-assembled growth of nanostructured CdSe films with (a) nucleation, (b) CdSe islands growth, (c) CdSe underlying film growth, (d, g) Se islands growth on CdSe, (e) starting growth of nanohorns (f) nanohorn growth, (h) starting growth of nanofibers, (i) nanofibers growth (A modified version of Fig. 5 from [I])

As the growth of thin and nanostructured films differs from each other, ED transients can be used in order to predict the morphology of the deposits. In the case of the CdSe nanostructured growth, Se-rich particles serve as nuclei. Their size as well as surface properties define the resulting morphology.

According to the SEM study, the structures of CdSe films electrodeposited from aqueous solutions with 0.025 M concentration of CdCl_2 vary from polycrystalline thin films to nanostructured thin films (Fig. 3.8). When the concentration of H_2SeO_3 in the solution is 10^{-3} M (solution B), the film grows with conical CdSe nanohorns on the top (Fig. 3.8) with a diameter of ~ 200 nm at the base and 30 nm on the top. The length of nanohorns varies in the range of 300–600 nm. The electrodeposited CdSe films from solutions C and D with concentrations of 5×10^{-3} M and 0.01 M of H_2SeO_3 , respectively, are covered with nanofibers with diameters varying in the range of 40–85 nm (Fig. 3.8). The film deposited in solution C has few aligned nanofibers and nanohorns. At a potential of -0.7 V (Ag/AgCl), high concentrations of Se and Cd species are necessary for the CdSe fiber shell arrangement.

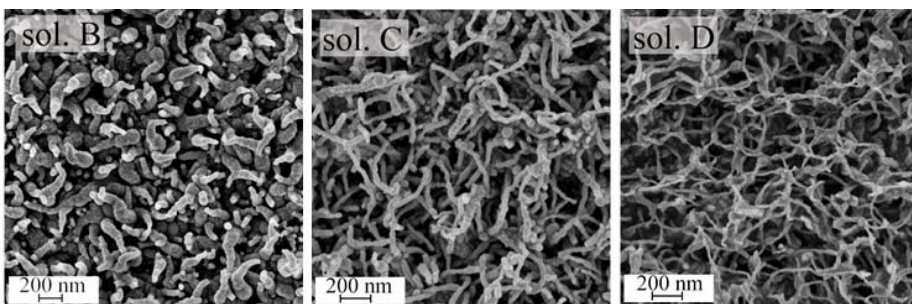


Fig. 3.8. SEM images of as-deposited CdSe films obtained at -0.7 V (Ag/AgCl) from B, C and D solutions at pH 2.5 for 20 min; all solutions contain 0.025 M $[\text{CdCl}_2]$ and various $[\text{H}_2\text{SeO}_3]$ equal to 10^{-3} M (solution B), 5×10^{-3} M (solution C), 0.01 M (solution D) (A modified version of Fig. 1 from [I])

3.2.1. Annealing on nanostructured CdSe films

The drawbacks of as-electrodeposited films are their poor crystallinity (Fig. 3.11) and mixed-phase structure, which can be improved by annealing. During the annealing process, recrystallization may cause sintering of the nanofibers, which should be avoided. Annealing of CdSe nanofibrous films in air may also improve the electrical properties by chemisorption of oxygen at the intergrain boundaries [140].

Annealing of nanohorn-structured CdSe films at 200 °C caused the evaporation of excess Se, transforming them into 100 nm thick hollow conical tubes (Fig. 3.9). Based on this phenomenon, we deduced that the as-electrodeposited nanohorn structure is composed of a Se core and CdSe shell, which is in accordance with the proposed self-assembling mechanism of CdSe nanostructured films (Fig. 3.7).

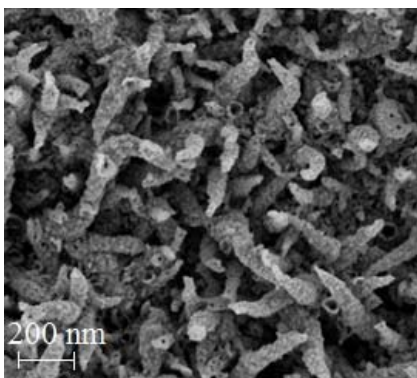


Fig. 3.9. SEM images of electrodeposited nanohorn CdSe film annealed at 200 °C for 1 h

CdSe films annealed at 250 °C show nanofibers with features similar to the as-deposited ones, but with smaller diameters in the range of 15 – 20 nm

(Fig. 3.10). The temperature of 250 °C assures the evaporation of excess Se but it is not sufficient for agglomeration of CdSe nanofibers. At temperatures equal to or greater than 350 °C agglomeration occurs. At 350 °C, CdSe fibers transform to a necklace-type structure accompanied by partial sintering of the nanofibers. Annealing at 410 °C causes more intensive agglomeration resulting in disappearance of the nanostructure.

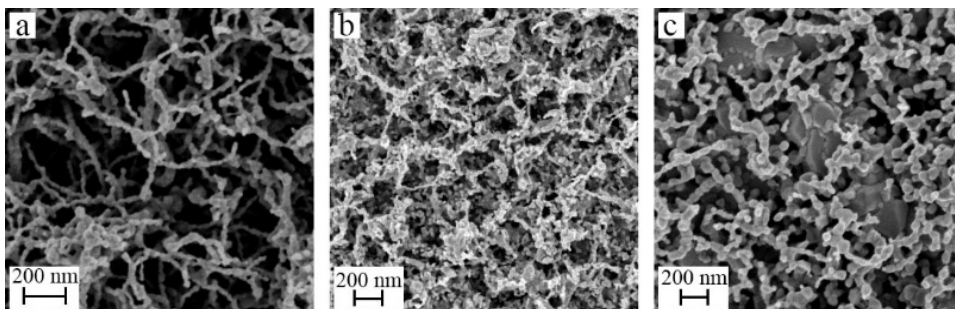


Fig. 3.10. CdSe films (solution D: $[\text{CdCl}_2] = 0.025 \text{ M}$ and $[\text{H}_2\text{SeO}_3] = 0.01 \text{ M}$ at pH 2.5 and -0.745 V (SCE) for 20 min) air annealed at (a) 250 °C, (b) 350 °C, (c) 410 °C (A modified version of Fig. 2 from [II])

3.2.2. Properties of nanostructured CdSe films

According to the XRD data, the as-deposited CdSe films exhibit a mixed-phase structure with (111) plane corresponding to a cubic structure [136] and (100), (110), and (200) planes of a hexagonal structure [141] (Fig. 3.11). The same mixed-phase crystalline structure with higher intensity of peaks was observed for CdSe annealed at 250 °C in air for 30 min. Diffraction patterns of CdSe films annealed at 350 °C and 410 °C show peaks corresponding to (100), (002), (101), (110), (103), (200), and (112) planes (Fig. 3.11), which can be attributed to the hexagonal structure [141]. A transition of mixed-phase to a wurtzite CdSe structure was indicated for the films annealed at temperature equal to or greater than 350 °C.

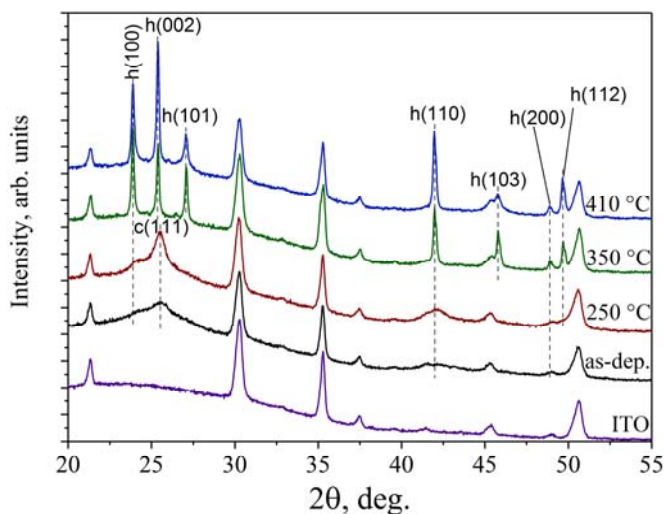


Fig. 3.11. XRD patterns of CdSe nanofibrous films before and after air annealing at various temperatures for 30 min (A modified version of Fig. 1 from [II])

The EDX measurements of the as-deposited nanofibrous CdSe showed that the Cd to Se ratio changes from 1:1 to 1:2 (Fig. 3.1) when the ED time is increased from 15 min to 25 min. On the other hand, all nanofibrous CdSe films annealed at 250, 350, and 410 °C show a stoichiometric composition.

The phase composition was described by Raman spectra of the as-electrodeposited and annealed CdSe films (Fig. 3.12). All the spectra show two peaks at 204 cm^{-1} and 410 cm^{-1} corresponding to a CdSe longitudinal phonon mode. The small peak at 170 cm^{-1} , which appeared for both the as-deposited and annealed at 410 °C films, may be attributed to the Se-Se vibrational mode [142] and/or CdSe transverse optical phonon mode [144]. In terms of stoichiometry and phase composition, annealing in air at temperatures of 250 °C and 350 °C is suitable for treatment of CdSe nanofibrous films.

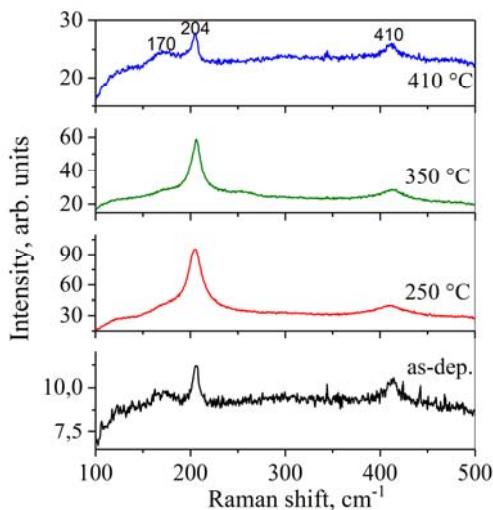


Fig. 3.12. Raman spectra of CdSe films ED from solution D ($[\text{CdCl}_2] = 0.025 \text{ M}$; $[\text{H}_2\text{SeO}_3] = 0.01 \text{ M}$) before and after air annealing at various temperatures

By increasing the annealing temperature from 250 °C to 410 °C, the absorption edge shifted from 767 nm to 731 nm (Fig. 3.13). In the visible range of spectra of up to 650 nm, the transmittance decreases with an increase in annealing temperature. At 600 nm the drop of transmittance from 15% to 2% occurs. However, at longer wavelengths, a higher transmittance was observed for films annealed at 250 °C and 350 °C, similar to the results for CdSe films reported by Mahato et al. [144]. The decrease in transmittance may occur owing to the increase in thickness of the CdSe underlying part of the film as a result of recrystallization, agglomeration, and fiber sintering (Fig. 3.10).

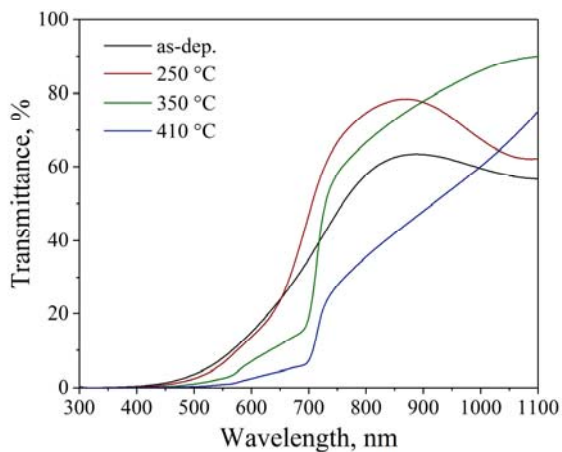


Fig. 3.13. Transmittance of nanofibrous CdSe films from solution D ($[\text{CdCl}_2] = 0.025 \text{ M}$; $[\text{H}_2\text{SeO}_3] = 0.01 \text{ M}$) before and after air annealing at various temperatures

The E_g values of the nanofibrous CdSe films obtained in solution D with 0.01 M concentration of H_2SeO_3 are shown in Fig. 3.14. The E_g of an as-deposited film is difficult to determine owing to the scattering effect in the amorphous film (Fig. 3.11). The E_g of the films air-annealed for 30 min at 250, 350, and 410 °C are 1.78 eV, 1.72 eV, and 1.71 eV, respectively (Fig. 3.14). The same was observed for the nanofibrous CdSe films obtained in solution C ($H_2SeO_3 = 5 \times 10^{-3}$ M). The E_g shifted from 1.77 eV to 1.68 eV when annealed at 250 °C and 410 °C, respectively. This red shift may occur owing to the increase in the crystallite size, lower dislocation concentration, decreased strain [145], and lower electrical resistivity [146].

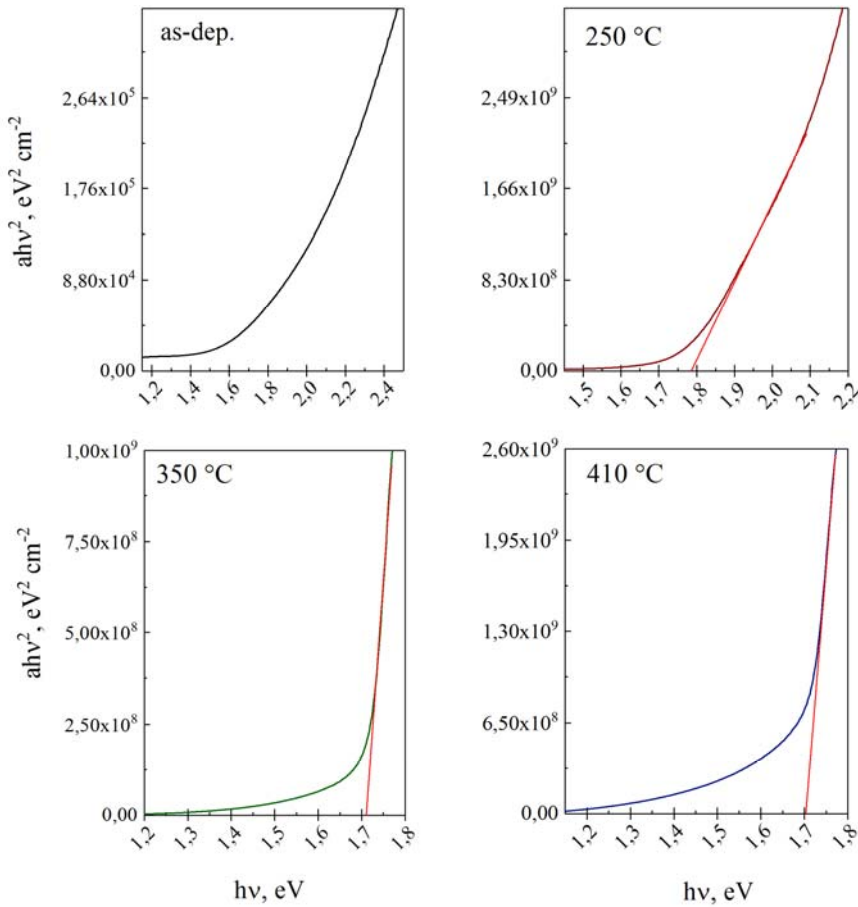


Fig. 3.14. E_g of nanofibrous CdSe films electrodeposited from solution D ($[CdCl_2] = 0.025$ M; $[H_2SeO_3] = 0.01$ M) before and after air annealing at various temperatures

To summarize, CdSe nanofibrous films with fiber diameters of 40–85 nm were electrodeposited from acidic aqueous solutions containing different concentrations of H_2SeO_3 (5×10^{-3} M and 0.01 M). The lower concentration of

H_2SeO_3 (10^{-3} M) allows the ED of core/shell nanohorn-structured CdSe films. Although the annealing improved the crystallinity and stoichiometry of the nanofibrous CdSe films, some pores appeared at the CdSe/ITO interface due to recrystallization [V]. These pores decrease the charge transport region, indicating the need for a buffer layer such as CdS.

3.3. Electrodeposition of CdS

Similar to the case of CdSe films, we studied the electrochemical formation of CdS films. Based on a cyclic voltammetry study [V] of the electrochemical systems, we propose the following steps in the formation of CdS (Fig. 3.15). First, $\text{S}_2\text{O}_3^{2-}$ reduction occurs on the surface of the ITO/glass substrate, followed by formation of S nuclei (R 1.16). This process is gradual and is followed by surface passivation of the WE as a result of the formation of a poorly conductive layer. Specifically adsorbed elemental S can form polysulfide anions (R 1.18). Moreover, a polysulfide colloid can be adsorbed from the solution (R 1.22). Gaining electrons, S^0 reduces to S^{2-} (R 1.17) or to H_2S (R 1.26) adsorbed onto the surface of the cathode. H_2S rapidly reacts with Cd^{2+} (R 1.27) and forms CdS (Fig. 3.14). However, considering the various species present in the solution and at the WE surface, CdS may also form as a result of Cd^{2+} interaction with $\text{S}_2\text{O}_3^{2-}$ (R 1.14, R 1.15) and polysulfides (R 1.23, R 1.23–R 1.25).

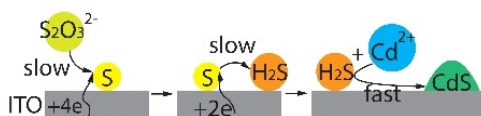


Fig. 3.15. Schematic representation of formation steps of CdS during ED (A modified version of Fig. 3 from [V])

The ED of CdS was performed in an initial solution of 0.01 M concentration of CdCl_2 , 0.05 M $\text{Na}_2\text{S}_2\text{O}_3$, and 0.02 M Na_2EDTA , where Na_2EDTA was used in order to shift the reduction potential of Cd towards a more negative region [V] and avoid the ED of metallic Cd^0 . According to the study of electrochemical systems described in detail in [V], an optimal potential value of -1.2 V vs. $\text{Hg}/\text{Hg}_2\text{SO}_4/\text{SO}_4^{2-}$ (-0.79 V vs. SCE) was chosen for the ED of CdS.

As discussed in Section 1.1, the temperature and pH of the electrolyte solution have a significant effect on the growth rate, morphology, and composition of films during ED. We studied the effect of these parameters on the composition of the CdS films and illustrated it in Fig. 3.16. The sulfur content in the CdS films changes as a function of pH from 2.5 to 4.5 in the initial solution at 80°C . Nearly stoichiometric CdS films with ~ 55 at.% of sulfur were obtained at pH 2.5. When the pH increases from 3.5 to 4.5, the content of S in the films rises from ~ 59 at.% to ~ 75 at.%, respectively. To investigate the temperature effect, a pH of 3.5 was chosen owing to the thiosulfate-containing-electrolyte stability in the pH range of 2.8 to 4.0. Poor adhesion of CdS onto the ITO/glass substrate was observed at

higher pH values [102]. S-rich composition of CdS thin films obtained at 20 °C may be caused by the gradual diffusion of Cd²⁺ ions towards the WE [147], which increases at higher temperatures. The content of S decreases from ~80 at.% to ~72 at.% by increasing the deposition temperature from 20 °C to 50 °C. Near-stoichiometric CdS films were electrodeposited at the highest temperature of 80 °C at pH values of 2.5 and 3.5. However, in terms of aqueous solution stability, a lower temperature of 50 °C is preferable.

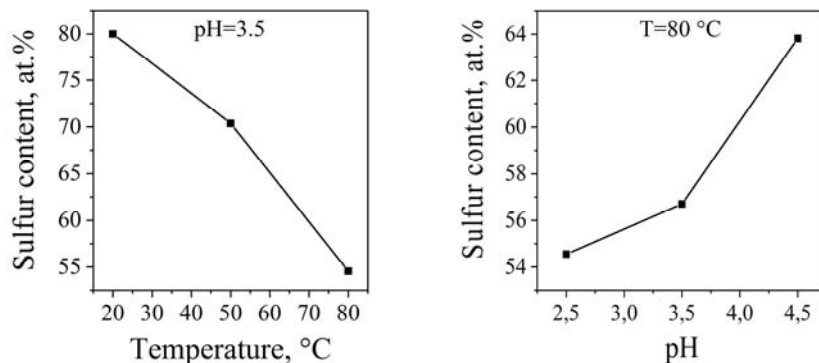


Fig. 3.16. Dependence of sulfur content as a function of (left) temperature and (right) pH for CdS films electrodeposited for 0.5 h at -0.79 V (SCE) (A modified version of Fig. 1 from [IV])

3.3.1. Influence of H₂SeO₃ microadditive on electrodeposition of CdS

In this thesis, we paid special attention on the effect of H₂SeO₃ additive onto the growth mechanism and properties of CdS thin films. We have found that the presence of H₂SeO₃ in the solution significantly affects the ED process of CdS. An idealized electrochemical formation mechanism of CdS in a thiosulfate solution in the presence of H₂SeO₃ is shown in Fig. 3.17. A positive reduction potential of H₂SeO₃ promotes its rapid electrochemical reduction (*R 1.8*), which initiates Se nucleation prior to S nucleation. The growth of Se nuclei is controlled by the diffusion rate of H₂SeO₃ to the WE, although the reduction reaction of S₂O₃²⁻ may occur on the surface of Se nuclei. In this case, the reactions taking place on the cathode occur faster owing to the higher electrical conductivity of Se in comparison to S [141,148]. Se itself may also be reduced to H₂Se (*R 1.9*), which go over into the solution. In addition, H₂SeO₃ may chemically react with H₂Se (*R 1.7*) in the solution and provide a higher number of conductive nucleation centers of Se, which contribute to the faster formation of CdS thin films with improved surface coverage.

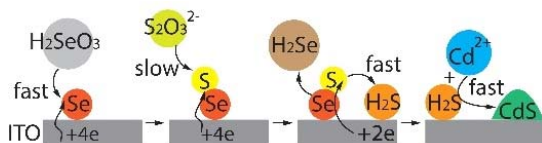


Fig. 3.17. Schematic representation of formation steps of CdS in the presence of H_2SeO_3 microadditive (A modified version of Fig. 3 from [V])

The influence of pH and temperature on the ED of CdS in the presence of micromolar concentrations of H_2SeO_3 (0 , 5×10^{-5} , 10^{-4} , and 5×10^{-4} M) was investigated (Fig. 3.18). More stoichiometric CdS films were obtained at low pH values of 2.5 and 3.5 (Fig. 3.18(a)). This observation is in agreement with the data obtained for CdS electrodeposited from a Se-free solution (Fig. 3.16). A decrease in pH from 4.5 to 2.5 reduces the excess sulfur from 63 at.% to 54 at.%, while an addition of H_2SeO_3 lowers the deviation in composition of the deposits. An increase in the solution temperature also decreases the deviation in composition and improves the stoichiometry of the deposited CdS films (Fig. 3.18(b)). At 20°C , an addition of 0.01 mM concentration of H_2SeO_3 reduces the excess sulfur from 80 at.% to 70 at.%, whereas higher concentrations of H_2SeO_3 (10^{-4} , 5×10^{-4} M) increase it again. At higher temperatures of 50°C and 80°C , the content of sulfur decreases from 70 at.% to 56 at.% and from 53 at.% to 52 at.% respectively, by adding H_2SeO_3 .

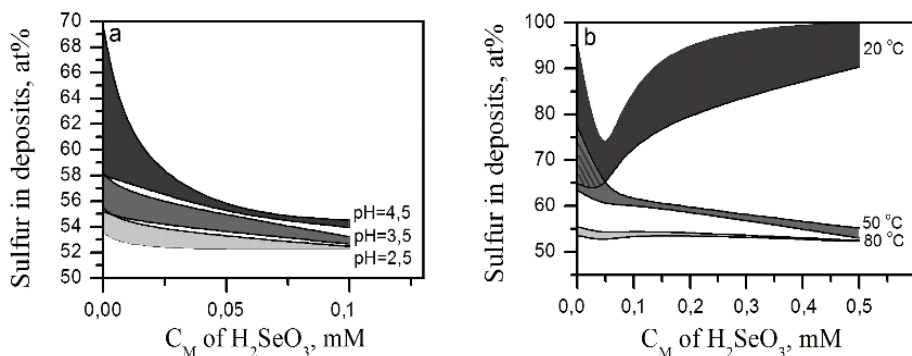


Fig. 3.18. Schematic representation of H_2SeO_3 influence on sulfur content in CdS films at (a) various pH at 80°C and (b) various temperatures at pH 3.5 (Fig. 2 from [IV])

CdS electrodeposited for a longer time (1.5 h) from the Se-free solution (Fig. 3.19) covers the substrate unevenly with islands of ~ 200 nm high. One can also observe a thin intermediate layer of several nanometers on the surface of ITO between the islands (Fig. 3.19(d)). An addition of 5×10^{-5} M concentration of H_2SeO_3 into the solution promotes the formation of a continuous uniform polycrystalline 100 nm thick CdS film; however, some voids are present. Such a changed microstructure of the CdS thin film confirms the effect of H_2SeO_3 on the mechanism of CdS ED. A higher concentration of 10^{-4} M H_2SeO_3 in a solution

decreases the island size and consequently, the film thickness to 64 nm. In addition, one can observe some adherent secondary particles on the surface of this film (marked with red circles) (Fig. 3.19(c)).

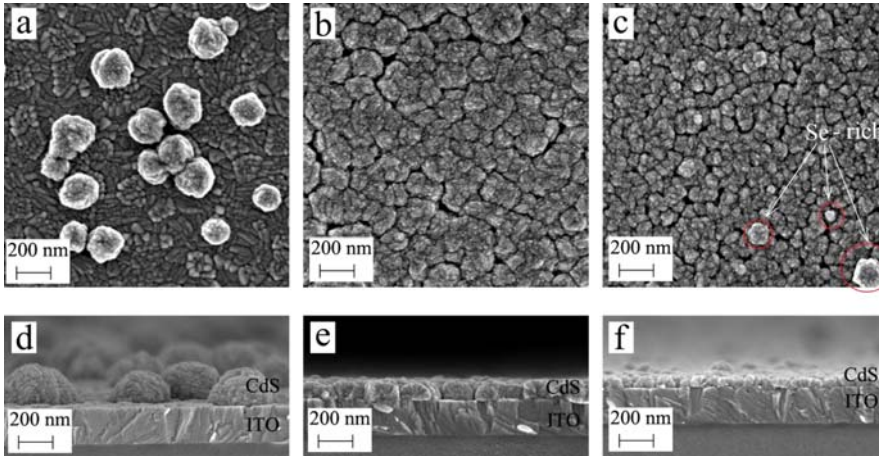


Fig. 3.19. SEM images of CdS films electrodeposited at pH 3.5 50 °C for 1.5 h at various $[H_2SeO_3]$ of (a,d) 0, (b,e) 10^{-5} M and (c,f) 10^{-4} M (Fig. 6 from [V])

According to the EDX measurements, the composition of CdS films deposited for 0.5 h at 5×10^{-4} $[H_2SeO_3]$ was found to be nearly stoichiometric with a Cd:S ratio of 1:1.08. Furthermore, no detectable Se peak was shown at 1.419 keV, indicating that Se is absent or very little ($< 0.3\%$) in the deposits [IV]. Similar compositional results were obtained for all CdS thin films deposited from Se-free solution and at low H_2SeO_3 concentrations. At longer duration of ED (1.5 h), an increase in the H_2SeO_3 concentration in the working solution shifts the stoichiometry of the as-deposited CdS. Se inclusions of 1.3 at.% and 4.7 at.% were detected in CdS films deposited at 5×10^{-5} M and 10^{-4} M H_2SeO_3 , respectively (Table 3.2).

In order to confirm the influence of H_2SeO_3 on ED, an in-situ monitoring of the current density during a potentiostatic ED (Fig. 3.20(a)) was conducted. The first 4–8 s is an induction time corresponding to the incubation time for nucleation, and no dependence on the concentration of H_2SeO_3 in the solution is observed (Fig. 3.20(b)) [105]. Further stages of the film growth are dependent on the concentration of H_2SeO_3 . The number of Se or S nuclei may increase with time, which agrees with the heterogeneous precipitation process present in the reduction-precipitation mechanism [105]. In the case of CdS electrodeposited from the Se-free solution the descending monotonous slope of the deposition curve indicates a steady-state growth of islands instead of a continuous film [149], which correspond to the SEM results shown in Fig. 3.19(a,d). An addition of H_2SeO_3 of up to 10^{-5} M and 5×10^{-5} M changes the transient shape, which suggests an increased amount of nucleation centers with time and further growth of the more compact CdS film. An addition of H_2SeO_3 of up to a concentration of

10^{-4} M intensifies the growth of the dense and uniform CdS thin film as shown in Fig. 3.19(c,f).

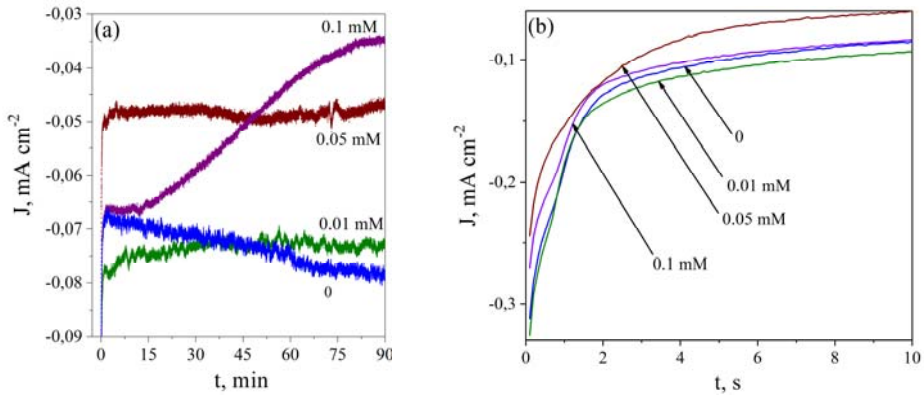


Fig. 3.20. (a) Current density vs time transients of CdS thin film ED at -0.79 V (SCE) for 1.5 h at 50 °C from solution containing various concentrations of H_2SeO_3 and (b) enlarged transients part in first 10 seconds (A modified version of Fig. 4 from [IV])

To summarize, the growth mechanism of the CdS thin film can be divided into several stages (Fig. 3.21). When no H_2SeO_3 is added into the working solution, there are two main stages (Fig. 3.21(a)): formation of S nuclei and gradual growth of CdS islands. The inclusion of H_2SeO_3 into the process generates a higher number of initial nuclei and additional stages that change the process of CdS formation into a more complex one (Fig. 3.21). In this case, the initial stage, which is the formation of Se nuclei, is followed by the adsorption of S on the surface of the cathode. This adsorbed S takes part in the growth of CdS islands. Finally, the secondary nucleation of Se may take place during the formation of a continuous CdS thin film.

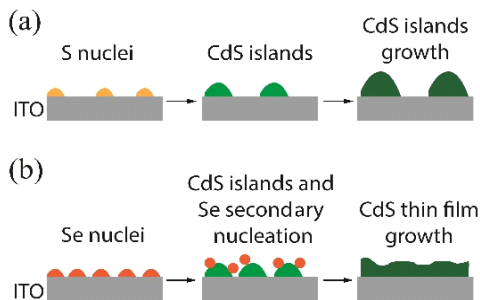


Fig. 3.21. The schematic representation of CdS thin film growth (a) without and (b) with H_2SeO_3 (Fig. 5 from [IV])

3.3.2. Properties of electrodeposited CdS thin film

CdS films electrodeposited for 0.5 h and 1.5 h from solutions with various concentrations of H_2SeO_3 were characterized and compared to reference films obtained from the initial Se-free solution.

The AFM study shows that the CdS film deposited from the initial solution for 0.5 h covers the ITO/glass substrate unevenly with agglomerated islands (Fig. 3.22). The average surface roughness was 11, 17, and 9 nm for the CdS films deposited at the concentration of H_2SeO_3 of 0, 10^{-4} M, and 5×10^{-4} M, respectively. On the other hand, CdS films deposited from solutions with H_2SeO_3 microadditive are better packed. The grain size decreases from 77 nm to 46 nm with an increase in the concentration of H_2SeO_3 . The formation of a more packed CdS film appears to depend more on H_2SeO_3 rather than on the deposition time (Fig. 3.19 and Fig. 3.22). The improved density of CdS films deposited from the Se-containing solution may be explained by the larger number of initial nucleation centers generated by the H_2SeO_3 microadditive. We can state that a higher concentration of H_2SeO_3 contributes to the thinning of CdS films (Table 3.1). This may be considered as a limiting aspect of the H_2SeO_3 microadditive; however, it is also advantageous as it simultaneously improves the film coverage and decreases the thickness of electrodeposited CdS films.

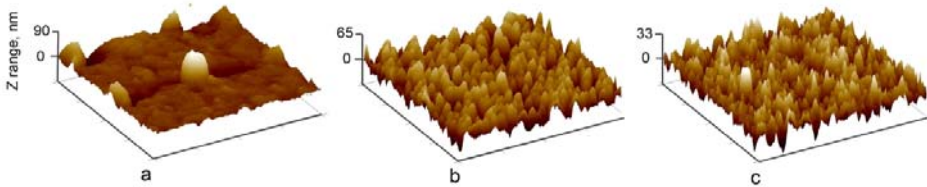


Fig. 3.22. AFM topography of CdS films electrodeposited for 0.5 h at various $[\text{H}_2\text{SeO}_3]$ (a) 0, (b) 10^{-4} M and (c) 5×10^{-4} M (Fig. 7 from [III])

Table 3.1. Thickness of CdS films deposited for 0.5 h and 1.5 h in the presence of various H_2SeO_3 concentrations

Molar concentration of H_2SeO_3 , mol/l	Thickness, nm	
	$t_{\text{dep}} = 0.5$ h	$t_{\text{dep}} = 1.5$ h
0	100	200
5×10^{-5}	66	103
10^{-4}	39	64
5×10^{-4}	44	47

Participation of Se in the growth of CdS is confirmed by the formation of the CdSe phase characterized by Raman peaks at 200 cm^{-1} and 400 cm^{-1} . Such evidences were observed only for the film deposited for 1.5 h at the highest H_2SeO_3 microadditive concentration of 5×10^{-4} M (Fig. 3.23). Besides the peaks at 300 cm^{-1} and 600 cm^{-1} attributed to longitudinal optical phonon vibrational modes of CdS [150], CdS films deposited at 10^{-4} M and 5×10^{-4} M concentration of H_2SeO_3 are characterized by peaks at 128 cm^{-1} and 173 cm^{-1} . These peaks are

attributed to sulfur vibrational modes [23]. In addition, a peak at 561 cm^{-1} was detected for all the CdS film except the film deposited at $5 \times 10^{-4}\text{ M}$ H_2SeO_3 concentration for 1.5 h. A peak at about 486 cm^{-1} that appears for the films electrodeposited at 10^{-4} M and $5 \times 10^{-4}\text{ M}$ $[\text{H}_2\text{SeO}_3]$ was attributed to CdS at near-resonance conditions [151]. A small peak at 188 cm^{-1} appears only for the films deposited for 0.5 h in the presence of 10^{-4} M and $5 \times 10^{-4}\text{ M}$ $[\text{H}_2\text{SeO}_3]$ in the electrolyte solution. This peak is attributed to pure S and S–Se [25,152].

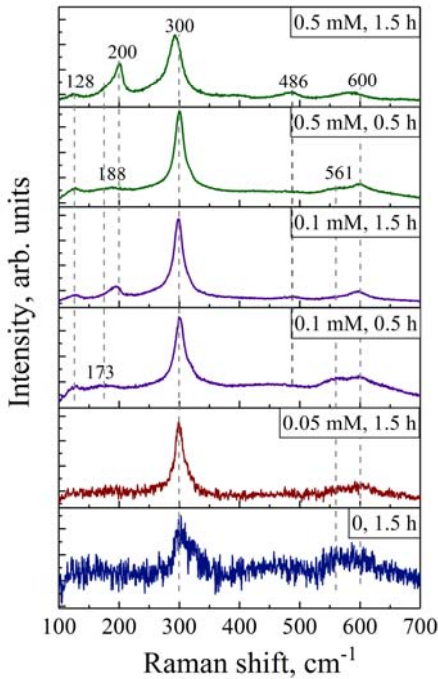


Fig. 3.23. Raman spectra of CdS films electrodeposited at $50\text{ }^\circ\text{C}$ pH 3.5 for 0.5 h and 1.5 h and various $[\text{H}_2\text{SeO}_3]$ (A modified version of Fig. 4 from [IV])

CdS films obtained from the Se-free solution exhibit both hexagonal and cubic structures corresponding to (100), (002), (101) and (220), (311) (Fig. 3.24) planes, respectively [107,153]. Other CdS peaks are suppressed by the strong ITO peaks, indicating a poor coverage of the substrate. An addition of $5 \times 10^{-5}\text{ M}$ of H_2SeO_3 into the solution promotes growth of only hexagonal CdS structure with (002) and (004) planes [107,108]. This change can be caused by a different nucleation initiated by Se traces identified in the XRD pattern at 24.0° (Fig. 3.21). This XRD peak corresponds to the (100) plane of hexagonal structure [154]. Such an improved ordering of the CdS structure may explain the decrease in thickness of CdS at higher concentrations of H_2SeO_3 in the solution (Table 3.1). At the highest H_2SeO_3 concentration, the CdS films exhibit the same hexagonal structure but with a weaker (002) peak and no Se peak. In terms of crystallinity, a concentration of $5 \times 10^{-5}\text{ M}$ of H_2SeO_3 appears to be optimal for the ED of CdS with an improved coverage and a stable hexagonal structure.

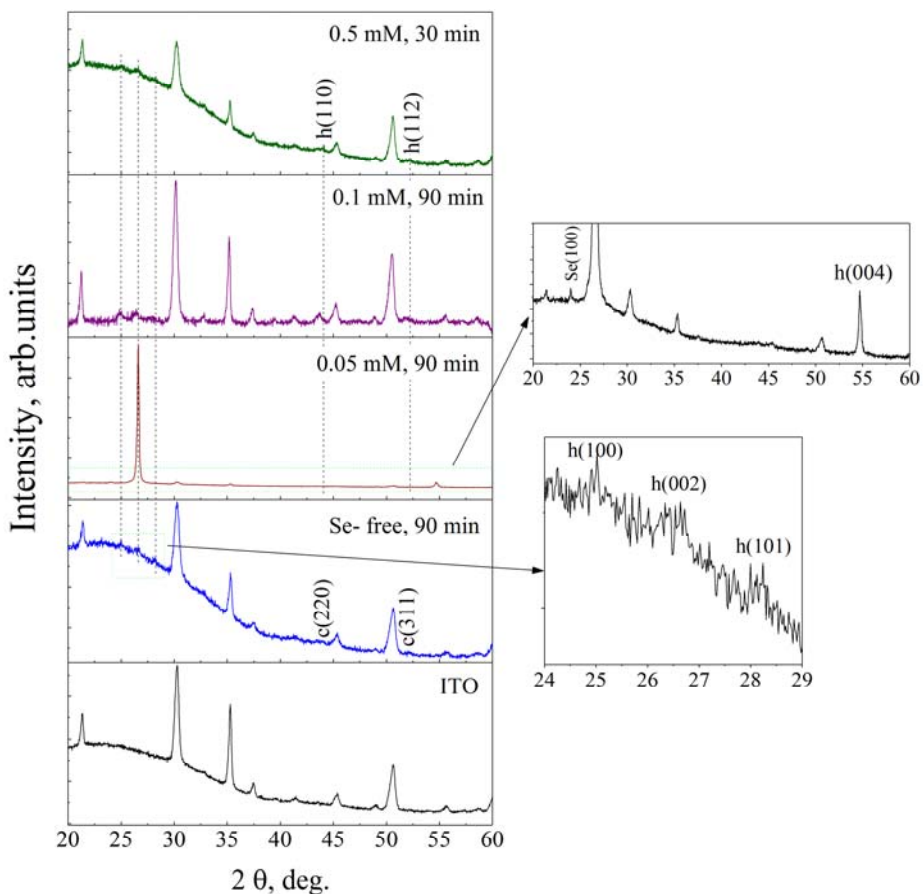


Fig. 3.24. XRD patterns of CdS films electrodeposited at 50 °C, pH 3.5 for 0.5 h and 1.5 h from solutions containing CdCl₂, Na₂Edta, Na₂S₂O₃ and various [H₂SeO₃] (0–5 × 10⁻⁴ M) (Combined from Fig. 5 [IV] and Fig. 7 [V])

The optical and electrical properties of electrodeposited CdS films are also influenced by the presence of the H₂SeO₃ microadditive in the working solution. Changes in the density of the CdS films are reflected in the optical transmittance (Fig. 3.25), which decreases from 81% to 75% at 600 nm with the addition of the H₂SeO₃ microadditive into the initial solution. This decrease in transmittance could occur owing to an improved coverage of the substrate by CdS, deviations in composition stoichiometry, scattering effects, and/or changes in thickness [IV]. At the same time, the optical E_g value slightly increased from 2.3 eV to 2.5 eV (Fig. 3.25 inset) and may be accompanied by a decrease in crystallite size [155].

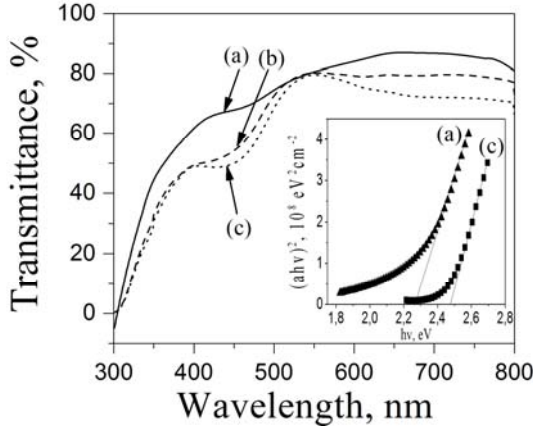


Fig. 3.25. Transmittance spectra of CdS films deposited at 50 °C, pH 3.5, -1.2 V vs. Hg/Hg₂SO₄/SO₄²⁻ for 0.5 h from initial solution: (a) Se-free, with [H₂SeO₃] of (b) 5 × 10⁻⁵ M, and (c) 5 × 10⁻⁴ M; inset- extrapolation of (αhν)² vs. hν plot for CdS films (a) and (b) (A modified version of Fig. 8 inset from [IV])

PEC and Kelvin probe measurements were performed in order to measure the photoresponse under white and red light, respectively, and to determine the type of photoconductivity and surface potential (Fig. 3.26). An *n*-type photoconducting behavior (Fig. 3.26(a)) was observed for all the analyzed CdS films as a result of semiconductor photodecomposition with participation of minority charge carriers (holes) generated in the CdS films [156]. CdS films electrodeposited in the presence of H₂SeO₃ show an improved PEC performance, which may be explained by the changed structural, morphological, and compositional properties of the films. In addition, the enhanced photocurrent densities indicate a delay in the *e*⁻-*h*⁺ pair recombination owing to the presence of more conducting Se species on the surface of CdS [157].

With addition of H₂SeO₃ the surface potential of CdS in the dark increases from approximately -0.34 V to approximately -0.53 V (Fig. 3.26(b)). This increase may be caused by incorporation of Se atoms into the surface causing the shift of the Fermi level. For CdS films deposited without Se, the photoresponse may appear due to secondary phases present in the film, whereas in the case of H₂SeO₃ presence, it appears owing to the trapped Se, which is photosensitive under a red light [158] or an imperfect stoichiometry of the films.

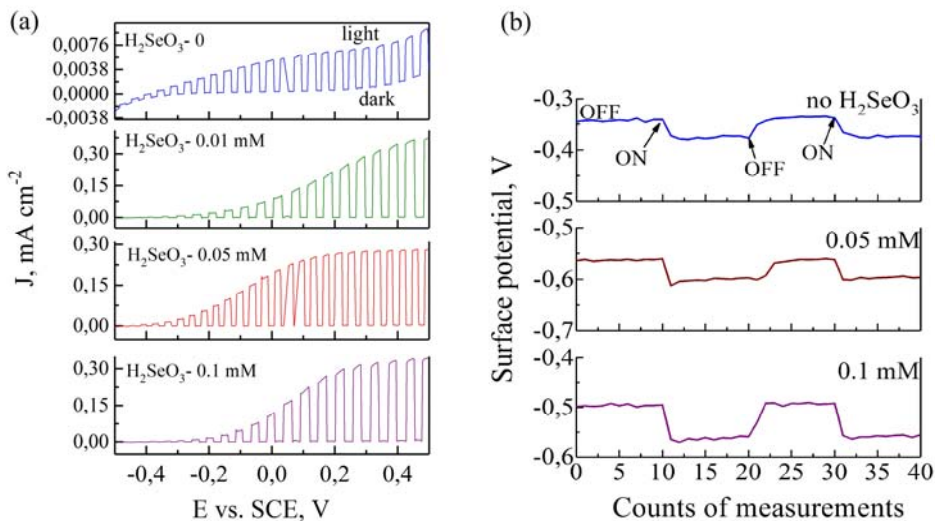


Fig. 3.26. (a) Current vs potential curves of as-deposited CdS/ITO/glass electrodes in 0.1 M Na₂SO₄ background electrolyte solution for CdS electrodeposited at various [H₂SeO₃] (Fig. 8 from [V]); (b) Kelvin probe measurements of CdS films electrodeposited at various [H₂SeO₃] (Fig. 9 from [V])

3.3.3. Annealing of CdS films

In order to improve the properties of CdS films, vacuum treatment was applied in a closed quartz tube. The detected Se in as-electrodeposited CdS is surface contaminating, as it was easily removed by the vacuum treatment (Table 3.2). However, we found that 1 at.% of Se remained in the CdS film deposited at 0.1 mM [H₂SeO₃]. It appears that the applied vacuum treatment at 120 °C for 1 h is not sufficient for the complete removal of 4.7 at.% of Se.

Table 3.2. Composition of CdS thin films (ED for 1.5 h) before and after annealing in vacuum at 120 °C for 1 h

Molar concentration C _M of H ₂ SeO ₃ in solution	Concentration in deposited films					
	Cd, at.%		S, at.%		Se, at.%	
	Asdep.	Treated	Asdep.	Treated	Asdep.	Treated
0	50.0	50.3	50.0	49.7	0.0	0.0
5 × 10 ⁻⁵	52.4	50.4	46.3	49.6	1.3	0.0
10 ⁻⁴	51.5	50.6	43.8	48.4	4.7	1.0

To summarize, H₂SeO₃ added into the working solution affects the mechanism of CdS formation and causes a transition of CdS crystalline structure from a mixed-phase to a hexagonal one. A micromolar concentration of H₂SeO₃ allows simultaneous deposition of a continuous CdS film with decreased grain size and

thickness, and lower deposition temperature of 50 °C. Secondary phases of Se can be removed by vacuum treatment at 120 °C. The obtained CdS films were deposited for application as a buffer layer in nanostructured hybrid SCs in order to improve the current transport from ITO to the CdSe nanostructured film.

3.4. Nanostructured hybrid solar cells based on electrodeposited CdSe

Nanocrystalline CdS and nanostructured CdSe thin films (described in Sections 3.2 and 3.3) were applied in initial hybrid SC structures. This section presents the preparation steps of nanostructured hybrid SCs based on electrodeposited CdS, CdSe, and CdTe films in combination with p-type conducting polymer (CP) films.

3.4.1. Glass/ITO/CdSe/P3OT:PCBM/graphite structure

For the application of a nanofibrous CdSe film in SCs, we chose a well-known structure with the commonly used spin-cast P3OT:PCBM as the absorber layer [III]. Nanofibrous CdSe films onto ITO/glass were annealed at various temperatures (Table 3.3) before spin-casting of the p-type polymer film (Fig. 3.27). P3OT:PCBM fills the upper fibrous part of the film uniformly and has a good adhesion.

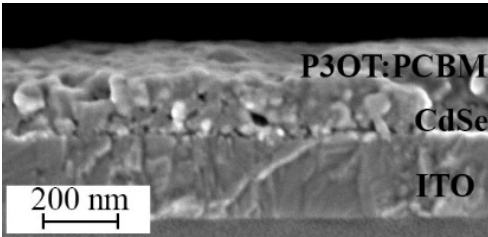


Fig. 3.27. SEM cross-sectional image of P3OT:PCBM/CdSe/ITO/glass structure, where CdSe was air annealed at 250 °C

Table 3.3. PV parameters of glass/ITO/CdSe/P3OT:PCBM/graphite SCs with nanofibrous CdSe films air annealed at various temperatures for 0.5 h

CdSe annealing temperature	V_{oc} , mV	J_{sc} , mA cm ⁻²	FF, %	η , %
250 °C	400	0.29	31	0.037
350 °C	500	0.30	29	0.044
410 °C	40	0.22	24	0.002

Hybrid SCs with a CdSe film annealed at 250 °C and 350 °C showed comparable PV properties, while an annealing temperature greater than 350 °C affects the V_{oc} value (Table 3.3). Usually the V_{oc} is affected by the back contact

material; however, we used the same material for all structures. It is more probable that in our case, the V_{OC} depends on the diameter of the nanofibers, similar to the study by Wright et al. [159], where a dependence on the size of nanocrystals was demonstrated. At the highest annealing temperature (450 °C), there are no nanofibers left and the V_{oc} value may be lowered owing to recombination losses or short carrier lifetime.

All glass/ITO/CdSe/P3OT:PCBM/graphite structures exhibit low photocurrent density (Table 3.3), which may indicate high series resistance. The possible reasons for this might be the poor contact between CdSe and P3OT:PCBM. One of the effective ways to improve the J_{sc} is to increase the light absorption yield of the polymer. The bandgap, composition and thickness of the polymer film play an important role on its absorbance, although another influencing parameter is the organic/inorganic interface of the SC [159]. It is important to adjust the thickness of the polymer film taking into account the exciton diffusion length [159].

Based on the obtained results, we can say that temperatures equal to or greater than 350 °C are suitable for air annealing of CdSe nanofibrous films. However, owing to the poor absorbing properties of P3OT:PCBM *p*-type layer, our SCs exhibit low J_{sc} values. An increase in the P3OT:PCBM thickness could improve the absorbance; however, the applied spin-casting method does not allow a precise control of the thickness. Therefore, we decided to solve the problem of insufficient absorption by adding a well-known absorber material, CdTe, to this SC structure.

3.4.2. Glass/ITO/CdSe/CdTe/P3OT:PCBM/graphite structure

For the improvement of the PV parameters of the previously discussed CdSe/P3OT:PCBM SC, we added CdTe between the polymer and nanofibrous CdSe films. In the new CdSe/CdTe/P3OT:PCBM structure, the polymer is a back-contact and an organic photoabsorber functional layer.

In order to fabricate the CdSe/CdTe core/shell structure, CdTe was electrodeposited onto a nanofibrous CdSe film [VI]. The formed core/shell structures have a diameter of ~100 nm, whereas the total thickness of the obtained CdTe/CdSe/ITO structure is ~700 nm (Fig. 3.28). CdSe core nanofibers are covered with a polycrystalline CdTe with an average grain size of 10–20 nm. Round-shaped caps with a diameter from 150–200 nm cover the tops of the CdSe/CdTe fibers (Fig. 3.28(a)). The observed morphology of the CdSe/CdTe structure confirms the preferable grain growth of CdTe as an “extension” of CdSe nanofibers. The mechanism of CdTe nucleation is similar to that of CdSe [76,95].

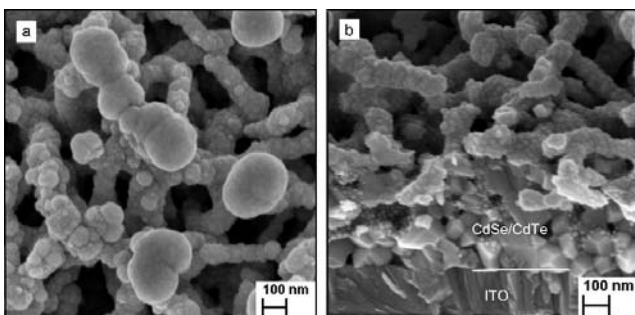


Fig. 3.28. SEM images of CdTe/CdSe/ITO/glass structure air-annealed at 200 °C for 1 h (A modified version of Fig. 2 from [V])

The Raman spectrum (Fig. 3.29) of the annealed CdTe/CdSe/ITO/glass structure shows peaks at 140 cm^{-1} , 163 cm^{-1} and 330 cm^{-1} belonging to CdTe [17] and peaks at 94 cm^{-1} and 120 cm^{-1} indicating the presence of Te secondary phase [90,160]. Furthermore, low-intensity CdSe peaks at 173 cm^{-1} , 204 cm^{-1} , and 411 cm^{-1} are observed as a result of an underlying CdSe film [77,78,143].

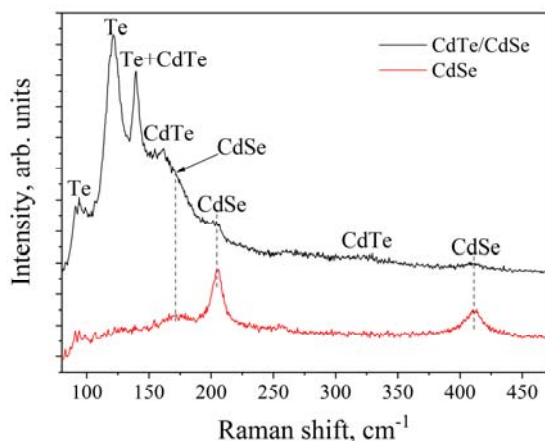


Fig. 3.29. Raman spectra of CdSe/ITO/glass air-annealed at 350 °C for 0.5 h and whole CdTe/CdSe/ITO/glass structure air annealed at 200 °C for 0.5 h (Fig. 3 from [V])

In the new SC structure, the CdSe nanostructure is not evident anymore as the polymer fills the empty spaces, with good adhesion, without cracks and holes (Fig. 3.30). Although the glass/ITO/CdSe/P3OT:PCBM/graphite structure was obtained with the CdTe layer, it has similar PV properties: $V_{oc} = 0.43\text{ V}$, $J_{sc} = 0.5\text{ mA cm}^{-2}$, FF = 33% (Fig. 3.31). Although the absorbance was improved by the inclusion of CdTe, the current density is still low, most probably because of interface issues, recombination losses or porosity of the CdSe film.

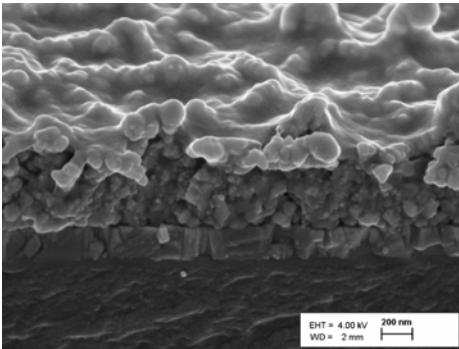


Fig. 3.30. SEM images of P3OT:PCBM/CdTe/CdSe/ITO/glass structure (A modified version of Fig. 2 from [V])

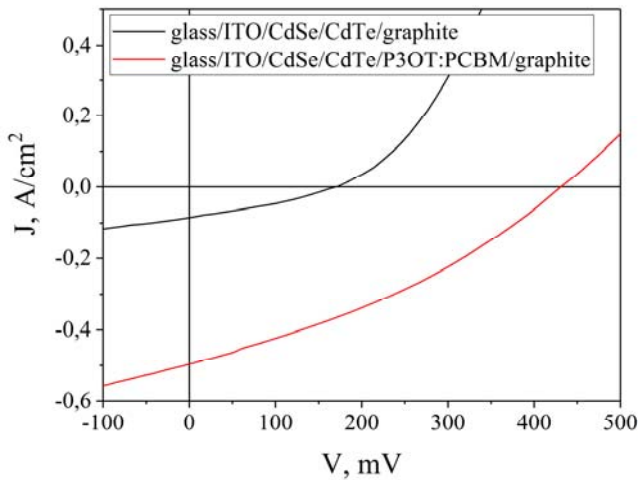


Fig. 3.31. J - V characteristics of glass/ITO/CdSe/CdTe structures uncoated and coated with P3OT:PCBM and with graphite back-contact, under illumination of 100 mW/cm^2 (Fig. 4 from [V])

In order to improve the polymer/CdSe interface and preserve the CdSe nanostructure, we applied a PPy polymer synthesized by PEC deposition method. Moreover, for the improvement of charge transport at the CdSe/ITO interface, a CdS buffer layer was deposited before the CdSe nanostructured film.

3.4.3. Glass/ITO/CdS/CdSe/PPy:NSA/graphite structure

For the deposition of CdS buffer onto ITO/glass structure, the knowledge gained in Section 3.3 was applied. Therefore, the ED of the CdS film with a thickness of $\sim 100 \text{ nm}$ was carried out at the following conditions: -0.79 V (SCE), $50 \text{ }^\circ\text{C}$, pH of 3.5, and with $5 \times 10^{-5} \text{ M}$ $[\text{H}_2\text{SeO}_3]$. CdS helped to reduce the number of pores at the interface between ITO and CdSe.

Py doped with NaNSA was electrodeposited onto CdSe/CdS/ITO/glass electrodes at a low potential of 0.2 V (SCE) under a Xe lamp illumination. Owing to the small applied potential value, PPy covered only the photoactivated surface of CdSe without deep penetration into the pores (Fig. 3.32). The thickness of the PPy film after 1 h deposition was ~ 10 nm.

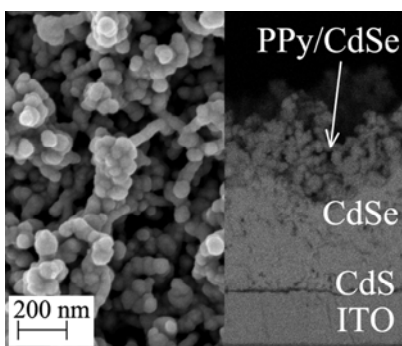


Fig. 3.32. SEM surface and cross-sectional images of nanostructured PPy/CdSe/CdS/ITO/glass structures with PPy electrodeposited for 1 h

Implementation of such a structure helped us to significantly improve the J_{sc} ($2.6 \text{ mA}\cdot\text{cm}^{-2}$); however, led to the decreased V_{oc} value (95 mV) at a FF of $\sim 27\%$. It is noteworthy that all layers of the latter SC structure are electrodeposited. We experimentally proved that electrodeposited nanofibrous CdSe films can be implemented in an electrodeposited hybrid SC. However, the fabrication technology of the complete device should be further optimized in order to improve the SC parameters.

CONCLUSIONS

This thesis was directed to the study of formation and growth mechanisms of electrodeposited CdSe and CdS films for application in electrodeposited nanostructured glass/ITO/CdS/CdSe/PPy/graphite hybrid solar cell structure. Conclusions from the studies are as follows:

1. The concentration of H_2SeO_3 determines the stoichiometry and morphology of CdSe films. The optimal concentration of H_2SeO_3 for the electrodeposition of stoichiometric CdSe thin films is $\leq 5 \times 10^{-4}$ M at exceeding concentrations of CdCl_2 . Higher concentration of H_2SeO_3 dictates formation of a nanostructured film. When $[\text{CdCl}_2]$ in the solution is 0.025 M, nanohorn films grow at 10^{-3} M $[\text{H}_2\text{SeO}_3]$, mixed nanohorn/nanofiber-structured films form at 5×10^{-3} M, and nanofibrous CdSe films are obtained at 10^{-2} M.
2. The formation of CdSe nanostructures is defined by the excess of Se^0 species at the electrode/electrolyte interface where strong affinity of Se atoms to each other lead to the formation of secondary Se nuclei on the underlying CdSe film. Still, the excess of Se in the nanostructured CdSe films can be easily removed by air-annealing.
3. Near-stoichiometric CdS films can be electrodeposited from the microadditive-free initial solution at the following conditions: -0.8 V (SCE), 80°C , $\text{pH} \leq 3.5$, 0.01 M $[\text{CdCl}_2]$, 0.05 M $[\text{Na}_2\text{S}_2\text{O}_3]$, 0.02 M $[\text{Na}_2\text{Edta}]$. Addition of the micromolar concentration of H_2SeO_3 into the initial solution modifies the growth of CdS films, improves the coverage and simultaneously decreases the thickness.
4. The optimal concentration of H_2SeO_3 (5×10^{-5} M) in the working solution assures the formation of CdS with stable hexagonal structure instead of the mixed-phase structure. Changes in morphology, structure, optical and electrical properties of CdS indicate to the inclusion of Se-containing phases, which can be easily removed by the vacuum treatment.
5. Electrodeposition of polycrystalline CdTe film onto CdSe nanofibers helps to improve the absorption and lead to increase of the photocurrent of the glass/ITO/CdSe/CdTe/P3OT:PCBM/graphite solar cell. With addition of the CdTe shell to CdSe core nanofibers the solar cell photovoltaic performance was improved from $V_{oc} = 400$ mV, $J_{sc} = 0.29$ $\text{mA}\cdot\text{cm}^{-2}$ to $V_{oc} = 430$ mV, $J_{sc} = 0.5$ $\text{mA}\cdot\text{cm}^{-2}$.
6. Spin-casted P3OT:PCBM was found to be an inappropriate absorber material for the electrodeposited nanofibrous CdSe/ITO/glass structure as the polymer fills the empty space in the fibrous part of the film.
7. Contrary, PPy deposited photoelectrochemically covers only the surface of CdSe nanofibers and preserves the nanostructure. All-electrodeposited nanostructured hybrid glass/ITO/CdS/CdSe/PPy/graphite solar cell structure is characterized by increased J_{sc} value up to 2.6 $\text{mA}\cdot\text{cm}^{-2}$; however lower V_{oc} value of 95 mV and FF of 27%.

8. The CdS film electrodeposited between CdSe and ITO front contact helps to eliminate pores in the CdSe film and, therefore, to improve the absorption and charge carriers transport in the solar cell.

REFERENCES

1. Electricity production, consumption and market overview, Data extracted in June 2017. Most recent data: Further Eurostat information, Main tables and Database, http://ec.europa.eu/eurostat/statistics-explained/index.php/Electricity_production,_consumption_and_market_overview.
2. M.T. Kibria, A. Ahammed, S.M. Sony, F. Hossain, S.-U.-Islam, A Review: Comparative studies on different generation solar cells technology, *Proceedings of 5th International Conference on Environmental Aspects of Bangladesh* (2014) 51–53.
3. <https://www.ise.fraunhofer.de/content/dam/ise/de/documents/publications/studies/Photovoltaics-Report.pdf>
4. S. Kumar, M. Nehra, A. Deep, D. Kedia, N. Dilbaghi, K.-H. Kim, Quantum-sized nanomaterials for solar cell applications, *Renew. Sust. Energ. Rev.* **73** (2017) 821–839.
5. K. Yoshikawa, H. Kawasaki, W. Yoshida, T. Irie, K. Konishi, K. Nakano, T. Uto, D. Adachi, M. Kanematsu, H. Uzu, K. Yamamoto, Silicon heterojunction solar cell with interdigitated back contacts for a photoconversion efficiency over 26%, *Nat. Energy* **2** (2017) 17032.
6. T. Dittrich, A. Belaidi, A. Ennaoui, Concepts of inorganic solid-state nanostructured solar cells, *Sol. Energy Mater. Sol. Cells* **95** (2011) 1527–1536.
7. G. Conibeer, Third-generation photovoltaics, *Mater. today* **10** (2007) 42–50.
8. M. A. Green, Y. Hishikawa, W. Warta, E.D. Dunlop, D.H. Levi, J. Hohl-Ebinger, A.W.Y. Ho-Baillie, Solar cell efficiency tables (version 50). *Prog. Photovolt: Res. Appl.* **25** (2017) 668–676.
9. H. Deligianni, S. Ahmed, and L.T. Romankiw, The Next Frontier: Electrodeposition for Solar Cell Fabrication, *Interface* **20** (2011) 47–53.
10. A. Jarkov, S. Bereznev, O. Volobujeva, R. Traksmaa, A. Tverjanovich, A. Öpik, E. Mellikov, Photo-assisted electrodeposition of polypyrrole back contact to CdS/CdTe solar cell structures, *Thin Solid Films* **535** (2013) 198–201.
11. X. Song, M. Wang, H. Zhang, J. Deng, Z. Yang, C. Ran, X. Yao, Morphologically controlled electrodeposition of CdSe on mesoporous TiO₂ film for quantum dot sensitized solar cells, *Electrochim. Acta* **108** (2013) 449–457.
12. W. Hou, Y. Xiao, G. Han, H. Zhou, Electro-polymerization of polypyrrole/multi-wall carbon nanotube counter electrodes for use in platinum-free dye-sensitized solar cells, *Electrochim. Acta* **190** (2016) 720–728.
13. R.Tena-Zaera, M.A. Ryan, A. Katty, G. Hodes, S. Bastide, C. Lévy-Clément, Fabrication and characterization of ZnO nanowires/CdSe/CuSCN *eta*-solar cell, *C. R. Chimie* **9** (2006) 717–729.

14. O.K. Echendu, F. Fauzi, A.R. Weerasinghe, I.M. Dharmadasa, High short-circuit current density CdTe solar cells using all-electrodeposited semiconductors, *Thin Solid Films* **556** (2014) 529–534.
15. O.K. Echendu, I.M. Dharmadasa, Graded-Bandgap solar cells using all-electrodeposited ZnS, CdS and CdTe thin-films, *Energies* **8** (2015) 4416–4435.
16. K. Fujimoto, T. Oku, T. Akiyama, Fabrication and Characterization of ZnO/Cu₂O Solar Cells Prepared by Electrodeposition, *Appl. Phys. Express* **6** (2013) 086503.
17. G. F. Alapatt, R. Singh, K. F. Poole, Fundamental Issues in Manufacturing Photovoltaic Modules Beyond the Current Generation of Materials, *Adv. Optoelectron.* **2012** (2012) 782150.
18. Д.М. Чижииков, Кадмий. Издание 2, издательство «Наука», Москва, 1967.
19. H. Jerominek, M. Pigeon, S. Patela, Z. Jakubczyk, C. Delisle, R. Tremblay, CdS microcrystallites-doped thin-film glass waveguides, *J. Appl. Phys.* **63** (1988) 957–959.
20. K.Senthil, D.Mangalaraj, S.K.Narayandass, Structural and optical properties of CdS thin films, *Appl. Surf. Sci.* **169-170** (2001) 476–479.
21. J. Schaffner, E. Feldmeier, A. Swirschuk, H.-J. Schimper, A. Klein, W. Jaegermann, Influence of substrate temperature, growth rate and TCO substrate on the properties of CSS deposited CdS thin films, *Thin Solid Films* **519** (2011) 7556–7559.
22. Z. Rizwan, A. Zakaria, M.S.M. Ghazali, A. Jafari, F.U. Din, R. Zamiri, Effect of Annealing Temperature on the Optical Spectra of CdS Thin Films Deposited at Low Solution Concentrations by Chemical Bath Deposition (CBD) Technique, *Int. J. Mol. Sci.* **12** (2011) 1293–1305.
23. H. Karami, A. Kaboli, Pulsed current electrochemical synthesis of cadmium sulphide nanofibers, *Int. J. Electrochem. Sci.* **5** (2010) 706–719.
24. J. Nishino, S. Chatani, Y. Uotani, Y. Nosaka, Electrodeposition method for controlled formation of CdS films from aqueous solutions, *J. Electroanal. Chem.* **473** (1999) 217–222.
25. G.P. Power, D. R. Peggs, A. I. Parker, The cathodic formation of photoactive cadmium sulfide films from thiosulfate solutions, *Electrochim. Acta* **26** (1981) 681–682.
26. S. Dennison, Studies of the cathodic electrodeposition of CdS from aqueous solution, *Electrochim. Acta* **38** (1993) 2395–2403.
27. M. Takahashi, S. Hasegawa, M. Watanabe, T. Miyuki, S. Ikeda, K. Iida, Preparation of CdS thin films by electrodeposition: effect of colloidal sulfur particle stability on film composition, *J. Appl. Electrochem.* **32** (2002) 359–367.
28. S.J. Lade, C.D. Lokhande, Electrodeposition of CdS from non-aqueous bath, *Mater. Chem. Phys.* **49** (1997) 160–163.
29. L. Zhao , L. Hu , and Xiaosheng Fang, Growth and Device Application of CdSe Nanostructures, *Adv. Funct. Mater.* **22** (2012) 1551–1566.

30. U. Farva, C. Park, Influence of thermal annealing on the structural and optical properties of CdSe nanoparticles, *Sol. Energy Mater. Sol. Cells* **94** (2010) 303–309.
31. T.C.M. Santhosh, K.V. Bangera, G.K. Shivakumar, Preparation of vacuum deposited cadmium selenide thin films for optoelectronic applications, *Mater. Today: Proceedings* **3** (2016) 2220–2224.
32. M.K. Khalaf, B.A.M. ALhilli, A.I. Khudiar, A.A. Alzahra, Influence of nanocrystalline size on optical band gap in CdSe thinfilms prepared by DC sputtering, *Photonic. Nanostruct.* **18** (2016) 59–66.
33. F. Laatar, A. Harizi, A. Smida, M. Hassen, H. Ezzaouia, Effect of deposition temperature on the structural and optical properties of CdSe QDs thin films deposited by CBD method, *Mater. Res. Bull.* **78** (2016) 83–95.
34. J.P. Szabo, M. Cocivera, Mechanism of electrodeposition of cadmium selenide from SeSO_3^{2-} solution, *Can. J. Chem.* **66** (1988) 1065.
35. M. Skyllas-Kazacos, Electrodeposition of CdSe and CdSe + CdTe thin films from cyanide solutions, *J. Electroanal. Chem.* **148** (1983) 233–239.
36. M. Skyllas-Kazacos, B. Miller, Studies in selenious acid and CdSe film deposition, *J. Electrochem. Soc.* **127** (1980) 869–873.
37. T.D. Lee, A.U. Ebong, A review of thin film solar cell technologies and challenges, *Renew. Sust. Energ. Rev.* **70** (2017) 1286–1297.
38. D. Bonnet, Manufacturing of CSS CdTe solar cells, *Thin Solid Films* **361-362** (2000) 547–552.
39. A.Romeo, M. Arnold, D.L. Bätzner, H. Zogg, A.N. Tiwari, Development of high efficiency flexible CdTe solar cells, PV in Europe - From PV Technology to Energy Solutions, 7–11 October 2002, Rome, Italy.
40. J.L. Boone, T.P. Van Doren, A.K. Berry, Deposition of CdTe by spray pyrolysis, *Thin Solid Films* **87** (1982) 259–264.
41. L-E. Lyons, G.C. Morris, D.H. Horton, J.G. Keyes, Cathodically electrodeposited films of cadmium telluride, *J. Electroanal. Chem.* **168** (1984) 101–116.
42. H. Gómez, R. Henríquez, R. Schrebler, R. Córdova, D. Ramírez, G. Riveros, E.A. Dalchiele, Electrodeposition of CdTe thin films onto n-Si(1 0 0): nucleation and growth mechanisms, *Electrochim. Acta* **50** (2005) 1299–1305.
43. M. Yoshii, Y. Murata, Y. Nakabayashi, T. Ikeda, M. Fujishima, H. Tada, Coverage control of CdSe quantum dots in the photodeposition on TiO₂ for the photoelectrochemical solar hydrogen generation, *J. Colloid Interf. Sci.* **474** (2016) 34–40.
44. J. Zhou, Y. Liu, J. Tang, W. Tang, Surface ligands engineering of semiconductor quantum dots for chemosensory and biological applications, *Mater. Today* **886** (in press).
45. F. A. Kröger, Cathodic Deposition and Characterization of Metallic or Semiconducting Binary Alloys or Compounds, *J. Electrochem. Soc.* **125** (1978) 2028–2034.

46. H.-G. Kim, M.-J. Gim, H.-J. Jeon, M. Kim, J.-H. Jeun, J.-M. Kim, Y.-S. Kim, Nonvolatile organic memory devices with CdTe quantum dots, *Microelectron. Eng.* **111** (2013) 210–213.
47. B.I. Ipe, M. Lehnig, C.M. Niemeyer, On the Generation of Free Radical Species from Quantum Dots, *Small* **1** (2005) 706–709.
48. A. Chen, C. Shang, G. Zeng, G. Chen, J. Shao, J. Zhang, H. Huang, Extracellular secretions of *Phanerochaete chrysosporium* on Cd toxicity, *International Biodeterioration & Biodegradation* **105** (2015) 73–79.
49. Z. Bujňáková, M. Baláž, E. Dutková, P. Baláž, M. Kello, G. Mojžišová, J. Mojžiš, M. Vilková, J. Imrich, M. Psočka, Mechanochemical approach for the capping of mixed core CdS/ZnS nanocrystals: Elimination of cadmium toxicity, *J. Colloid Interface Sci.* **486** (2017) 97–111.
50. A. Ramos-Ruiz, C. Zeng, R. Sierra-Alvarez, L.H. Teixeira, J.A. Field, Microbial toxicity of ionic species leached from the II–VI semiconductor materials, cadmium telluride (CdTe) and cadmium selenide (CdSe), *Chemosphere* **162** (2016) 131–138.
51. J.H. Werner, Second and Third Generation Photovoltaics – Dreams and Reality, *Adv. Solid State Phys.* **44** (2004) 51–67.
52. E. Placzek-Popko, Top PV market solar cells 2016, *Optoelectron. Rev.* **25** (2017) 55–64.
53. M.A. Green, K. Emery, Y. Hishikawa, W. Warta, E.D. Dunlop, D.H. Levi, A.W.Y. Ho-Baillie, Solar cell efficiency tables (version 49), *Prog. Photovolt: Res. Appl.* **25** (2017) 3–13.
54. <https://www.energy.gov/eere/sunshot/cadmium-telluride>
55. T. Dittrich, A. Belaidi, A. Ennaoui, Concepts of inorganic solid-state nanostructured solar cells, *Sol. Energy Mater. Sol. Cells* **95** (2011) 1527–1536.
56. S. Mathew, A. Yella, P. Gao, R. Humphry-Baker, B.F.E. Curchod, N. Ashari-Astani, I. Tavernelli, U. Rothlisberger, Md. K. Nazeeruddin, M. Grätzel, Dye-sensitized solar cells with 13% efficiency achieved through the molecular engineering of porphyrin sensitizers, *Nature Chem.* **6** (2014) 242–247.
57. N. McElroy, R.C. Page, D. Espinbarro-Valazquez, E. Lewis, S. Haigh, P. O'Brien, D.J. Binks, Comparison of solar cells sensitised by CdTe/CdSe and CdSe/CdTe core/shell colloidal quantum dots with and without a CdS outer layer, *Thin Solid Films* **560** (2014) 65–70.
58. H.K. Jun, M.A. Careem, A.K. Arof, Quantum dot-sensitized solar cells—perspective and recent developments: A review of Cd chalcogenide quantum dots as sensitizers, *Renew. Sust. Energ. Rev.* **22** (2013) 148–167.
59. R. Zhou, L. Wan, H. Niu, L. Yang, X. Mao, Q. Zhang, S. Miao, J. Xu, G. Cao, Tailoring band structure of ternary CdS_xSe_{1-x} quantum dots for highly efficient sensitized solar cells, *Sol. Energy Mater. Sol. Cells* **155** (2016) 20–29.

60. Y. Xie, Q. Tan, Z. Zhang, K. Lu, M. Li, W. Xu, D. Qin, Y. Zhang, L. Hou, H. Wu, Improving performance in CdTe/CdSe nanocrystals solar cells by using bulk nano-heterojunctions, *J. Mater. Chem. C* **4** (2016) 6483.
61. E.M. El-Menyawy, I.T. Zedan, A.A. Azab, One-pot solvothermal synthesis and characterization of CdS nanotubes decorated with graphene for solar cell applications, *J. Alloys Compd.* **695** (2017) 3429–3434.
62. H. Majidi, M.E. Edley, L.C. Spangler, J.B. Baxter, Tailoring Absorber Thickness and the Absorber-Scaffold Interface in CdSe-Coated ZnO Nanowire Extremely Thin Absorber Solar Cells, *Electrochim. Acta* **145** (2014) 291–299.
63. J. Xu, X. Yang, H. Wang, X. Chen, C. Luan, Z. Xu, Z. Lu, V.A.L. Roy, W. Zhang, C.-S. Lee, Arrays of ZnO/Zn_xCd_{1-x}Se Nanocables: Band Gap Engineering and Photovoltaic Applications, *Nano Lett.* **11** (2011) 4138–4143.
64. X. Wang, R. Li, D. Fan, Nanostructured Al-ZnO/CdSe/Cu₂O ETA solar cells on Al-ZnO film/quartz glass templates, *Nanoscale Research Lett.* **6** (2011) 614.
65. V. Mittal, *Polymers for energy storage and conversion*, Scrivener Publishing LLC, 2013.
66. S. Gunes, N.S. Sariciftci, Hybrid solar cells, *Inorg. Chim. Acta* **361** (2008) 581–588.
67. F. Kadirgan, D. Mao, W. Song, T. Ohno, B. McCandless, Properties of Electrodeposited Cadmium Sulfide Films for Photovoltaic Devices With Comparison to CdS Films Prepared by Other Methods, *Turk. J. Chem.* **24** (2000) 21–33.
68. C. Li, L. Yang, J. Xiao, Y.-C. Wu, M. S ndergaard, Y. Luo, D. Li, Q. Meng, B.B. Iversen, ZnO nanoparticle based highly efficient CdS/CdSe quantum dot-sensitized solar cells, *Phys. Chem. Chem. Phys.* **15** (2013) 8710.
69. T. D. Lee, A.U. Ebong, A review of thin film solar cell technologies and challenges, *Renew. Sust. Energ. Rev.* **70** (2017) 1286–1297.
70. A. Ray, Electrodeposition of Thin Films for Low-cost Solar Cells, Chapter 7, In: *Electroplating of Nanostructures*. Ed. Mahmood Aliofkhaezai, InTech, 2015.
71. A.J. Bard, L.R. Faulkner. *Electrochemical methods: Fundamentals and applications*. Ed. D. Harris, E. Swain, C. Robey, E. Aiello, 2nd edition. New York: John Wiley & Sons, Inc., 2001, pp. 9–23.
72. S. S. Djokić, Editor, *Electrodeposition and Surface Finishing: Fundamentals and Applications*, Springer-Verlag New York, 2014, p. 223.
73. V. G. Dubrovskii, *Nucleation Theory and Growth of Nanostructures*, 1, NanoScience and Technology, Springer-Verlag Berlin Heidelberg, 2014.
74. A. Bewick, M. Fleischmann, H. R. Thirsk, Kinetics of the Electrocrystallization of Thin Films of Calomel, *Trans. Faraday Soc.* **58** (1962) 2200–2216.
75. S.B. Hendricks, Screw dislocations and charge balance as factors of crystal growth, *American Mineralogist* **40** (1955) 139–146.

76. N.B. Hannay, Semiconductors, Reinhold publishing corporation, New York, 1959.
77. T. E. Schlesinger, K. Rajeshwar, N.R. de Tacconi, Electrodeposition of semiconductors, Modern Electroplating, Fifth Edition, John Wiley & Sons, Inc., 2010.
78. M.-R. Gao, Y.-F. Xu, J. Jiang, S.-H. Yu, Nanostructured metal chalcogenides: synthesis, modification, and applications in energy conversion and storage devices, *Chem. Soc. Rev.* **42** (2013) 2986–3017.
79. A.V. Shaikh, R.S. Mane, H.M. Pathan, B.-K. Min, O.-S. Joo, S.-H. Han, CdSe thin film growth: Primarily amorphous nanograins to self-assembled nanowires, *J. Electroanal. Chem.* **615** (2008) 175–179.
80. E.M. Mkawi, K. Ibrahim, M.K.M. Ali, M.A. Farrukh, A.S. Mohamed, N.K. Allam, Effect of complexing agents on the electrodeposition of Cu-Zn-Sn metal precursors and corresponding Cu₂ZnSnS₄-based solar cells, *J. Electroanal. Chem.* **735** (2014) 129–135.
81. L. Liu, S. Yellinek, I. Valding, A. Donval, D. Mandler, Important implications of the electrochemical reduction of ITO, *Electrochim. Acta* **176** (2015) 1374–1381.
82. A. Ghazali, Z. Zainal, M.Z. Hussein, A. Kassim, Cathodic electrodeposition of SnS in the presence of EDTA in aqueous media, *Sol. Energy Mater. Sol. Cells* **55** (1998) 237–249.
83. P. Radhakrishnu, A.K.N. Reddy, Mechanism of action of selenious acid in the electrodeposition of manganese, *J. Appl. Electrochem.* **7** (1977) 113–117.
84. L.L. Shreir, J.W. Smith, Effects of addition agents on the cathode polarization potential during the electrodeposition of copper, *Trans. Faraday Soc.* **50** (1954) 393–403.
85. M. Fracastoro-Decker, J.L.S. Ferreira, N.V. Gomes, F. Decker, Optically monitored electrodeposition of thin CdSe films, *Thin Solid Films* **147** (1987) 291–297.
86. B. Shan, W.Wu, K. Feng, H. Nan, Electrodeposition of wurtzite CdTe and the potential dependence of the phase structure, *Mater. Lett.* **166** (2016) 85–88.
87. S. Hamilakis, D. Balgis, K. Milonakou-Koufoudaki, C. Mitzithra, C. Kollia, Z. Loizos, Electrodeposition of CdSe photoabsorbent thin films in the presence of selected organic additives, *Mater. Lett.* **145** (2015) 11–14.
88. M. P. R. Panicker, M. Knaster, F. A. Kroger, Cathodic deposition of CdTe from aqueous electrolytes, *J. Electrochem. Soc.: Electrochemical science and technology* **125** (1978) 566–572.
89. G.C. Morris, R. Vanderveen, Cadmium sulphide films prepared by pulsed electrodeposition, *Sol. Energ. Mater. Sol. Cells* **27** (1992) 305–319.
90. R. K. Pandey, Handbook of semiconductor electrodeposition, CRC Press, 1996.
91. X. Fang, L. Wu, Handbook of innovative nanomaterials from syntheses to applications, CRC Press, Taylor & Francis Group, 2013.

92. O.I. Olusola, V. Patel, I.M. Dharmadasa, Optimization of pH for electrodeposition of n CdSe thin films for applications in photovoltaic devices, 29th European Photovoltaic Solar Energy Conference and Exhibition (2014) 1852–1856.
93. S. Thanikaikarasan, C. Vedhi, X.S. Shajan, T. Mahalingam, Investigation of solution pH effect on electrochemical, microstructural, optical and photoelectrochemical properties of CdSe thin films, *Solid State Sci.* **15** (2013) 142–151.
94. S.A.M. Al-Bat'hi, *Electrodeposition of Nanostructure Materials*, Chapter 1, 2015.
95. M. Bouroushian, *Electrochemistry of Metal Chalcogenides*, Monographs in Electrochemistry, Springer-Verlag Berlin Heidelberg, 2010.
96. M. Bouroushian, *Electrochemistry of Metal Chalcogenides*, Springer Berlin Heidelberg, 2010.
97. M. Osial, J. Widera, K. Jackowska, Influence of electrodeposition conditions on the properties of CdTe films, *J. Solid State Electrochem.* **17** (2013) 2477–2486.
98. A. Kampmann, P. Cowache, J. Vedel, D. Lincot, Investigation of the influence of the electrodeposition potential on the optical, photoelectrochemical and structural properties of as-deposited CdTe, *J. Electroanal. Chem.* **387** (1995) 53–64.
99. R.K. Pandey, S.N. Sahu, S. Chandra, *Handbook of Semiconductor Electrodeposition*, Markel Dekker, Inc., 1996.
100. M. Fathy, S. Elyamny, S. Mahmoud, A.El-H.B. Kashyout, Effect of Thermal and Chemical Treatment on Electrodeposited CdTe Thin Films for Solar Cell Applications, *Int. J. Electrochem. Sci.* **10** (2015) 6030–6043.
101. W. Song, D. Mao, Y. Zhu, J. Tang, J.U. Trefny, Fabrication of high efficiency CdTe thin film solar cells using electrodeposition, Conference Record of the Twenty Fifth IEEE Photovoltaic Specialists Conference (1996) 873 – 876.
102. N. Takeno, *Atlas of Eh-pH diagrams*, 2005.
103. B. N. Levonovich, Effect of the annealing atmosphere on the recrystallization of polycrystalline films of cadmium selenide, *Doklady Phys.* **55** (2010) 127–129.
104. U. Farva, C. Park, Influence of thermal annealing on the structural and optical properties of CdSe nanoparticles, *Sol. Energy Mater. Sol. Cells* **94** (2010) 303–309.
105. J.D. Phillip, P.S. Anura, D.S. Dilip, M.P. Laurence, Synthesis of cadmium and zinc semiconductor compounds from an ionic liquid containing choline chloride and urea, *Thin Solid Films* **515** (2007) 5751–5754.
106. H.H. Huang, “STABCAL”, Thermodynamic Software, Metallurgical and Materials Engineering Department, Montana Tech, Butte, Montana, 2007.
107. S. Dennison, Studies of the cathodic electrodeposition of CdS from aqueous solution, *Electrochim. Acta* **38** (1993) 2395–2403.

108. B.E. McCandless, A. Mondal, R.W. Birkmire, Galvanic deposition of cadmium sulfide thin films, *Sol. Energ. Mater. Sol. Cells* **36** (1995) 369–379.
109. D.K. Roe, L. Wenzhao, H. Gerischer, Electrochemical deposition of cadmium sulfide from DMSO solution, *J. Electroanal. Chem.* **136** (1982) 323–337.
110. C-FYou, Y-J. Lin, C.-J. Liu, C.-A. Wu, Dependences of the structural, compositional and photoluminescent properties of electrodeposited CdS films upon thermal annealing, *J. Luminescence* **146** (2014) 109–113.
111. E. Fatas, P. Herrasti, Effect of thermal treatment on some properties of electrodeposited CdS thin films, *Mat. Chem. Phys.* **19** (1988) 315–325.
112. N. Maticiuc, N. Spalatu, V. Mikli, J. Hiie, Impact of CdS annealing atmosphere on the performance of CdS–CdTe solar cell, *Appl. Surf. Sci.* **350** (2015) 14–18.
113. M. Kaur, A. Gopal, R.M. Davis, J.R. Heflin, Concentration gradient P3OT/PCBM photovoltaic devices fabricated by thermal interdiffusion of separately spin-cast organic layers, *Sol. Energy Mater. Sol. Cells* **93** (2009) 1779–1784.
114. M.C. Arenas, N. Mendoza, H. Cortina, M.E. Nicho, H. Hu, Influence of poly3-octylthiophene (P3OT) film thickness and preparation method on photovoltaic performance of hybrid ITO/CdS/P3OT/Au solar cells, *Sol. Energ. Mater. Sol. Cells* **94** (2010) 29–33.
115. B. Garcia, D. Belanger, Electrochemical preparation and characterization of polypyrrole doped with bis(trifluoromethanesulfone) imide anions, *Synthetic Metals* **98** (1998) 135–141.
116. J.I. Martins, S.C. Costa, M. Bazzaoui, G. Goncalves, E. Fortunato, R. Martins, Electrodeposition of polypyrrole on aluminium in aqueous tartaric solution, *Electrochim. Acta* **51** (2006) 5802–5810.
117. S. Skaarup, L. Bay, K. Vidanapathirana, S. Thybo, P. Tofte, K. West, Simultaneous anion and cation mobility in polypyrrole, *Solid State Ionics* **159** (2003) 143–147.
118. S. Asavapiriyant, G.K. Chandler, G.A. Gunawardena, D. Pletcher, The electrodeposition of polypyrrole films from aqueous solutions, *J. Electroanal. Chem.* **117** (1984) 229–244.
119. A. Bhattacharya, A. De, S. Dast, Electrochemical preparation and study of transport properties of polypyrrole doped with unsaturated organic sulfonates, *Polymer* **37** (1996) 4375–4382.
120. P. Wang, Y. Li, Electrochemical and electrocatalytic properties of polypyrrole film doped with heteropolyanions, *J. Electroanal. Chem.* **408** (1996) 77–81.
121. Handbook of conducting polymers. 2nd ed., rev. and expanded. c1998, edited by Terje A. Skotheim and John R. Reynolds, Taylor & Francis Group, LLC., 2007.
122. T. V. Vernitskaya, O. N. Efimov, Polypyrrole: a conducting polymer; its synthesis, properties and applications, *Russ. Chem. Rev.* **66** (1997) 443–457.

123. T.-H. Le, Y. Kim, H. Yoon, Electrical and Electrochemical Properties of Conducting Polymers, *Polymers* **9** (2017) 150.
124. E. Beelen, J. Riga, J.J. Verbist, Electrochemical doping of polypyrrole: XPS study, *Synthetic Metals* **41-43** (1991) 449–454.
125. K. West, T. Jacobsen, B. Zachau-Christiansen, M.A. Careem, S. Skaarup, Electrochemical synthesis of polypyrrole: Influence of current density on structure, *Synthetic Metals* **55-57** (1993) 1412–1417.
126. H. Yoneyama, K. Wakamoto, H. Tamura, Photo-assisted electrochromic behavior of polyaniline and polypyrrole films coated on platinized n-type silicon, *Mater. Chem. Phys.* **15** (1986) 567–575.
127. C. Janákya, K. Rajeshwar, The role of (photo)electrochemistry in the rational design of hybrid conducting polymer/semiconductor assemblies: From fundamental concepts to practical applications, *Progress in Polymer Sci.* **43** (2015) 96–135.
128. Z.-D. Ni, Y.-T. Song, H.-Q. Chen, L.-Y. Lin, UV Light-assisted Electropolymerization of Pyrrole on TiO₂ for Supercapacitors: Investigating the Role of TiO₂, *Electrochim. Acta* **190** (2016) 313–321.
129. A. Jarkov, S. Bereznev, O. Volobujeva, R. Traksmaa, A. Tverjanovich, A. Öpik, E. Mellikov, Photo-assisted electrodeposition of polypyrrole back contact to CdS/CdTe solar cell structures, *Thin Solid Films* **535** (2013) 198–201.
130. R. Singh, A.K. Narula, R.P. Tandon, S.U.M. Rao, V.S. Panwar, A. Mansingh, S. Chandra, Growth kinetics of polypyrrole, poly (N-methyl pyrrole) and their copolymer, poly (N-methyl pyrrole-pyrrole): effect of annealing on conductivity and surface structure, *Synthetic Metals* **79** (1996) 1–6.
131. R. Ansari, G.G. Wallace, Effect of thermal treatment on the electrochemical properties of conducting polypyrrole polymers, *Polymer* **35** (1994) 2372–2377.
132. V.-T. Truong, B. C. Emus, M. Forsyth, Ion exchange, anisotropic structure and thermal stability of polypyrrole films, *Synthetic Metals* **69** (1995) 479–480.
133. R. Saxena, K. Sharma, N.S. Saxena, T.P. Sharma, Effect of Annealing on Structural and Optical Properties of Polypyrrole Doped With Different Acids, *Polymer Composites* **30** (2009) 820–826.
134. H. Sowa, *Solid State Sci.* **7** (2005) 1384.
135. D.R. McCann, L. Cartz, *J. Appl. Phys.* **43** (1972) 4473.
136. V.M. Goldschmidt Skr. Nor. Vidensk.-Akad., Kl. 1: Mat.-Naturvidensk. K 1.9, 1926.
137. Lai, F. Liu, J. Li, Z. Zhang, Y. Liu, Nucleation and growth of selenium electrodeposition onto tin oxide electrode, *J. Electroanal. Chem.* **639** (2010) 187–192.
138. H. Majidi, J.B. Baxter, Electrodeposition of CdSe coatings on ZnO nanowire arrays for extremely thin absorber solar cells, *Electrochim. Acta* **56** (2011) 2703–2711.

139. G. Pilania, T. Sadowski, R. Ramprasad, Oxygen Adsorption on CdSe Surfaces: Case Study of Asymmetric Anisotropic Growth through ab Initio Computations, *J. Phys. Chem. C* **113** (2009) 1863–1871.
140. M.T.S. Nair, P.K. Nair, R.A. Zingaro, E.A. Meyers, Enhancement of photosensitivity in chemically deposited CdSe thin films by air annealing, *J. Appl. Phys.* **74** (1993) 1879.
141. K.E. Murphy, B.B. Wunderlich, B. Wunderlich, Effect of Structure on the Electrical Conductivity of Selenium, *J. Phys. Chem.* **86** (1982) 2827–2835.
142. Editors: D. Abou-Ras, T. Kirchartz, U. Rau, Advanced Characterization Techniques for Thin Film Solar Cells, Wiley-VCH Verlag GmbH & Co. KGaA., 2016.
143. E. Belandria, Ch. Power, J. Marquina, J. Gonzalez, E. Flahaut, Raman scattering on DWCNT filled with 1D CdSe nanowire, *Revista mexicana de fisica S* **53** (7) 182–184.
144. S. Mahato, A.K. Kar, The effect of annealing on structural, optical and photosensitive properties of electrodeposited cadmium selenide thin films, *J. Sci.: Adv. Mater. Devices 2* (2017) 165–171.
145. M.S. Al-Kotb, J.Z. Al-Waheidi, M.F. Kotkata, Investigation on microstructural and optical properties of nano-crystalline CdSe thin films, *Thin Solid Films* **631** (2017) 219–226.
146. M. Aliofkhaeaei, Nanocoatings: Size Effect in Nanostructured Films, Springer-Verlag Berlin Heidelberg, 2011.
147. Editor-in-Chief: D.R. Lide, CRC Handbook of Chemistry and Physics, 78th edition, CRC Press LLC, 1997.
148. <http://periodictable.com/Properties/A/ElectricalConductivity.an.html>
149. J.F. McCann, M. Skylas-Kazacos, The electrochemical deposition and formation of cadmium sulphide thin film electrodes in aqueous electrolytes, *J. Electroanal. Chem.* **119** (1981) 409–412.
150. J. Singh, Semiconductor optoelectronics: Physics and Technology, New York, McGraw-Hill, Inc., 1995.
151. A. Gichuhi, B.E. Boone, C. Shannon, Resonance Raman scattering and scanning tunneling spectroscopy of CdS thin films grown by electrochemical atomic layer epitaxy—thickness dependent phonon and electronic properties, *J. Electroanal. Chem.* **522** (2002) 21–25.
152. S.N. Yannopoulos, K.S. Andrikopoulos, Raman Scattering study on a structural and dynamical features of noncrystalline selenium, *J. Chem. Phys.* **121** (2004) 4747–4758.
153. G.C. Morris, R. Vanderveen, Cadmium sulphide films prepared by pulsed electrodeposition, *Sol. Energ. Mater. Sol. Cells* **27** (1992) 305–319.
154. J. Nishino, S. Chatani, Y. Uotani, Y. Nosaka, Electrodeposition method for controlled formation of CdS films from aqueous solutions, *J. Electroanal. Chem.* **473** (1999) 217–222.
155. L. Huang, Z.L. Wei, F.M. Zhang, X.S. Wu, Electronic and optical properties of CdS films deposited by Evaporation, *J. Alloys Compd.* **648** (2015) 591–594.

156. H.Gerischer, Photoassisted interfacial electron transfer, *Surf. Sci.* **101** (1980) 518–530.
157. C. Liu, J. Chen, H. Che, K. Huang, P.A. Charpentier, W.Z. Xu, W. Shi, H.J. Dong, Construction and enhanced photocatalytic activities of a hydrogenated TiO₂ nanobelt coated with CDs/MoS₂ nanosheets, *RSC Adv.* **7** (2017) 8429–8442.
158. K.J. Siemsen, H.D. Riccius, Infrared photoconductivity of polycrystalline selenium, *Solid State Commun.* **11** (1972) 1379–1383.
159. M. Wright, A. Uddin, Organic—inorganic hybrid solar cells: A comparative review, *Sol. Energy Mater. Sol. Cells* **107** (2012) 87–111.
160. A.P. Samantilleke, M.F.Cerqueira, B.Mari, Segregation of Te at the back contact in electrochemically deposited CdTe thin film solar cells, *J. Crystal Growth* **320** (2011) 13–17.
161. http://sites.chem.colostate.edu/diverdi/all_courses/CRC%20reference%20data/electrochemical%20series.pdf

ACKNOWLEDGEMENTS

This thesis is based on the experimental work carried out at the Department of Materials Science (now the Department of Materials and Environmental technology), Tallinn University of Technology.

I would like to thank Prof. Enn Mellikov and Prof. Andres Öpik for giving me the opportunity to join and work in the research group at the Department of Materials Science and to participate actively in the Doctoral School.

I wish to thank Dr. Malle Krunks, Head of the Department of Materials and Environmental Technology, for giving me the possibility to carry out this doctoral thesis, for useful remarks and discussions.

I sincerely appreciate the guidance, support and motivation of my supervisors Dr. Julia Kois, Dr. Sergei Bereznev and Dr. Natalia Maticiuc. During these years, they also gave me opportunity to attend conferences and other meetings concerning my PhD topic that gave me additional experience, extending my knowledge and also in establishing valuable collaborations with partner institutes abroad.

This work could not be completed without great support and advice of my colleagues and friends: Dr. Revathi Naidu, MSc Denisa Dosenovicova, PhD students Anna Kidakova, Inga Gromõko and Svetlana Polivtseva.

I am thankful for useful discussions with Dr. Mare Altosaar, Dr. Atanas Katerski, Dr. Jaan Hiie, Dr. Juri Krustok, Dr. Nicolae Spalatu, for SEM and EDX studies held by Dr. Olga Volobujeva and Dr. Valdek Mikli.

I thank all the colleagues from the Laboratory of Photovoltaic Materials and their leader Dr. Marit Kauk-Kuusik, from the Laboratory of Optoelectronic Materials Physics and their leader Dr. Maarja Grossberg, and from the Laboratory of Thin Film Chemical Technologies and their leader Dr. Ilona Oja Acik.

This work was financially supported by the institutional research funding IUT19-28 and IUT19-4 and Grants SF0140099s08 and SF0140033s12 of the Estonian Ministry of Education and Research, the Estonian Science Foundation G8655 and G8714, the Archimedes Project “New materials for solar energetics” code 3.2.0501.10.0014, the European Union through the European Regional Development Fund, Project TK141, by ERA.NET RUS PLUS Project Flexapp (ETAG15028), the University Base finance B54, PUT1495 Project and European Social Fund’s Doctoral Studies and Internationalisation Programme DoRa, which is carried out by Foundation Archimedes. This work has been partially supported by ASTRA “TUT Institutional Development Program for 2016-2022” Graduate School of Functional Materials and Technologies (2014-2020.4.01.16-0032).

My profound gratitude I express to my family, my husband Anatoly, parents Irina and Arkadi, and sisters Svetlana and Tatjana, for their unconditional belief and support.

Jelena Maricheva

ABSTRACT

Cd-chalcogenide compounds have been shown as suitable candidates for second- and third-generation photovoltaics. The emerging interest in the third-generation solar cell (SC) devices is due to the developing technologies in the field of materials research towards low-cost and highly efficient devices. One of the promising concepts is a nanostructured hybrid SC, which combines the advantages of inorganic and organic materials accompanied with a highly active interface area. A highly developed surface area of the heterojunction is beneficial in terms of higher fraction of generated electron-hole pairs. Inorganic semiconductors as well as conducting polymers can be synthesized by a cost-effective and relatively simple method as electrodeposition. This technique allows deposition of self-assembled nanostructured Cd-chalcogenide films, which can be used as a matrix for nanostructured hybrid SCs. Furthermore, on all-electrodeposited hybrid structures there are few or no publications.

The aim of this dissertation was to study the nucleation and growth mechanisms of CdS and CdSe compounds during the electrodeposition process and to investigate the influence of H_2SeO_3 microadditive on the electrodeposition of CdS, in order to apply electrodeposited films as a matrix for all-electrodeposited nanostructured hybrid SC.

This thesis is based on six publications and is divided into three Chapters. Following the Introduction, Chapter 1 includes a literature overview on the main properties of CdS, CdSe, and CdTe, and possible applications of these materials including third-generation SCs and electrochemistry of binary Cd-chalcogenides. Chapter 2 describes the experimental details of the synthesis, post-deposition treatment, and characterization of the obtained CdSe and CdS films, as well as the fabrication of hybrid SCs based on nanofibrous CdSe films. Chapter 3 is divided into four sections, which include the results and discussion on the electrochemical growth mechanisms of thin and nanostructured CdSe films as well as CdS films. CdS films were obtained without and in the presence of H_2SeO_3 microadditive, followed by the application of these electrodeposited films in hybrid SCs.

CdSe and CdS films were electrodeposited from acidic aqueous electrolyte solutions. Variables such as concentrations of reagents, pH, and temperature were varied in order to determine the appropriate conditions for stoichiometric film formation. We also determined the conditions for the synthesis of nanostructured CdSe films. As-electrodeposited CdSe films were annealed in air at temperatures from 250 °C to 410 °C. The growth of near-stoichiometric CdS at 50 °C was improved by addition of H_2SeO_3 microadditive. As-deposited CdS films were annealed in vacuum at 120 °C.

Prior to electrodeposition, electrochemical systems were analyzed by cyclic voltammetry to determine the possible electrochemical reactions and choose the potential for film deposition. Based on the data obtained from the cyclic voltammetry and thermodynamic data, we proposed the mechanisms for CdSe thin and nanostructured film formation as well as for CdS film formation without

and in the presence of H_2SeO_3 . We showed that for both CdSe and CdS, the formation of Se nuclei is growth defining.

CdSe nanohorn or nanofibrous films arrange as a result of exceeding the concentration of Se^0 species at the electrode/electrolyte interface. The initial diameter of a nanohorn or a nanofiber is determined by the diameter of the Se nucleus, which in the case of a nanohorn, decreases in the vertical direction during the deposition process. According to a morphological study performed using a high-resolution scanning electron microscope, nanohorns have a diameter of ~ 200 nm at the base and 30 nm on the top, while nanofibers have a uniform diameter of 40–85 nm. According to an energy dispersive X-ray spectroscopy, stoichiometric CdSe films can be deposited at H_2SeO_3 equal to or less than 5×10^{-4} M and exceeding the concentration of CdCl_2 . The optical properties were characterized by UV-Vis spectroscopy. Air annealing of CdSe nanofibers promotes the transition of the mixed-phase crystalline structure to a more stable hexagonal one.

The morphology of CdS films electrodeposited from an initial solution at 50°C and pH of 3.5 is non-continuous with islands of ~ 200 nm in diameter; however, an addition of 10^{-5} M H_2SeO_3 improves the coverage and decreases the film thickness two times. When depositing CdS at 50°C , stoichiometric films can be obtained only in the presence of a H_2SeO_3 additive. The presence of Se secondary phase in as-deposited CdS films was also confirmed by scanning Kelvin probe measurements and X-ray diffraction. Nevertheless, stoichiometry of the films was improved by annealing. A transition of the mixed-phase to hexagonal structure was observed for CdS electrodeposited in the presence of 5×10^{-5} M concentration of H_2SeO_3 .

Finally, electrodeposited nanofibrous CdSe films were applied as matrix in the initial hybrid SCs separately and as a bilayer structure with electrodeposited CdS and CdTe. The hybrid glass/ITO/CdSe/P3OT:PCBM/graphite structure showed diodic behavior and photosensitivity but with relatively low photocurrent value. In order to improve the insufficient absorption, a CdSe-core/CdTe-shell structure was fabricated. This helped to slightly improve the open circuit voltage (V_{oc}), short circuit current (J_{sc}) and fill factor; however, the values stayed below those of an efficient SC grade. Taking into account interface problems or possible high recombination losses electrodeposited PPy/CdSe/CdS structure was implemented. The fabricated electrodeposited hybrid glass/ITO/CdS/CdSe/PPy/graphite SC showed a maximal J_{sc} value of $2.6 \text{ mA}\cdot\text{cm}^{-2}$ but with reduced V_{oc} . The results show a potential of electrodeposited nanostructured CdSe films for application in hybrid SCs; however, further optimization of the fabrication conditions is necessary.

KOKKUVÕTE

Kaadmiumi (Cd) kalkogeniide kasutatakse laialdaselt teise ja kolmanda põlvkonna päikesepatareides, mille vastu on tekkinud huvi tänu vajadusele valmistada odavaid ning efektiivseid seadmeid. Nanostruktuurne hübriidne päikesepatarei on lootustandev kontseptsioon, milles kasutatakse koos anorgaanilisi ja orgaanilisi materjale. Hübriid-päikesepatareide tehnoloogia eeliseks on lihtsalt valmistatavate odavate ning suure absorptsioonikoefitsiendiga polümeeride ja kõrge stabiilsusega anorgaaniliste materjalide ühendamine. Nanostruktuursete kilede kasutamine võimaldab suurendada *p-n* ülemineku pindala. Nii anorgaanilisi pooljuhte kui ka juhtivaid polümeere on võimalik sünteesida kasutades odavat ja suhteliselt lihtsat elektrokeemilise sadestuse meetodit. Lisaks on antud meetodiga võimalik valmistada ise-organiseeruvaid nanostruktuurseid Cd-kalkogeniide, mida saab kasutada maatriksina nanostruktuursetes hübriid-päikesepatareides. Hübriid-päikesepatareide saamise tehnoloogia, kus kõik kihid on elektrokeemiliselt sadestatud, on aktuaalne ja pakub huvi, kuna informatsiooni sellel teemal on vähe.

Antud doktoritöö eesmärgiks oli uurida elektrokeemilisel sadestamisel kaadmiumsulfiidi (CdS) ja kaadmiumseleniidi (CdSe) kilede idumoodustumise ning kasvu mehhanisme, leida nanostruktuurse CdSe kasvu tingimusi ning uurida seleenishappe (H_2SeO_3) lisandi mõju CdS sadestamisele. Lisaks kasutati elektrokeemiliselt sadestatud nanostruktuurseid Cd-kalkogeniid kilesid funktsionaalsete materjalidena hübriid-päikesepatareides.

Käesolev töö baseerub kuuel publikatsioonil ning on jagatud kolmeks peatükiks. Sissejuhatusele järgnev esimene peatükk on kirjandusülevaade, milles käsitletakse CdS, CdSe ja CdTe peamisi omadusi ning rakendusi teise ja kolmanda põlvkonna päikeseelementides. Lisaks kirjeldatakse Cd-kalkogeniidide ja polümeeride elektrokeemilise sadestuse põhialuseid. Teises peatükis antakse ülevaade eksperimentaalsest katsekorraldusest õhukeste kilede elektrokeemiliseks sadestamiseks, kuumutamiseks, päikeselementide valmistamiseks ning karakteriseerimismeetoditest. Kolmas peatükk on jaotatud neljaks alapeatükiks ning sisaldab eksperimentaalsete tulemuste analüüsi, CdS ning CdSe kilede kasvumehhanismide kirjeldust ning nende rakendamist hübriidsetes fotovolt-struktuurides.

Antud uurimustöös sadestati CdSe ning CdS kiled elektrokeemiliselt happelises vesilahuses. Varieeriti reagentide kontsentratsiooni, pH väärtust ja sadestustemperatuuri, et leida sobivad parameetrid stõhhiomeetriliste kilede elektrokeemiliseks sadestamiseks. Lisaks leiti tingimused nanostruktuursete CdSe kilede sadestamiseks. CdSe kilesid lõõmutati õhu käes erinevatel temperatuuridel 250 °C-st kuni 410 °C-ni. Seleenishappe lisamisega lahusele leiti võimalus CdS kilede elektrokeemiliseks sadestamiseks 50 °C juures. Uuriti vaakumis 120 °C juures lõõmutamise mõju CdS kilede koostisele. Kilede struktuurilisi omadusi ja faasikoostist uuriti XRD ning Raman spektroskoopia abil ning optilisi omadusi uuriti kasutades UV-Vis spektroskoopiat.

Võimalike elektrokeemiliste reaktsioonide määramiseks ning sadestuspotsiaali valimiseks kasutati elektrokeemiliste süsteemide analüüsimeetodit - tsüklilist voltamperomeetria. Tsüklilise voltamperomeetria ning termodünaamiliste andmete põhjal kirjeldati CdSe ja CdS elektrokeemilise sadestamise mehhanisme. Näidati, et mõlema materjali puhul kasvavate kilede morfoloogia on määratud seleeni idutsentrite tekke poolt. CdSe nanosarve või nanokiu kujulised struktuurid moodustuvad, kui on Se^0 ülekontsentratsioon elektroodi/lahuse piirpinnal. Nanosarve või nanokiu algdiameeter sõltus seleeni idutsentri suuruselt. Vastavalt SEM uuringutele leiti, et nanosarvede diameeter alumises osas on ~200 nm ning tipus ~30 nm. Nanokiudude diameeter varieerub 40 nm ja 85 nm vahel. Leiti, et CdSe nanokiudude kuumutamisel 250 °C juures toimub diameetri vähenemine ilma kokkupaakumiseta ja mitmefaasilise struktuuri üleminek heksagonaalseks. Sarnane kristallstruktuuri muutus toimub ka CdS kiledes, mis sadestati H_2SeO_3 kontsentratsioonil 5×10^{-5} M.

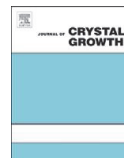
Leiti, et CdS kihtide sadestamisel 50 °C juures lahusest, mille pH on 3.5, moodustuvad pideva kile asemel CdS-di saarekesed, mille teket ja kuju on võimalik juhtida seleenishappe lisamisega lahusele. Lisades 10^{-5} M seleenishappe kontsentratsiooni, sadestub õhem CdS kile, mis katab aluse ühtlaselt. Seleenishappe lisandi kasutamine võimaldab sadestada stöhhiomeetria-lähedase koostisega CdS kilesid 50 °C juures. XRD analüüs näitas, et CdS kiled sisaldavad elementaarse Se faasi, mille eemaldati sadestusjärgse kuumutamisega vaakumis 120 °C juures.

Elektrokeemiliselt sadestatud nanostruktuurseid CdSe kilesid rakendati hübriid-päikesepatareides nii ühe kui ka kahekihilise struktuurina koos elektrokeemiliselt sadestatud CdS-i ja CdTe-ga. Päikesepatarei voolu-pinge kõverad näitasid, et klaas/ITO/CdSe/P3OT:PCBM/grafiit fotovolt-struktuuril on diodi omadused, kuid madalate fotovolt-parameetritega. Antud struktuurile lisati CdTe kiht CdSe peale, et parandada valguse absorptsiooni. Täiendatud struktuuri fotovolt-parameetrid paranesid, kuid nende väärtused on madalad efektiivsete päikesepatareide jaoks. Madalad fotovolt parameetrite väärtused võivad olla põhjustatud piirpinna kontaktprobleemide või laengukandjate suure rekombinatsioonikao tõttu. Arvestades saadud tulemusi, valmistati elektrokeemiliselt sadestatud PPy/CdSe/CdS struktuur ITO/klaas alusele. Saadud klaas/ITO/CdS/CdSe/PPy/grafiit päikesepatarei lühisvoolu väärtus on $2.6 \text{ mA} \cdot \text{cm}^{-2}$, kuid avatud vooluahela pinge on 95 mV. Tulemused näitavad, et elektrokeemiliselt sadestatud nanostruktuurseid CdSe kilesid võib kasutada hübriid-päikesepatareides, kuid paremate tulemuste saavutamiseks peab selliste struktuuride valmistamise tehnoloogiat optimeerima ning täiustama.

APPENDIX A

Paper I

J. Kois, S. Bereznev, O. Volobujeva, **J. Gurevits**, E. Mellikov, Electrocrystallization of CdSe from aqueous electrolytes: Structural arrangement from thin films to self-assembled nanowires, *J. Cryst. Growth* 320 (2011) 9–12.



Electrocrystallization of CdSe from aqueous electrolytes: Structural arrangement from thin films to self-assembled nanowires

Julia Kois*, Sergei Bereznev, Olga Volobujeva, Jelena Gurevits, Enn Mellikov

Tallinn University of Technology, Department of Material Science, Ehitajate tee 5, 19086 Tallinn, Estonia

ARTICLE INFO

Available online 5 January 2011

Keywords:

A1. Nanowires
A1. Thin films
A3. Electrochemical deposition
B1. Cadmium selenide

ABSTRACT

In the present paper, the method of electrochemical deposition was employed for the growth of CdSe structures with various morphologies from thin film to self-assembled crystalline nanowires. CdSe films electrodeposited from aqueous solutions on indium tin oxide (ITO) coated glass substrates were characterized for their structural, morphological, compositional and electrochemical properties. Influence of composition of electrolyte, pH and deposition time on composition, morphology and crystallinity of the deposited films was studied. The scanning electron microscopy (SEM) study of CdSe structures shows the difference of the morphology from thin films and spherical grains to 200 nm-long self-assembled nanowires depending on conditions of the deposition.

© 2011 Elsevier B.V. All rights reserved.

1. Introduction

In recent years, many studies have focused on the investigation of chemical/electrochemical synthesis of CdSe thin films [1–3], 2D structures [4] and nanostructures including wires [5,6], rods [7] and dots [8].

A wide range of studied experimental conditions was examined in order to determine the best way of electrosynthesis of the material with the proper elemental stoichiometric ratio and of the suitable dimensions. The controllable synthesis of thin films was achieved by deposition from aqueous [2,4,9], so organic solutions [1,3], changing the species and concentrations of the reducing agents, the reduction potential and the reaction temperature.

The formation of 2D microstructures was achieved by cathodic electrodeposition of CdSe on different type of templates [4,10] and membranes [13,11]. The interesting investigations on formation of self-assembled nanorods, nanowires and nanotubes were recently presented in several works [5–7].

The present work continues an investigation on electrocrystallization of CdSe with various morphology structures from thin film to self-assembled crystalline nanowires. The electrochemical deposition was provided in aqueous acidic medium, at room temperatures. The influence of the electrodeposition parameters on chemical composition and structural characteristics of the deposited CdSe were investigated.

2. Experimental

The CdSe thin films were electrodeposited on indium tin oxide (ITO) coated glass substrates from aqueous electrolytic bath containing 1–200 mM CdSO₄ and 0.25–20 mM H₂SeO₃. The electrodeposition process was carried out in standard three-electrode electrochemical cell equipped with a platinum wire as the counter electrode and Ag/AgCl 3 M KCl reference electrode. Voltalab PGZ100 potentiostat/galvanostat was applied for the voltammetry and the electrodeposition of CdSe thin film. The synthesis was carried out on the substrate area around 1.5 cm² at potentiostatic regime at room temperature without stirring. The pH value of the solution was around 2, adjusted by hydrochloric acid.

The morphology of deposited films was studied by using a high-resolution scanning electron microscope (SEM) Zeiss ULTRA 55. The chemical composition and the distribution of components on the specimen surface was determined by using energy dispersive X-ray analysis (EDX) system of Röntex.

The UV–Vis transmission and reflection spectra have been taken with a spectro 320 R5 apparatus (Instrument Systems GmbH) equipped with integrating sphere in the wavelength region from 250 to 1400 nm. The thickness and refractive indices values were obtained using specular reflectance measurements recorded on Filmetrics F20 using Cauchy fitting method. Cross-section SEM micrographs from selected samples were also used to evaluate the film's thickness.

3. Results and discussion

According to previous works [12–14] CdSe electrodeposition process is controlled by selenium species diffusion at the

* Corresponding author. Tel.: +372 6203367.
E-mail address: julia@staff.ttu.ee (J. Kois).

cathode/electrolyte interface. The growth mechanism of CdSe films in acidic media could be described as follows.

On reduction of H_2SeO_3 ,



and formation of CdSe takes place according to the chemical reaction,



In our first experiments, CdSe was electrodeposited from aqueous solutions with $\text{pH}=2$ at room temperature for 15 min. The films were grown at the optimized deposition potential of -700 mV with respect to Ag/AgCl. The concentrations of reactants were varied to optimize the electrochemical conditions for the growth the stoichiometric CdSe films.

The composition and the thickness of deposited films depend on the concentration of selenium in solution as it is shown in Figs. 1 and 2. For deposition from solution with high concentration of H_2SeO_3 (> 1 mM) it was revealed that the thickness and the ratio of Se to Cd in deposited films grows proportionally to the concentration of H_2SeO_3 in solution. Those dependences could be attributed to that the rate of deposition and is limited by the diffusion of selenium species to cathode. From solution with high Cd^{2+} concentration, the thinner and more stoichiometric CdSe films were deposited.

The dependence of thickness and composition of deposited CdSe films was not observed for solutions with low selenium content (< 1 mM H_2SeO_3). Regardless of the concentration of Cd

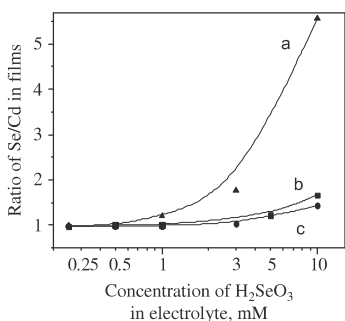


Fig. 1. Chemical composition of CdSe thin films vs. concentration of H_2SeO_3 in electrolyte. Concentration of CdSO_4 is: (a) 10 mM, (b) 25 mM and (c) 100 mM. Deposition time is 15 min.

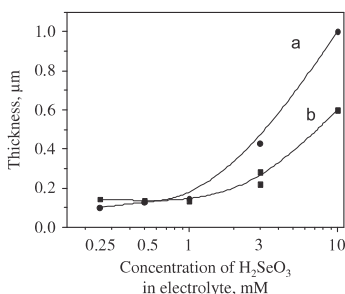


Fig. 2. Thickness of CdSe thin films vs. concentration of H_2SeO_3 in electrolyte. Concentration of CdSO_4 is: (a) 10 mM and (b) 100 mM. Deposition time is 15 min.

and Se in electrolytes, deposited films have near stoichiometric composition (around 50 at% Se, 50 at% Cd). All films show uniform compact polycrystalline morphology with thickness about 120 nm, as seen in Figs. 3a, 4a and 5a. Under this condition of electrodeposition, all Se atoms precipitated at the surface of cathode (1) reduce to H_2Se (2) and then react with Cd^{2+} and form CdSe colloidal particles. The new formed CdSe particles could be charged and hardly precipitate on ITO surface.

Fig. 3 shows SEM images of thin films deposited from aqueous solution containing high Cd^{2+} concentration (100 mM) and various concentrations of H_2SeO_3 under potential of -700 mV for 15 min. The surface morphology of the CdSe films deposited from 0.25 to 0.5 mM H_2SeO_3 shows compact polycrystalline films, as seen in Fig. 3a. The grains look like a lentil with grain size about 20 nm. The grains are packed very compact and form thin film with thickness about 100–120 nm.

XRD patterns of CdSe structures are shown in Fig. 4. Fig. 4a–c shows the XRD patterns of the products with thin compact polycrystalline films. All the XRD patterns of the films in Fig. 4c correspond to a zinc-blende crystal structure.

When 1 mM H_2SeO_3 solutions were used, white round drops and multi-foots rod crystals were formed on the layer of polycrystalline film (Fig. 3b). Both drop and multi-foots rod could form on the same substrate. White drops content containing excess of Se (70 at% Se, 30 at% Cd) and their formation could be attributed to the H_2Se reaction with selenous acid to form

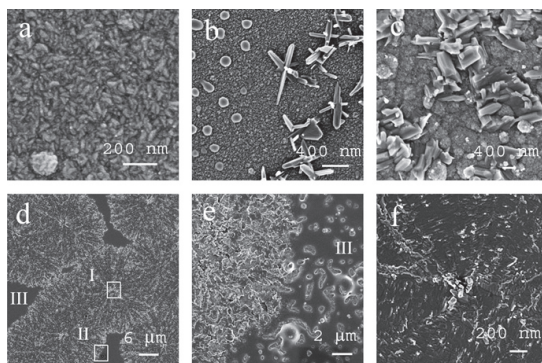


Fig. 3. SEM images of CdSe films deposited from solution contained 100 mM CdSO_4 and H_2SeO_3 (a) 0.5 mM, (b) 1 mM, (c) 3 mM and (d–f) 10 mM H_2SeO_3 for 15 min. Zone I on (d) corresponds to image in (f). Zone II on (d) corresponds to image in (e). Zone III in (d) and (e) is Se-rich films.

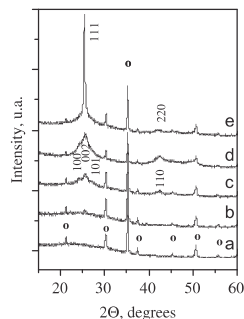


Fig. 4. X-ray diffraction pattern of CdSe films deposited for 15 min from solution contained 100 mM CdSO_4 and (a) 0.25 mM, (b) 0.5 mM, (c) 1 mM, (d) 3 mM and (e) 10 mM H_2SeO_3 . Circles indicate contributions of ITO substrate.

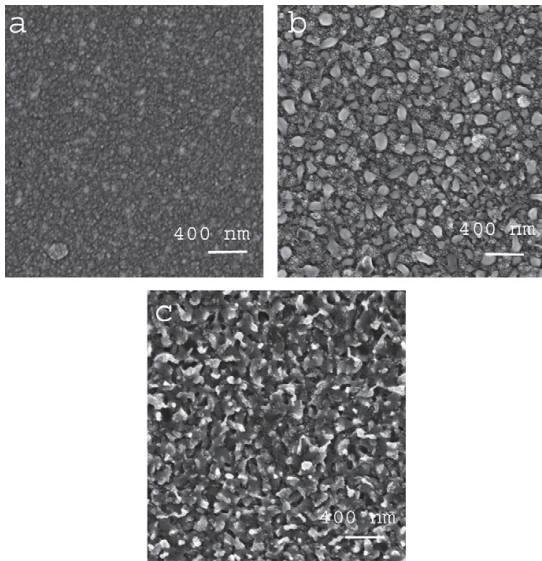


Fig. 5. SEM images of CdSe films deposited from solution contained 25 mM CdSO₄ and H₂SeO₃ (a) 0.5 mM, (b) 1 mM and (c) 5 mM for 15 min.

elemental Se. This result is similar to results described in [15]. The amorphous Se-rich film (Zone III in Fig. 3c and d) forms on the bottom polycrystalline layer when the rate of deposition of Se (1) exceeds the rate of reduction of Se (2).

Multi-foots rods consist of four or more arms and correspond to the formation of the wurtzite structure of CdSe (Fig. 4c–e). The rod-like crystals (diameter of the rod is 50 nm) formed from the center area of the nuclei (Zone I in Fig. 3c and d) and grow at amorphous Se-rich regions forming large round conglomerates (with diameter for 20 μm).

As XRD and SEM measurements are shown, films deposited from low Cd²⁺ solutions could be slightly Se-rich and show more amorphous morphology. Figs. 5 and 6 show SEM images of films deposited from 25 mM CdSO₄ and 10 mM CdSO₄ solution. The bottom of polycrystalline film is formed from round grains and covered by amorphous drops. With increase in the content of Se in solution, Se-rich drops have tendency grow to “islands” and cover the bottom polycrystalline film and growing to branched structures in further (Fig. 6d). The size and the density of distribution of Se-rich drops depend on the concentration of electrolyte. The Se-rich drops are seeds for growing Se-rich films (Fig. 6c) or CdSe nanowires (Fig. 5c).

In order to investigate the formation mechanism of the wires, the films obtained at different growth stages were analyzed. Fig. 7 shows the CdSe films prepared at four different deposition times: 7, 10, 15 and 25 min.

During the initial stages of growth, thin polycrystalline films from densely packed, uniformly distributed nanograins were formed. Next step was formation over the surface of polycrystalline films spherical Se-rich drops of 30–40 nm in diameter (Fig. 7a).

The SEM images of CdSe films deposited for 10 min show a vermiculated structure (Fig. 7b). For 15 min deposition forming rods (in length 50 nm and diameter 20 nm) on vermiculated structure are clearly visible (Fig. 7c). CdSe deposited for 25 min is made of nanowires with 200–300 nm in length and 20–40 nm in diameters randomly distributed over the substrate surface (Fig. 7d).

It is also observed that both diameter and length of the CdSe nanowires increase with respect to the deposition time, indicating

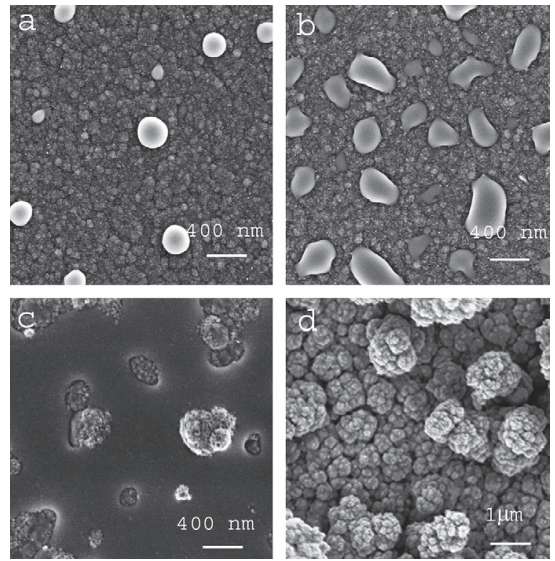


Fig. 6. SEM images of CdSe thin films prepared from solution contained 10 mM CdSO₄ and H₂SeO₃ (a) 0.25 mM, (b) 0.5 mM, (c) 1 mM deposited for 15 min and (d) 1 mM H₂SeO₃ deposited for 30 min.

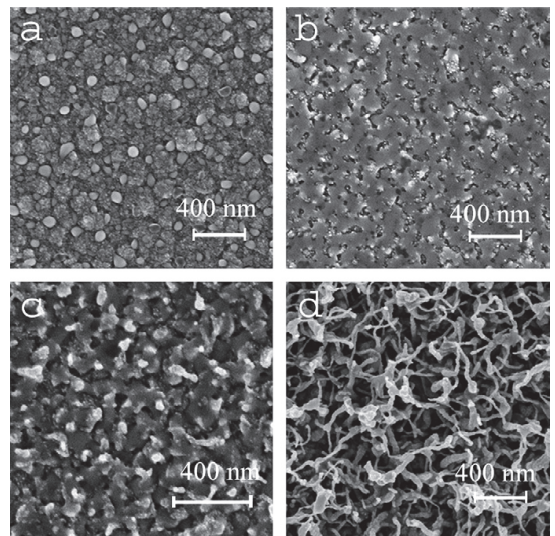


Fig. 7. SEM images of CdSe films deposited from solution contained 25 mM CdSO₄ and 5 mM H₂SeO₃ for (a) 7 min, (b) 10 min, (c) 15 min and (d) 25 min.

that the surface morphology of the CdSe films is strongly correlated with the amount of CdSe deposited.

Thus, the preparation of morphologically and crystal phase controlled CdSe thin films and nanowire structures by electro-deposition from aqueous solutions without any surfactants has been achieved.

Fig. 8 illustrates the growth process of thin polycrystalline films, rods, nanowires and branched structures from solutions with different concentration of active components. The inserted

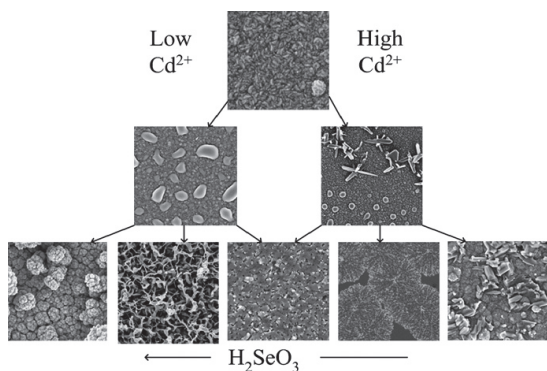


Fig. 8. The growth of thin film structures depending on Cd^{2+} and H_2SeO_3 concentration in electrolytic bath. SEM image insets show the products prepared at different stages and concentrations.

SEM images show the morphology of structures formed at -700 mV.

4. Conclusions

In summary, we presented the preparation of stoichiometric CdSe thin films and nanowire structures via direct electrochemical route from aqueous electrolytes. It was observed initially formation of thin polycrystalline films (about 100 nm) from densely packed, uniformly distributed CdSe nanograin. The formation CdSe structure over the surface of polycrystalline film was determined by concentration of selenin species and cadmium ions.

CdSe thin polycrystalline films and rod-like wurtzite crystals formed from solutions with high Cd^{2+} concentration in the solution. From solution with low Cd^{2+} content the CdSe forms nanowire and branched structures. The formation of nanowire from initially amorphous CdSe films was discussed.

Acknowledgements

Our group is grateful to the financial support from the Estonian Ministry of Education and Research under Grant SF0140099s08 and from the Estonian Science Foundation (G7669 and G7595).

References

- [1] K. Premaratne, S.N. Akuranthilaka, I.M. Dharmadasa, A.P. Samantilleka, *Renew. Energy* 29 (2004) 549.
- [2] M. Bouroushian, D. Karoussos, T. Kosanovic, *Solid State Ionics* 177 (2006) 1855.
- [3] J. Datta, C. Bhattacharya, S. Bandyopadhyay, *Appl. Surf. Sci.* 253 (2006) 2289.
- [4] L.K. Teh, V. Furin, A. Martucci, M. Guglielmi, C.C. Wong, F. Romanato, *Thin Solid Films* 515 (2007) 5787.
- [5] S.-K. Min, O.-S. Joo, K.-D. Jung, R.S. Mane, *Electrochem. Commun.* 8 (2006) 223.
- [6] A. Shaikh, R.S. Mane, H.M. Pathan, *J. Electroanal. Chem.* 615 (2008) 175.
- [7] S.-H. Kim, J.-Y. Lee, W.-K. Han, J.-H. Lee, *Thin Solid Films* 518 (2010) 7222.
- [8] S.M. Rabchynski, D.K. Ivanou, E.A. Streltsov, *Electrochem. Commun.* 6 (2004) 1051.
- [9] K. Bieñkowski, M. Strawski, B. Maranowski, M. Szklarczyk, *Electrochim. Acta* (2010) 8908.
- [10] G. Vijaya Prakash, R. Singh, A. Kumar, R.K. Mishra, *Mater. Lett.* 60 (2006) 1744.
- [11] X.S. Peng, J. Zhang, X.F. Wang, Y.W. Wang, L.X. Zhao, G.W. Meng, L.D. Zhang, *Chem. Phys. Lett.* 343 (2001) 470.
- [12] St. Kutzmutz, G. Lång, K.E. Heusler, *Electrochim. Acta* 47 (2001) 955.
- [13] Z. Bouroushian, Loizos, N. Spyrellis, *Appl. Surf. Sci.* 156 (2000) 125.
- [14] C.M. Shen, X.G. Zhang, H.L. Li, *Appl. Surf. Sci.* 240 (2005) 34.
- [15] L. Beaunier, H. Cachet, M. Froment, et al., *J. Electrochem. Soc.* 147 (2000) 1835.

Paper II

J. Kois, **J. Gurevits**, S. Bereznev, O. Volobujeva, A. Öpik, E. Mellikov, CdSe nanofiber and nanohorn structures on ITO substrates fabricated by electrochemical deposition, *Appl. Surf. Sci.* 283 (2013) 982–985.



CdSe nanofiber and nanohorn structures on ITO substrates fabricated by electrochemical deposition



Julia Kois*, Jelena Gurevits, Sergei Bereznev, Olga Volobujeva, Andres Öpik, Enn Mellikov

Department of Materials Science, Tallinn University of Technology, Ehitajate tee 5, 19086 Tallinn, Estonia

ARTICLE INFO

Article history:

Received 8 February 2013

Received in revised form 12 July 2013

Accepted 12 July 2013

Available online 20 July 2013

Keywords:

CdSe

Electrodeposition

Nanofiber

Nanostructure

ABSTRACT

Self assembled 3-D CdSe structures have been successfully electrodeposited from aqueous solutions. Proposed method allows a control of self-assembled nanostructures formation with a different morphology by varying the composition of the electrolyte in electrochemical bath. The two types of 3-D nanostructures: CdSe nanofibers (\varnothing 30 nm, length of 1–2 μm) and Se core–CdSe shell nanohorns (\varnothing 200 nm, length of 600 nm) were fabricated and investigated. The possible mechanism of electrochemical formation of CdSe nanofibers and nanohorns has been proposed.

© 2013 Published by Elsevier B.V.

1. Introduction

Nanostructured II–VI CdSe materials have progressively attracted attention for its potential applications in photoelectrochemical solar cells, optoelectronic devices, biosensors, thin film transistors and gamma ray detectors [1–5].

Various methods have been brought forward to the synthesis of CdSe nanostructures e.g. chemical bath deposition, dip-coating, ionic layer adsorption, molecular beam epitaxy and chemical vapour deposition [4,6,7]. As an alternative synthesis technique, electrodeposition is a commercially important process because of its simplicity, low cost as well as possibility for large-scale production.

CdSe compounds have been successfully electrochemically synthesized from aqueous [8–10] and non-aqueous solutions [11,12]. Apart from previous studies, a method for electrochemical deposition of template-free CdSe nanowire structures was developed [8,9,12–14].

However, in order to control the morphology and the roughness of the CdSe electrodeposits, most of these approaches require the presence of special additives in the electrochemical bath and controlling electrical quantities, current density, or deposition potential.

The aim of the present work is to study the electrochemical nucleation and growth mechanism of CdSe nanowires and nanohorns in aqueous solution. The structural, morphological and

optical properties of obtained nanostructures have been studied and discussed.

2. Experimental

A potentiostat/galvanostat Voltalab PGZ100 was applied for a voltamperometric measurement and an electrodeposition of CdSe structures. All experiments were carried out in a three-electrode cell with Pt counter electrode and Ag/AgCl/KCl 3 M reference electrode. A working electrode was commercial indium tin oxide (ITO) coated glasses $8 \Omega/\text{cm}^2$. All CdSe structures were electrodeposited potentiostatically under cathodic potential value of $-700 \text{ mV vs. Ag/AgCl}$ at room temperature. For the electrodeposition of CdSe, aqueous solutions containing 25 mM CdCl₂ and 0.5–5 mM H₂SeO₃ with pH of 2.1–2.5 were prepared in 18.2 M Ohm Millipore water.

X-ray diffraction (Rigaku Ultima IV diffractometer with Cu K α radiation ($\lambda = 1.5406 \text{ \AA}$, 40 kV at 40 mA) and the silicon strip detector D/teX Ultra) and an energy dispersive X-ray spectroscopy (EDS, Röntex) were used to investigate a chemical composition of the samples. A high-resolution scanning electron microscope (HR SEM) Zeiss ULTRA 55 was used to characterize a morphology of synthesized samples.

An UV–vis–NIR spectrophotometer (SIMADZU UV-1800) was used to investigate an optical properties of the synthesized nanostructures in the wavelength region from 250 to 1100 nm.

3. Results

In order to investigate the effect of concentration of Cd and Se species on the morphology and particle size, the composition of

* Corresponding author. Tel.: +372 6203367.
E-mail address: julia.kois@ttu.ee (J. Kois).

electrolyte solution was varied, while the other parameters which include pH, applied potential and temperature of deposition were kept constant.

The optimal parameters for electrodeposition of the stoichiometrical CdSe nanostructures with various morphologies from thin film to nanowires have been discussed in our previous work [13,15].

The phase composition and the morphology of CdSe nanostructures induced by a variation concentration of the electrolyte agents are listed in Table 1. The morphological changes of the CdSe films with respect to the electrochemical bath composition were investigated by SEM at Fig. 1. Stoichiometric CdSe thin films with the thickness around 250 nm were electrodeposited from the solution I (Fig. 1a). The obtained CdSe thin film shows nanocrystalline structures with densely packed, uniformly distributed over the surface nanograins (5–10 nm in diameter).

The two types of 3-D CdSe nanostructures: nanohorns and nanofibers were formed by direct electrochemical deposition. Thin fiber-like morphology was observed on the CdSe structures deposited from the solution III (Fig. 1d and g). The cross-sectional image (Fig. 1g) of the films reveals a bottom monolithic CdSe layer of about 150 nm growing on ITO surface. The bottom CdSe layer is covered by winding nanowires with uniform diameter of about 30 nm and length of 1–2 μm . An inner morphology of as-deposited CdSe wires is not clearly seen in the SEM micrographs.

It should be noted that the part of electrodeposited structures were annealed at 200 °C during 1 h. This value of annealing temperature is high enough for an evaporation of an excess of selenium without a recrystallization of CdSe. The CdSe layers annealed at temperature of 200 °C demonstrate shape-tailored porous nanofiber structure (Fig. 1f).

Conical CdSe nanohorns were grown from the solution II as shown in Fig. 1c. Nanohorns have an diameter have about 200 nm at the base and have about 30 nm on the bottom of wire. The length of nanohorns is varied from 300 to 600 nm. After annealing at 200 °C as evaporation of excess of selenium, hollow conical CdSe tubes were obtained at Fig. 1d. CdSe wall has uniform thickness about 5–10 nm. It could be deduced that as-deposited CdSe nanohorn structure composes as “Se core–CdSe shell” structure.

XRD patterns of the three CdSe structures are shown in Fig. 2. The peaks marked with an asterisk stem from ITO. The XRD patterns (Fig. 2b and c) of CdSe films prepared from solutions I and III exhibit an amorphous structure with nanocrystalline cubic structure. The diffraction peaks observed close to 25.3°, 42.0° and 49.7° are attributed to (1 1 1), (2 2 0), (3 1 1) planes of zinc blend structures of CdSe. The XRD pattern of CdSe films deposited from solution I (Fig. 2c) exhibits single (1 1 1) peak, which is more sharp then in Fig. 1b. The characteristic planes of (1 1 1), (2 2 0), (3 1 1) of wurtzite structures coincide with planes (0 0 2), (1 1 0), (2 0 1) of zinc blend structures on pattern of Fig. 2a. There are also weak peaks at 27° and 45° corresponding (1 0 1) and (1 0 3) plane of hexagonal phase of CdSe.

In order to gain a better understanding of the growth of the nanowire structures, the evolution of the morphology as a function of current density (deposition time) was studied. The current density–time dependence of the electrodeposition process of CdSe nanofibers is shown in Fig. 3 (solution III) and formation of the CdSe thin films (solution I).

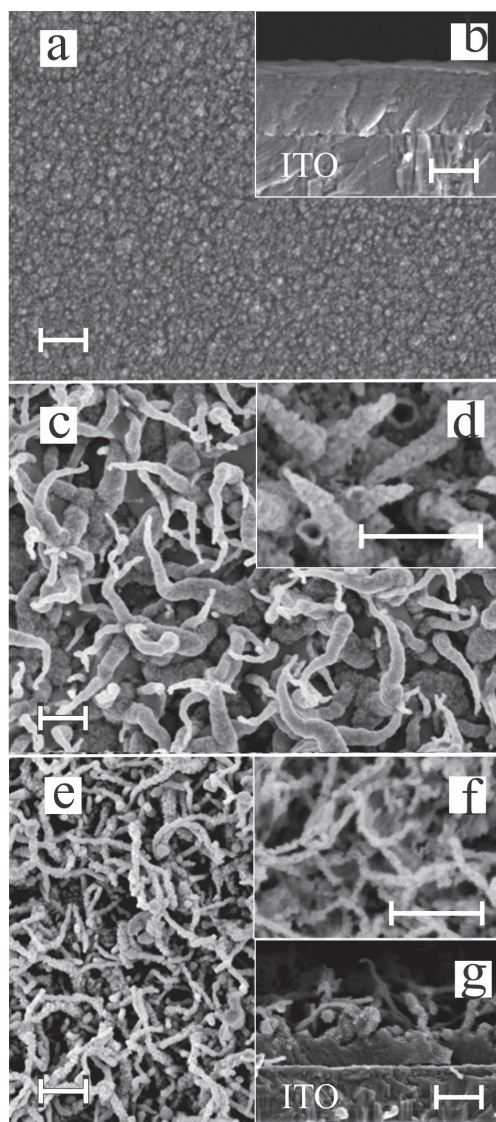


Fig. 1. Surface and cross-sectional SEM images of the CdSe samples electrodeposited from different solution I (a and b); solution II (c and d); solution III (e–g). The films annealed at 200 °C for 1 h (d and f). The white bar indicates the length of 200 nm.

In a process of formation of CdSe the current density decreases rapidly and then gradually stabilizes. The sharp drop in the initial current density could be explained by charging of formed double layer. When the current density reaches the minimum at the time

Table 1
Morphological and structural properties of CdSe deposits with respect to composition of electrochemical bath.

Solution no.	Concentration of solution (Cd):(Se), mM	Phase	Morphology
I	25:0.5	Wurtzite	Film, grain 5–10 nm
II	25:3	Wurtzite, zinc blend	Tube \varnothing 200 nm
III	25:05:00	Wurtzite, zinc blend	Fiber \varnothing 30 nm

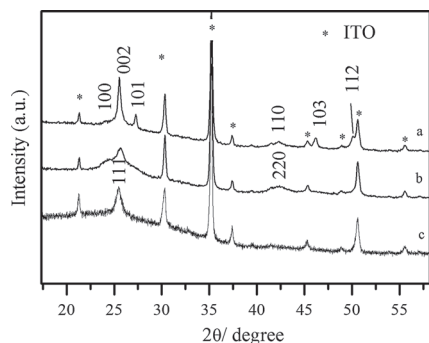


Fig. 2. XRD pattern of CdSe electrodeposited from solution I (a), solution II (b) and solution III (c).

point of 50 s. CdSe layer composed of nanoparticles (10 nm) with clusters of Se (50 nm) on the nanoparticle layer forms (point (a) in Fig. 3). Analogical structures were described in our previous work [13]. The formation of Se cluster islands was confirmed by secondary electron imaging method in use of high resolution scanning electron microscope with energy selective backscattered electron detector (EsB) for compositional contrast.

The followed decreasing of the current density corresponds to the transition of 2D Se clusters into 3D nucleus clusters (point (b) in Fig. 3). When the current density reaches the transition point, the fiber nanostructures start to grow accompanied by the linear increase in the current (point (c) in Fig. 3).

4. Discussions

The mechanism of electrochemical synthesis of cadmium selenide could be consider as follows (Fig. 4): the formation Se solid islands on cathode is achieved through a diffusion controlled reduction of H_2SeO_3 species to Se^0 , which is followed the reduction to H_2Se . Synthesis of CdSe nanoparticles is immediately followed through chemical reaction of Se with Cd^{2+} ions.

Under condition of overpotential deposition and excess of cadmium ions in solution, we can say about the electrochemical process of formation CdSe controlled by a rate of reduction of selenium species. At overpotential deposition the rate of diffusion of Se species into electrode surface is expected to be sluggish in comparison to the rate of diffusion when the Se nucleolus are reduced

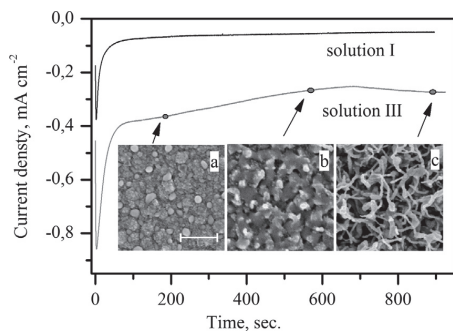


Fig. 3. Current density–time curve recorded during CdSe electrodeposition at -0.7 V vs. Ag/AgCl. The SEM images correspond to the CdSe deposits obtained at different deposition times; 3.5 min (a), 10 min (b) and 15 min (c). The white bar indicates the length of 200 nm.

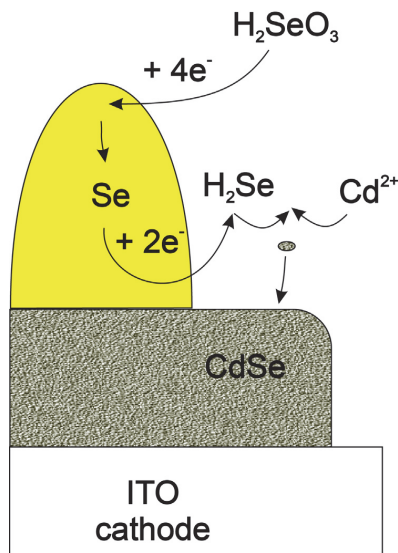


Fig. 4. Schematic representation of the electrochemical process of formation of CdSe deposits.

to H_2Se at the surface of working electrode and CdSe synthesized. As the result, stoichiometric CdSe film is formed [13].

Electrochemical deposition of CdSe nanowire structures was investigated in [8,12,14]. Feng supposed the growth mechanism CdSe nanowires along a uniform direction of $[0001]$ [14]. However HRTEM image of single CdSe nanofibers reveals the tubular space and the presence of CdSe thick layer surrounding the central tubule [8].

On the basis of the above results, we have proposed the possible growth mechanism for the formation of CdSe nanowires (Fig. 5).

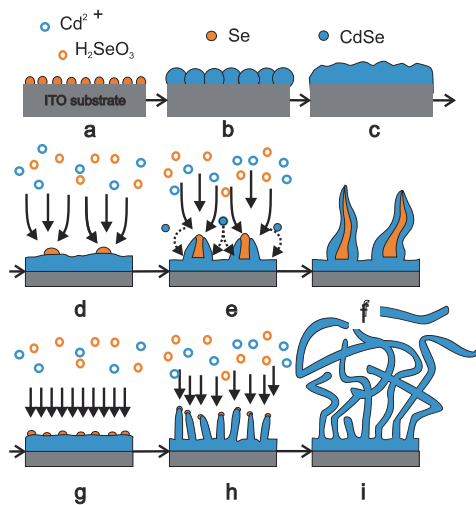


Fig. 5. Schematic representation of the patterning approach: Se absorption on ITO surface (a), CdSe nucleus formation (b), growth of CdSe underlayer (c), formation of Se nucleus on CdSe underlayer (d and g), growth of CdSe nanorods (h and i) and nanohorns (e and f).

The mechanism of a formation includes two growth stages. The first stage is formation of CdSe underlayer, the second one is formation of CdSe nanowire structures.

Initially, Se species are adsorbed on the ITO substrate surface (Fig. 5a). Then, CdSe nuclei are formed (Fig. 5b) and further coalesced through the above nucleation processes (Fig. 5c). The formation of the CdSe layer is described as 2-D growth, when condensing particles have strong affinity to the ITO layer.

The formation of 3-D nanowire structures is enabled if the rate of surface diffusion is expected to be fast in comparison to the rate of diffusion when the metal ions are reduced to metal atoms at the surface.

The Se adsorbed atoms have a stronger affinity one to another than to CdSe surface, resulting in the formation of selenium islands grow in all directions (Fig. 5d and g). The size and an real density of Se islands depend on the rate of reduction of selenium. The bigger size and scattered selenium islands are formed at more sluggish deposition rate. Deposition of CdSe occurs preferentially at the Se islands interface, so that nanowire nucleation takes place. The growth of nanowires is restrained by the diameter of the Se islands.

An anisotropic growth of CdSe nanofibers is induced by an impingement of CdSe nanoparticles on Se tips located at the end of nanowires (Fig. 5g–i). The formation of curvature of CdSe nanowires can be attributed to re-deposition or the accumulation of atomic disorder in CdSe.

The formation core shell Se–CdSe nanohorns from selenium islands is characterized by the radial growth occurring when species diffuse and incorporate on the nanowire side-walls (Fig. 5d–f).

As a result, the initial selenium core becomes smaller during the electrodeposition. Finally, thin nanowires (diameter 30 nm) were formed on the selenium tip as shown in Fig. 5.

5. Conclusions

In summary, we have demonstrated a simple one-step electrochemical synthesis of CdSe nanofiber layers and nanohorn structures from aqueous solutions. The two types of 3-D nanostructures: CdSe nanofibers (\varnothing 30 nm, length of 1–2 μ m) and Se core–CdSe shell nanohorns (\varnothing 200 nm and length of 600 nm) were obtained and investigated. It was found the mechanism of a formation of CdSe nanostructures includes two growth stages. The first stage is absorption of Se on the ITO surface and formation of CdSe underlayer. The second one is a growth and a formation of CdSe nanofibers and nanohorn on an underlayer of CdSe. An anisotropic growth is induced by an impingement of reduced CdSe nanoparticles on Se seeds located at the end of nanowires. This method can be

extended for the controlled synthesis of other inorganic functional nanomaterials with different morphologies.

Acknowledgements

Our group is grateful to the financial support from the Estonian Ministry of Education and Research under Grant SF0140099s08 and SF0140033s12, the Estonian Science Foundation G8655 and G8714 and the Archimedes Project “New materials for solar energetics” code 3.2.0501.10.0014.

References

- [1] K.R. Murali, A. Austine, B. Jayasutha, D.C. Trivedi, Photoelectrochemical cells based on CdSe films brush plated on high-temperature substrates, *Sol. Energy Mater. Sol. Cells* 90 (2006) 753–759.
- [2] I. Gerdova, A. Haché, Third-order non-linear spectroscopy of CdSe and CdSe/ZnS core shell quantum dots, *Opt. Commun.* 246 (2005) 205–212.
- [3] M. Zheng, Y. Cui, X. Li, S. Liu, Z. Tang, Photoelectrochemical sensing of glucose based on quantum dot and enzyme nanocomposites, *J. Electroanal. Chem.* 656 (2011) 167–173.
- [4] H.J. Joyce, Q. Gao, H.H. Tana, C. Jagadish, Y. Kim, et al., III–V semiconductor nanowires for optoelectronic device applications, *Prog. Quantum Electron.* 35 (2011) 23–75.
- [5] M. Roth, Advantages and limitations of cadmium selenide room temperature gamma ray detectors, *Nucl. Instrum. Methods Phys. Res. Sect. A* 283 (1989) 291–298.
- [6] P. Němec, M. Šimurda, I. Němec, P. Formánek, Y. Němcová, D. Sprinzl, F. Trojánek, P. Malý, Highly luminescent CdSe nanocrystalline films prepared by chemical bath deposition, *J. Cryst. Growth* 292 (2006) 78–86.
- [7] Y. Murase, T. Noma, K. Maehashi, H. Nakashima, Formation and photoluminescence of stacked CdSe quantum dots grown by molecular beam epitaxy, *J. Vac. Sci. Technol. B* 19 (2001) 1459–1463.
- [8] S.-K. Min, O.-S. Joo, K.-D. Jung, R.S. Mane, S.-H. Han, Tubular end-capped electrodeposited CdSe nanofibers: Enhanced photochemistry, *Electrochem. Commun.* 8 (2006) 223–226.
- [9] A.V. Shaikh, R.S. Mane, H.M. Pathan, B.-K. Min, O.-S. Joo, S.-H. Han, CdSe thin film growth: primarily amorphous nanograins to self-assembled nanowires, *J. Electroanal. Chem.* 615 (2008) 175–179.
- [10] M. Bouroushian, Z. Loizos, N. Spyrellis, G. Maurin, Influence of heat treatment on structure and properties of electrodeposited CdSe of Cd(Te, Se) semiconducting coatings, *Thin Solid Films* 229 (1993) 101–106.
- [11] J. Datta, C. Bhattacharya, S. Bandyopadhyay, Cathodic deposition of CdSe films from dimethyl formamide solution at optimized temperature, *Appl. Surf. Sci.* 253 (2006) 2289–2295.
- [12] K. Singh, S.S.D. Mishra, Photoelectrochemical studies on galvanostatically formed cadmium selenide films using mixed solvents, *Sol. Energy Mater. Sol. Cells* 63 (2000) 275–284.
- [13] J. Kojs, S. Bereznev, O. Volobujeva, J. Gurevits, E. Mellikov, Electrocrystallization of CdSe from aqueous electrolytes: structural arrangement from thin films to self-assembled nanowires, *J. Cryst. Growth* 320 (2011) 9–12.
- [14] Z. Feng, Q. Zhang, L. Lin, H. Guo, J. Zhou, Z. Lin, (001)-Preferential growth of CdSe nanowires on conducting glass: template-free electrodeposition and application in photovoltaics, *Chem. Mater.* 22 (2010) 2705–2710.
- [15] J. Kojs, S. Bereznev, J. Gurevits, O. Volobujeva, Electrochemically synthesised CdSe nanofibers and pearl-chain nanostructures for photovoltaic app, *Mat. Lett.* 95 (2013) 110–113.

Paper III

J. Kois, S. Bereznev, **J. Gurevits**, O. Volobujeva, Electrochemically synthesized CdSe nanofibers and pearl-chain nanostructures for photovoltaic applications, *Mater. Lett.* 95 (2013) 110-113.



Electrochemically synthesised CdSe nanofibers and pearl-chain nanostructures for photovoltaic applications

J. Kois*, S. Bereznev, J. Gurevits, O. Volobujeva

Department of Materials Science, Tallinn University of Technology, Ehitajate tee 5, 19086 Tallinn, Estonia

ARTICLE INFO

Article history:

Received 17 October 2012

Accepted 22 November 2012

Available online 5 December 2012

Keywords:

CdSe
Electrodeposition
Nanofibers
Photovoltaic
Hybrid solar cell

ABSTRACT

Self-assembled arrays of CdSe nanofibers with diameter of 40 nm and length about 2 μm were electrodeposited onto glass/ITO substrates in aqueous media. Thermal treatments of CdSe nanofibers were applied and the influence of treatment on morphology, optical and electrical parameters were investigated. Scanning electron microscopy (SEM) study of CdSe structures revealed the change in the morphology of CdSe structures from nanofibers to pearl chain-like nanostructures after thermal treatment at 350 °C in air. Also CdSe nanostructures were characterized by UV–vis absorption spectroscopy and X-ray diffraction spectroscopy (XRD). The poly(3-octylthiophene) (P3OT) functional layers were deposited on CdSe nanowires by spin-casting technique to prepare hybrid photovoltaic (PV) structures. Obtained CdSe nanowires/P3OT PV structures were characterized and partially optimized by additional post-deposition thermal treatment.

© 2012 Elsevier B.V. All rights reserved.

1. Introduction

In the last decades, controllable synthesis of various metal chalcogenide semiconductor crystals with dimensions from nanometer to micrometer scale including CdTe [1], ZnS [2], CdS [3], CdSe [4] and ZnO [5] have been reported in connection of their potential applications in electronics and optoelectronics.

CdSe is an important II–VI semiconductor with high absorption coefficient and nearly optimum band-gap energy (1.7 eV), and is an interesting material for fabrication of photovoltaic devices [6] in photoelectrochemical solar cells [7], optoelectronic and gas-sensing devices [8].

Up to now, different CdSe nanostructures including nanodots [9], nanorods and tetrapods [10], nanowires and branched structures [11] have been synthesized by different methods.

Among them, most CdSe nanostructures were grown on the basis of vapor-phase-based techniques as molecular beam epitaxy, ionic layer adsorption [12], and solution-based techniques including chemical deposition process [11], solvothermal method [9], hydrothermal treatment [13] and also electrochemical deposition.

Electrodeposition has been successfully applied as a simple and low cost fabrication technique to obtain CdSe with different morphology: from thin films to self-assembled nanorods and nanofibers [7,14]. As a rule, the crystallinity of electrodeposited

structures can be improved significantly by additional thermal treatment.

In our previous work we reported about successful electro-deposition of stoichiometric self-assembled nanofiber CdSe films [15]. The aim of present work was to study the effect of annealing on the structural, morphological, optical and electrical properties of the electrodeposited CdSe nanofibers.

2. Experimental details

The CdSe nanofiber films were electrodeposited on commercial indium tin oxide (ITO) coated glass substrates from aqueous solutions of CdCl₂ and H₂SeO₃ (Aldrich) in concentrations 25 mM and 10 mM respectively. The pH value of the solution was around 2, adjusted by hydrochloric acid. Voltalab PGZ100 potentiostat/galvanostat was applied for the voltammetry and electrodeposition of CdSe. The electrodeposition process was carried out in standard three-electrode electrochemical cell equipped with a platinum wire as the counter electrode and Ag/AgCl 3 M KCl reference electrode. Thin film was deposited on the substrate area around 1.5 cm² under standard conditions: under cathodic potential –700 mV at room temperature during 15 min without stirring. Finally, as-grown CdSe nanofibers were annealed at 250 °C, 350 °C or 410 °C for 30 min in air and characterized by using different techniques.

The morphology of deposited films was studied by using a high-resolution scanning electron microscope (HRSEM) Zeiss ULTRA 55. The chemical composition of deposits was determined by using energy dispersive X-ray analysis (EDX) system of Röntex.

* Corresponding author. Tel./Fax: +372 6203366.
E-mail address: julia.kois@ttu.ee (J. Kois).

The phase composition of films was determined by X-ray diffraction analysis using Bruker AXS D5005 diffractometer with Cu K_{α} radiation. UV–vis transmission spectra have been scanned with a SIMADZU UV-1800 spectrophotometer in the wavelength region from 250 to 1100 nm.

The hybrid PV structures were fabricated using the CdSe nanofibers (both annealed and as-synthesized) and conductive polymer poly(3-octylthiophene-2,5-diyl) (P3OT).

Organic functional layers of conductive polymer P3OT regioregular (Aldrich) and composite layers of P3OT mixed with methanofullerene phenyl C61 butyric acid methyl ester (PCBM) (Aldrich) were deposited by using the spin-casting technique from 1.5% solution of P3OT and P3OT(1.5%):PCBM(1.5%) solution in chlorobenzene (Aldrich). Chemat Technology KW-4A double speed spin-coater was used for organic layers deposition (first rotating speed—800 rpm; second rotating speed—3000 rpm; film thickness—around 20–40 nm). Finally, highly-conductive graphite suspension contacts (Alfa Aesar) were painted onto the glass/ITO/CdSe/P3OT structure and dried for 1 h at 60 °C. The active area of the prepared ITO/CdSe/P3OT/graphite structures was about 1 mm².

White light with an intensity of 100 mW/cm² from a tungsten–halogen lamp was applied to measure current–voltage characteristic of prepared glass/ITO/CdSe/P3OT/graphite PV structures.

3. Results and discussion

CdSe nanofiber films: CdSe nanofiber films were synthesized under the standard electrochemical deposition conditions: from 25 mM CdCl₂ and 10 mM H₂SeO₃ under potential –700 mV vs. Ag/AgCl during 15 min. The chemical composition of as-deposited nanofibers was determined as 40 at% Cd and 60 at% Se by EDX analysis.

Fig. 1 shows the X-ray diffraction scans for CdSe electrodeposited on ITO. The low intensity of diffraction peaks indicates that as-deposited CdSe film is amorphous and/or nanocrystalline. Reported in the literature structural studies on CdSe nanowires electrodeposited from aqueous electrolytes showed that the as-grown nanowires were amorphous and/or have zinc-blende crystal structure, changed to a hexagonal structure after thermal treatment [16,17].

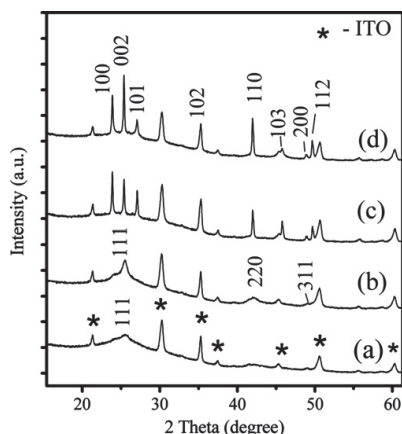


Fig. 1. XRD patterns of the CdSe nanofiber films: (a) electrodeposited, (b) annealed at 250 °C, (c) 350 °C and (d) 410 °C.

Well defined diffraction peaks appeared after annealing at 250 °C, indicating an improvement in the crystalline quality of the CdSe nanofibers (Fig. 1). Broad humps at about 25 °C and 44 °C correspond to the (111) and (220) reflections of face centered-cubic structure of the CdSe (JCPDS no. 19-191) [18]. The absence of (103) and (102) peaks of the hexagonal phase at about 48 °C and 37 °C confirms this cubic structure.

The transformation of zinc-blende structure to wurtzite-type CdSe was indicated for the CdSe annealed at 350 °C. The XRD pattern of CdSe film annealed at 350 °C and 410 °C shows appearance of sharp diffraction peaks in the positions (100), (002/111), (110) and (112/311) planes of mixture wurtzite and zinc-blende type CdSe structure. It should be noted that the hexagonal structure dominates in the CdSe nanofiber film annealed at 350 °C.

The morphology of the CdSe nanowires synthesized under the standard electrochemical deposition conditions and annealed at different temperatures are shown in Fig. 2. It seems that the distorted CdSe fibers with rough surfaces were formed during deposition (Fig. 2a). Diameter of the as-deposited nanofibers varied within 30–40 nm and length in the order of few micrometers. The diameter of fibers are slightly thickened at the base (not shown in the micrograph).

As a result of annealing process at 250 °C for 30 min, the evaporation of excess of selenium occurs; however the temperature applied is not sufficient for recrystallization of CdSe nanofibers. The EDX analysis confirms stoichiometric composition (Cd/Se = 1:1) of all annealed CdSe fiber films.

The influence of annealing conditions on the surface morphology of CdSe nanofibers is shown in Fig. 2(b–d). The CdSe films annealed at temperature 250 °C demonstrate shape-tailored porous fibers with features similar to the as-deposited fibers, but with smaller diameter of nanowires (about 15–20 nm).

Fig. 2(c) reveals the presence of some pearl necklace type CdSe fibers after annealing at 350 °C during 30 min. CdSe beads with diameters 15–20 nm were obtained, that practical corresponds the diameters of the as-deposited CdSe fiber. Some of the CdSe structures exhibit segmented structure with some variations in the length of segments and nearly uniform diameter. According to our assumption, low temperature prevents grain agglomeration of the CdSe nanoparticles, instead they form pearl necklace-like structure [19].

At annealing temperature of 410 °C the recrystallization and the conglomeration of CdSe fibers to solid films of about 200 nm were observed on the surface of ITO (Fig. 2(d)). A number of micro-scaled particles with diameter 10–100 nm can be clearly observed on the surface of the CdSe films.

Fig. 3 shows the absorption spectrum of CdSe nanofiber electrodeposited and annealed on ITO. The absorbance of all films increases steeply in the wavelength range shorter than 750 nm.

It can be seen that optical absorption increases with the increase in annealing temperature [20]. It may be due to evaporation of excess of Se and recrystallization of amorphous CdSe films. Slow evolution and red shift of the spectra occur at annealing temperature 350–410 °C, due to recrystallization of nanocrystallites into effectively larger crystallites [7,11,16].

Characterization of hybrid photovoltaic structured: The hybrid photovoltaic structure were fabricated for rough estimate of electrical characteristics of CdSe fiber films. The polymers poly(3-octylthiophene) (P3OT) mixed with methanofullerene phenyl C61 butyric acid methyl ester (PCBM) have been used for this PV application. The structure was finished by graphite back contact.

Table 1 shows performance (V_{oc} , J_{sc} , FF and power conversion efficiency) of hybrid photovoltaic structure under simulated 100 mW/cm² solar irradiation for cells.

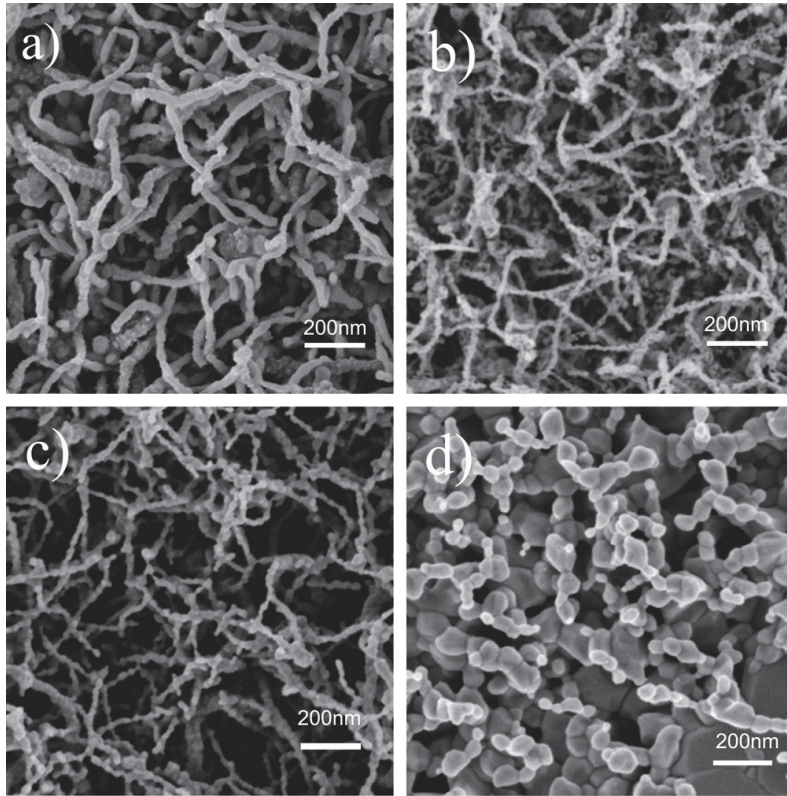


Fig. 2. SEM images of CdSe nanofiber films: (a) electrodeposited and annealed (b) at 250 °C, (c) 350 °C and (d) 410 °C.

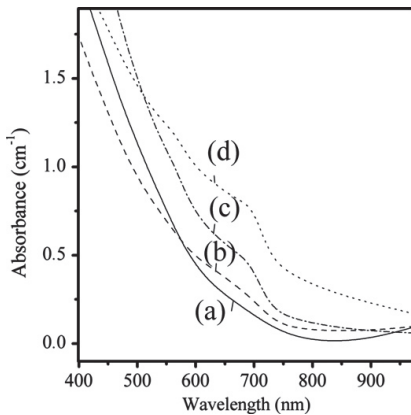


Fig. 3. Optical absorption spectra of CdSe films: (a) electrodeposited and annealed (b) at 250 °C, (c) 350 °C and (d) 410 °C.

Without heat treatment of CdSe nanofibers, CdSe/P3OT structure does not form any p–n barrier junction as revealed by the ohmic characteristic in Fig. 4. The photovoltaic parameters remarkably improved after the heat-treatment of CdSe nanofibers. The CdSe structure annealed at 250 °C/P3OT shows the short-circuit current density (J_{sc}) at about 0.1 mA cm^{-2} and the open circuit voltage (V_{oc}) 200 mV. The power conversion

Table 1

Characteristic parameters of ITO/CdSe/P3OT/graphite photovoltaic structures.

Structure	Open-circuit voltage, V_{oc} (V)	Short-circuit current density, J_{sc} (mA cm^{-2})	Fill factor, FF	Power conversion efficiency
As-deposited CdSe/P3OT-PCBM	0	0		
Annealed at 250 °C CdSe/P3OT	0,2	0,1	0,38	0,07
Annealed at 250 °C CdSe/P3OT-PCBM	0,41	0,29	0,31	0,36
Annealed at 350 °C CdSe/P3OT-PCBM	0,5	0,3	0,29	0,44
Annealed at 410 °C CdSe/P3OT-PCBM	0,04	0,22	0,24	0,02

efficiency of this structure has been improved by the addition of fullerene (PCBM) to (P3OT) polymer, mainly due to the increased conductivity of polymer.

The maximum open current voltage (V_{oc}) was observed in the structure with CdSe annealed at 350 °C.

The dependence of J_{sc} on annealing temperature of CdSe was not observed, it could be attributed to the thickly aggregated CdSe nanofibers or pore-filling problem associated with P3OT.

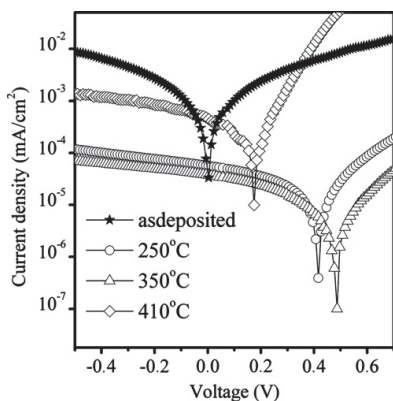


Fig. 4. The J - V photoresponse of a ITO/CdSe/(P3OT)-(PCBM) photovoltaic structures under illumination.

The structure with CdSe annealed at 410 °C demonstrates the degradation of power conversion efficiency owing to the significant degradation of the open circuit voltage (V_{oc}) and fill factor.

4. Conclusion

The electrodeposition technique was successfully applied for the synthesis of self-assembled arrays of CdSe nanofibers with diameter 40 nm and length about 2 μ m.

Significant improvement in the crystallinity and optical absorbance of CdSe nanostructures was observed after thermal annealing (temperatures 250–410 °C). Formation of new pearl chain-like CdSe nanostructures after thermal treatment at 350 °C was found.

On the base of electrodeposited and thermally treated CdSe deposits, hybrid CdSe/P3OT photovoltaic structures were formed. The hybrid photovoltaic structures on the base of pearl chain-like CdSe nanostructures show the best photovoltaic parameters.

Acknowledgments

We are grateful to the financial support from the Estonian Ministry of Education and Research under Grant SF0140099s08 and from the Estonian Science Foundation (G8655 and G8714).

References

- [1] Yang L, Wu R, Li J, Sun YF, Jia JK. CdTe nanosheets and pine-like hyperbranched nanostructures prepared by a modified film technique: catalyst-assisted vacuum thermal evaporation. *Mater Lett* 2011;65:17–20.
- [2] Moore D, Ronning C, Ma C, Wang L. Wurtzite ZnS nanosaws produced by polar surfaces. *Chem Phys Lett* 2004;385:8–11.
- [3] Gao T, Wang T. Catalyst-assisted vapor–liquid–solid growth of single-crystal CdS nanobelts and their luminescence properties. *J Phys Chem B* 2004;108:20045–9.
- [4] Barth S, Hernandez-Ramirez F, Holmes JD, Romano-Rodriguez A. Synthesis and applications of one-dimensional semiconductors. *Prog Mat Sci* 2010;55:563–627.
- [5] Allsop N, Schönmann A, Belaidi A, Muffler H-J, Mertesacker B, Bohne W, et al. Indium sulfide thin films deposited by the spray ion layer gas reaction technique. *Thin Solid Films*, 513; 2006 52–56.
- [6] Dayal S, Kopidakis N, Olson DC, Ginley DS, Rumbles G. Photovoltaic devices with a low band gap polymer and CdSe nanostructures exceeding 3% efficiency. *Nano Lett* 2010;10:239–42.
- [7] Min S-Ki, Joo O-S, Mane RS, Jung K-D, Lokhande CD, Han S-H. CdSe nanofiber based photoelectrochemical cells: influence of annealing temperatures. *J Photochem Photobiol A* 2007;187:133–7.
- [8] Joshi SS, Lokhande CD, Han S-H. A room temperature liquefied petroleum gas sensor based on all-electrodeposited n-CdSe/p-polyaniline junction. *Han. Sens Actuators, B* 2007;123:240–5.
- [9] Li J, Tang X, Lu Z, Qian Y. Synthesis of CdSe micro/nanocrystals with controllable multimorphologies and crystal phase. *J Alloys Compd* 2010;497:390–5.
- [10] Li YC, Zhong HZ, Li R, Zhou Y, Yang CH, Li YF. High-yield fabrication and electrochemical characterization of tetrapodal CdSe, CdTe, and CdSexTe1-x nanocrystals. *Adv Funct Mater* 2006;16:1705–16.
- [11] Fan H, Liang J, Zhang Y, Zhang M, Xi B, Wang X, et al. Phase transition of CdSe nanocrystallines with controlled morphologies induced by ratios of ethanamine and water in their mixed solution. *Solid State Sci* 2008;10:901–7.
- [12] Pathan HM, Sankpal BR, Desai JD, Lokhande CD. Preparation and characterization of nanocrystalline CdSe thin films deposited by SILAR method. *J Mater Chem Phys* 2003;78:11–4.
- [13] Xi L, Lam YM, Ping Y, Li L. Synthesis and characterization of one-dimensional CdSe by a novel reverse micelle assisted hydrothermal method. *J Colloid Interface Sci* 2008;320:491–500.
- [14] Min S-K, Joo O-S, Jung K-D, Mane RS, Han S-H. Tubular end-capped electrodeposited CdSe nanofibers: enhanced photochemistry. *Electrochem Commun* 2006;8:223–6.
- [15] Kois J, Bereznev S, Volobujeva O, Gurevits J, Mellikov E. Electrocrystallization of CdSe from aqueous electrolytes: structural arrangement from thin films to self-assembled nanowires. *J Cryst Growth* 2011;320:9–12.
- [16] Bouroushian M, Charoud-Got J, Loizos Z, Spyrellis N. A phase modification of CdSe electrodeposits induced by substrate roughness. *J Mater Sci Lett* 2000;19:2201–3.
- [17] Erat S, Metin H, Ari M. Influence of the annealing in nitrogen atmosphere on the XRD, EDX, SEM and electrical properties of chemical bath deposited CdSe thin films. *Mater Chem Phys* 2008;111:114–20.
- [18] Riveros G, Vásquez J, Gómez H, Makarova T, Silva D, Marotti RE, et al. Single-step electrodeposition of polycrystalline CdSe microwire arrays: structural and optical properties. *Appl Phys A* 2008;90:423–30.
- [19] Kale RB, Lokhande CD. Influence of air annealing on the structural, optical and electrical properties of chemically deposited CdSe nano-crystallites. *Appl Surf Sci* 2004;223:343–51.
- [20] Shinde VR, Lokhande CD, Mane RS, Han S-H. Hydrophobic and textured ZnO films deposited by chemical bath deposition: annealing effect. *Appl Surf Sci* 2005;245:407–13.

Paper IV

J. Maricheva, S. Bereznev, R. Naidu, N. Maticiuc, V. Mikli, J. Kois, Improved electrodeposition of CdS layers in presence of activating H₂SeO₃ microadditive, *Mater. Sci. Semicond. Process.* 54 (2016) 14–19.



Contents lists available at ScienceDirect

Materials Science in Semiconductor Processing

journal homepage: www.elsevier.com/locate/mssp

Improved electrodeposition of CdS layers in presence of activating H₂SeO₃ microadditive



J. Maricheva*, S. Bereznev, R. Naidu, N. Maticiuc, V. Mikli, J. Kois

Department of Materials Science, Tallinn University of Technology, Ehitajate tee 5, 19086 Tallinn, Estonia

ARTICLE INFO

Article history:

Received 15 March 2016

Received in revised form

26 May 2016

Accepted 21 June 2016

Available online 9 July 2016

Keywords:

Selenious acid

Addition agent

Cadmium sulfide

Electrodeposition

Thin film

Characterization

ABSTRACT

CdS thin films were deposited electrochemically onto indium tin oxide (ITO)/glass substrates from aqueous solutions containing 0.01 M CdCl₂, 0.05 M Na₂S₂O₃ and 0.02 M Edta-Na₂ at –1.2 mV versus saturated sulfate reference electrode. Depositions were carried out at various temperatures (20, 50 and 80 °C) and different pH (2.5, 3.5 and 4.5) in a three electrode electrochemical cell. All above mentioned electrochemical syntheses were reproduced in presence of H₂SeO₃ microadditive to compare resulted CdS layers. Electrodeposited CdS thin films were characterized by different instrumental techniques to know the influence of deposition conditions on the quality of the obtained layers. It was found that the presence of 0.05–0.5 mM of H₂SeO₃ in the electrolyte changes the mechanism of the CdS film formation that facilitates nucleation and a growth of a more dense and uniform polycrystalline CdS film. Addition of 0.5 mM of H₂SeO₃ into the initial solution allowed us to obtain nearly stoichiometric (sulfur content ~52 at%) CdS films at reduced temperature value of 50 °C vs. higher temperature values used in a conventional electrodeposition process of CdS layers. No Se-containing phases were detected by EDX, Raman and XRD analyses in the CdS films. The presence of H₂SeO₃ tends to rearrange polytype crystalline structure of CdS to more stable hexagonal structure. The band gap value of CdS was increased from 2.3 eV to 2.5 eV as a result of H₂SeO₃ addition.

© 2016 Elsevier Ltd. All rights reserved.

1. Introduction

Cadmium sulfide is one of the most attractive semiconductors for application in solar cells [1] and other optoelectronic devices [2,3] due to its appropriate properties: wide band gap of about 2.5 eV at 300 K, n-type conductivity, Hall mobility of electrons ~10⁴ cm²/V s, and optical transmittance > 70% [4]. CdS thin films are produced using different techniques such as chemical vapor deposition [5], chemical bath deposition [6], spray pyrolysis [7], sputtering [8], and electrodeposition [9,10]. CdS can be deposited electrochemically from ionic liquids [9], aqueous [10] and organic solutions [11]. Electrodeposition is a relatively simple and inexpensive technology which allows the control of film properties through the change of growth parameters such as applied potential, pH, temperature and composition of the electrolyte. Generally, the use of specific additives in aqueous solutions may shift the optimal potential of electrodeposition [12], helps to refine grain size, and controls surface morphology, influencing crystalline structure and electrical properties of the layers [10]. In the electrodeposition of metals the presence of H₂SeO₃ shifts the

reduction reaction of metals to lower current densities, and influences the polarization of the electrode, affecting the current efficiency and energy consumption of the electrodeposition process [13,14]. The studies concerning the properties of CdS thin films by the electrodeposition method [15,16] were held by different groups, though there are few reports on the influence of additives in the solution on the properties of CdS films.

In this work we show the effect of the H₂SeO₃ microadditive on the growth mechanism. Improvement of morphology, crystalline structure, and optical properties of the electrodeposited CdS thin films were observed at lower deposition temperature.

2. Experimental

CdS layers were electrodeposited onto indium tin oxide (ITO) coated glass substrates (15 Ω sq⁻¹) in a potentiostatic mode using a Voltalab PGZ100 potentiostat/galvanostat. All the electrochemical experiments were carried out in a conventional three-electrode cell. Platinum wire was used as a counter electrode (CE), an ITO/glass as a working electrode (WE), and a saturated sulfate reference electrode (SSE) as a reference. The glass/ITO substrates were cleaned in heated concentrated sulfuric acid, then rinsed with deionized Millipore water.

* Corresponding author.

E-mail address: jelena.maricheva@ttu.ee (J. Maricheva).

An initial solution was prepared in Millipore water by using reagent grade anhydrous cadmium chloride (CdCl₂, 99.0%, Alfa-Aesar), ethylenediaminetetraacetic acid disodium salt concentrate (EDTA-Na₂, Sigma-Aldrich) and sodium thiosulfate pentahydrate (Na₂S₂O₃ · 5H₂O, >99.0%, Alfa-Aesar) in concentrations 0.01 M, 0.02 M and 0.05 M, respectively. The CdS films were electrodeposited at –1.2 V vs. SSE from the initial solution at the temperatures of 20, 50 and 80 °C. As growth rate is usually temperature-dependent, we used different deposition times at different temperatures (20 °C – 60 min, 50 °C – 30 min, 80 °C – 20 min) to obtain films with a comparable thickness. The pH of the electrolyte was adjusted by addition of 0.1 M H₂SO₄ up to the values of 2.5, 3.5 and 4.5. The H₂SeO₃ microadditive was added into the initial solution in the concentration range of 0–0.5 mM.

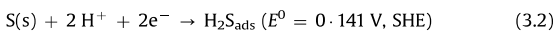
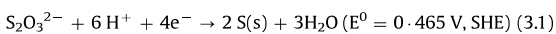
The composition of the deposited CdS films was determined by energy-dispersive X-ray microanalysis (EDX) method using Bruker Esprit 1.8 system. Due to very thin CdS layers minimum acceptable accelerating voltage of 7 kV was used. Quantification of the EDX results was performed by the help of interactive PB-ZAF standardless method. For determination of the presence of Se in film 4 kV accelerating voltage was used. Phase composition was studied using Micro Raman spectroscopy (Horiba LabRam HR spectrometer). X-ray diffractometer (Rigaku Ultima IV diffractometer with Cu-Kα radiation) was applied to analyze the crystalline nature and phase composition of the deposited films. The average crystallite size was calculated from the full width at half maximum (FWHM) intensity of the preferred peak using the Scherrer equation (1.1), where *D* is the average crystallite size, *K* is the constant related to crystallite shape (normally taken as 0.9), λ is the X-ray wavelength, β is the FWHM, and θ is the angle of the diffraction. Morphology and thickness of the films was imaged using high-resolution scanning electron microscopy (HR-SEM, Zeiss ULTRA 55). The surface topography of the prepared CdS thin films as well as surface roughness and average grain size were investigated by atomic force microscopy (AFM, Bruker Multimode 8.0 with application module based on Nanoscope V controller). Optical properties were measured using the SHIMADZU UV-1800 UV–vis spectrophotometer in the wavelengths region of 300–800 nm. Optical transmission and reflection data were used to determine the absorption coefficient of the deposited CdS thin films. Based on the Tauc relation [17], the values of *E_g* were estimated by extrapolating the linear portion of (α*hν*)² versus *hν* plot.

$$D = (K \cdot \lambda) / (\beta \cdot \cos \theta) \tag{2.1}$$

3. Results and discussion

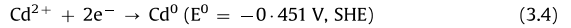
3.1. Mechanism of electrochemical formation of CdS

Electrochemical formation of CdS thin film in acidic medium takes place according to the sequential reactions (3.1–3.3) on the surface of the WE [10].



Initially, thiosulfate anions reduce to sulfur on the surface of the WE (3.1), where SHE is the saturated hydrogen electrode, and then sulfur reduces to hydrogen sulfide H₂S_{ads} (3.2). The molecules of H₂S_{ads} react with Cd cations and form CdS (4). Because metallic

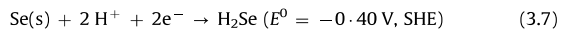
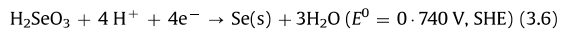
cadmium can be reduced at the potential of –0.45 V vs. SHE (3.4), we used EDTA-Na₂ as a complexing agent in order to shift the deposition potential of Cd to a more negative region.



In parallel with electrochemical reactions, chemical disproportionation reaction of the thiosulfate anions (3.5) can occur at pH lower than 5 [14]. There is a high probability that sulfur in a form of nanoparticles could be incorporated into the CdS film during the deposition process.



A small amount of selenious acid added into the initial solution influences the mechanism of electrodeposition and may cause changes in the chemical, structural and optical properties of CdS films [13,16]. According to our assumption, Se reduces from H₂SeO₃ under a more positive potential (3.6) than sulfur from the thiosulfate ions (3.1). Se contributes to the formation of a larger number of nucleation centers on the surface of the WE. This may promote the growth of a denser film with smaller grain size. Then Se can be reduced to H₂Se at the cathodic potential of 0.40 V vs. SHE (3.7). H₂Se may react with Cd²⁺ ions forming CdSe as nucleation centers (3.8) or return back into the electrolyte. Then Se may be replaced by S with following formation of CdS layer.



3.2. Electrodeposition from Se-free solution

The temperature and pH of an electrolyte have a great influence on the growth rate and morphology of the CdS films during the electrodeposition [16,18]. The changes of sulfur content in the films as a function of a pH from 2.5 to 4.5 in the initial solution at 80 °C are shown in Fig. 1 (curve a). Nearly stoichiometric CdS films with the sulfur content ~55 at% were obtained at the pH 2.5. When the pH increases from 3.5 to 4.5 the content of sulfur in the films raises from ~59 at% to ~75 at%, respectively.

Changes of the film stoichiometry as a function of deposition temperature (20–80 °C) at the pH 3.5 are shown in Fig. 1 (curve b). The pH 3.5 was chosen due to the electrolyte stability in the range of pH from 2.8 to 4.0 and because at higher pH values a poor adhesion of CdS to the ITO/glass substrate was observed [19].

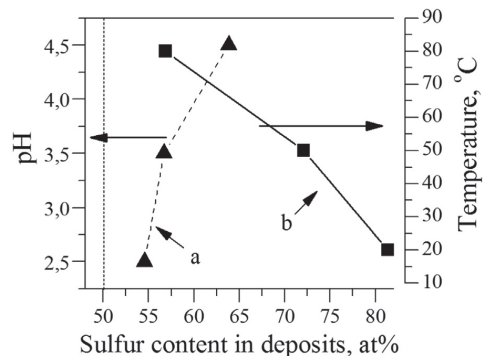


Fig. 1. Content of sulfur in CdS films electrodeposited from initial Se-free solution at –1.2 V vs. SSE at a) pH 2.5 – 4.5, 80 °C, b) 20 °C – 80 °C, pH 3.5.

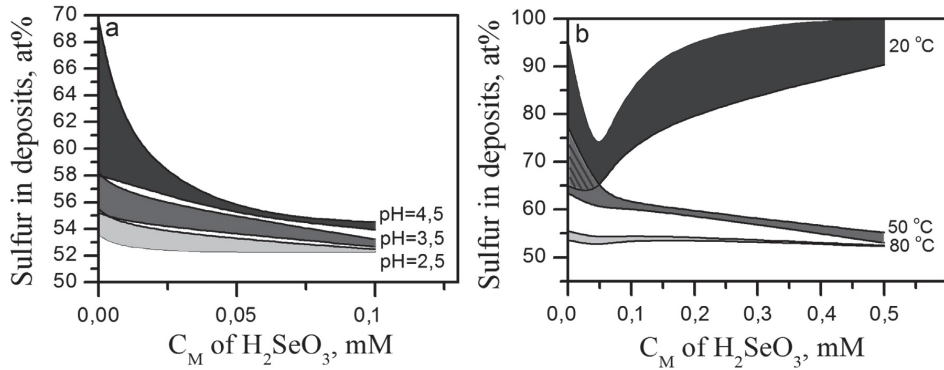


Fig. 2. Content of sulfur in CdS films as function of H₂SeO₃ concentration (CM) deposited from initial solution at a) different pH at 80 °C and; b) various temperatures at pH 3.5.

Sulfur content decreases from ~80 at% to ~72 at% by raising the deposition temperature from 20 °C to 50 °C. In terms of stoichiometry (53–55 at%), the best films deposited from Se-free initial solution were obtained at the highest temperature of 80 °C at the pH values of 2.5 and 3.5. However, in terms of stability of aqueous solution a lower temperature of 50 °C is preferable.

3.3. CdS electrodeposited from Se-containing solutions

In order to study the influence of H₂SeO₃ on the electro-deposition of CdS, a micromolar concentration of H₂SeO₃ (0, 0.05, 0.1, 0.5 mM) was added into the initial solution. The properties of the CdS films deposited at different H₂SeO₃ concentrations were studied as a function of pH and temperature. More stoichiometric CdS films were obtained at lower pH values 2.5 and 3.5 (Fig. 2(a)), which is in an agreement with the data obtained for CdS electro-deposited from the Se-free solution (Fig. 1). The decrease of the pH from 4.5 to 2.5 reduces the excess of sulfur from ~63 at% to 54 at%, while addition of H₂SeO₃ lowers deviation in the composition of the deposits.

The raise of the solution temperature decreases the deviation of composition, and improves the stoichiometry of the deposited CdS films (Fig. 2(b)). At 20 °C the addition of 0.01 mM of H₂SeO₃ diminishes the excess of sulfur from 80 at% to 70 at%, whereas higher concentrations of the H₂SeO₃ (0.1, 0.5 mM) increase it back. S-rich composition of the CdS thin films obtained at 20 °C may be caused by slow diffusion of the Cd²⁺ ions towards the WE at low temperature. At higher temperatures the content of sulfur is

decreased by the addition of H₂SeO₃ from ~70 at% to ~56 at% and from ~53 at% to ~52 at% at 50 °C and 80 °C, respectively. We can conclude that the presence of H₂SeO₃ microadditive allows to obtain nearly stoichiometric CdS at lower deposition temperature (50 °C).

The elementary analysis of the CdS films deposited from the solution with maximal concentration of H₂SeO₃ (0.5 mM) at the pH 3.5, at –1.2 V vs. SSE, at 50 °C for 30 min is shown in Fig. 3. Strong peaks corresponding to Cd at L_α of 3.13 keV and S at K_α of 2.307 keV were observed (Fig. 3-a). Composition of the CdS films was found to be nearly stoichiometric with a ratio of Cd:S equal to 1:1.08. Small excess of sulfur may occur as a result of sulfur nanoparticles trapping in the CdS layer. Peaks of indium and oxygen appear from ITO. As no detectable L_α Se peak at 1.419 keV was revealed (Fig. 3-b), it is reasonable to assume that Se is absent or very low (less than 0.3 m%) in the deposits. Similar compositional results were obtained for all the CdS thin films deposited from the solutions Se-free and containing 0.05–0.5 mM of H₂SeO₃.

Raman spectra of the CdS films deposited at various concentrations of H₂SeO₃ are shown in Fig. 4. Peaks at 300 cm⁻¹ and 600 cm⁻¹ are attributed to longitudinal optical (LO) phonon vibrational modes of CdS [20], whereas peaks at 91, 128, 170 and 561 cm⁻¹ correspond to sulfur vibrational modes [21]. Peak at 300 cm⁻¹ is the dominant for CdS, and its intensity increases with addition of a higher concentration of H₂SeO₃ to the working solution. A small peak at 188 cm⁻¹ appears only for the CdS thin films deposited with the presence of 0.5 mM of H₂SeO₃ in the electrolyte. According to literature, this peak is attributed to

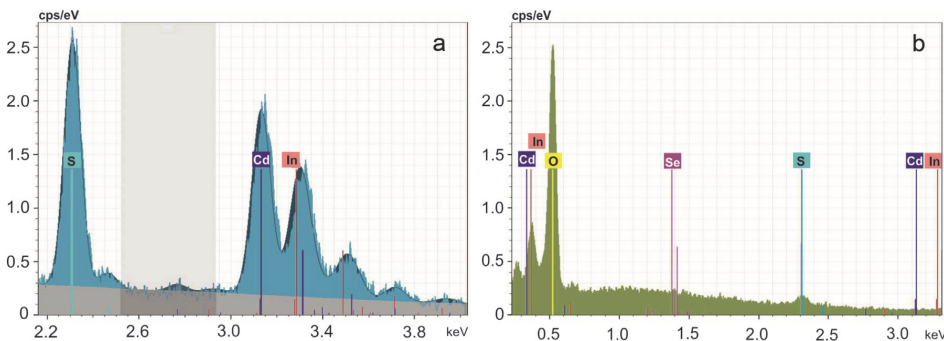


Fig. 3. EDX elemental microanalysis of CdS film deposited at pH 3.5, –1.2 V vs. SSE, 50 °C for 30 min from initial solution with 0.5 mM of H₂SeO₃ measured at accelerating voltage of (a) 7 kV and (b) 4 kV.

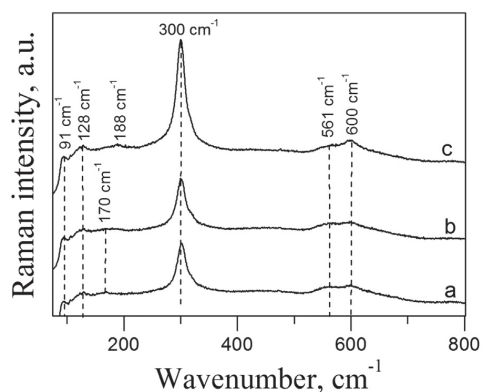


Fig. 4. Raman spectra of CdS films deposited at pH 3.5, -1.2 V vs. SSE, 50 °C for 30 min from initial solution with different H_2SeO_3 concentrations: a) 0, b) 0.1, c) 0.5 mM.

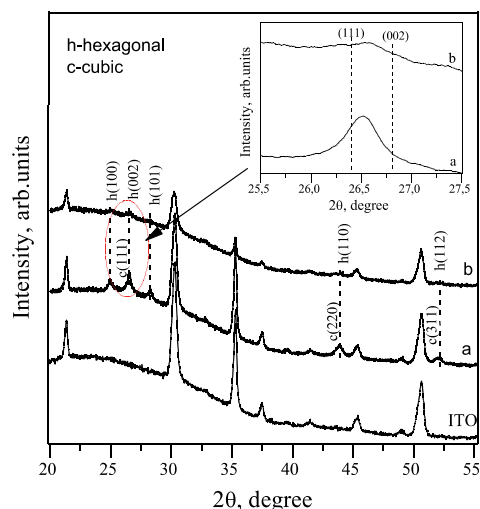


Fig. 5. XRD spectra of CdS films electrodeposited at 50 °C, pH 3.5 for 30 min from initial solution: a) Se-free, b) with 0.5 mM of H_2SeO_3 , and ITO as reference. In the inset: diffraction peak at 26.5° .

surface optical (SO) phonon modes of CdSe or to vibrational modes of pure S and S-Se [22,23]. H_2SeO_3 microadditive seems to promote the inclusion of Se into the crystalline structure of electrodeposited CdS thin films without forming Se-containing phases.

XRD analysis (Fig. 5) confirms the absence of Se-containing phases (or very low amount, in the frames of accuracy ($\sim 1\%$) of XRD measurement) in CdS thin films deposited from Se-containing solution. The CdS thin films deposited from Se-free solution exhibit both hexagonal and cubic structures with peaks (100), (002), (101), (110), (112) corresponding to the hexagonal structure, and (111), (220) and (311) planes related to the cubic structure [24]. All diffraction peaks were identified by using ICDD database [25,26]. With addition of 0.5 mM of H_2SeO_3 into the working solution, dominant hexagonal crystalline structure of the CdS thin films can be observed (Fig. 5). Transformation of the main peak at around 26.5° from mixed-phase to the hexagonal structure was detected. In order to study this transition the XRD pattern in the 2θ region 25.5 – 27.5° (Fig. 5-inset) was magnified. In both cases the peak at around 26.5° does not clearly belong to any of (111) and (002) planes. The diffraction peak at $2\theta=26.49^\circ$ is shifted towards the higher angle side equal to 26.61° with addition of 0.5 mM of H_2SeO_3 to the working solution. This may be attributed to the lattice distortion due to changes in the stacking order. Crystalline modifications in the CdS thin films may be influenced with a Se-modified growth mechanism of the film related to the surface and interface energy. In addition, lattice constants of the CdS film increase from $a=4.13$ Å to $a=4.14$ Å and from $c=6.67$ Å to $c=6.69$ Å. The average crystallite size decreases from 15 nm to 8 nm with addition of 0.5 mM of H_2SeO_3 . These changes in the crystal lattice support our assumption of Se inclusion into the CdS lattice.

Thus H_2SeO_3 microadditive in the solution tend to rearrange the usual mixed-phase [27,28] structure of CdS film to hexagonal. Moreover, it seems that the transformation tendency of the mixed-phase structure to a more hexagonal in the obtained CdS layers is connected with the initial formation of Wurtzite-hexagonal nuclei of CdSe [29,30], where Se is replaced with S as described in part 3.1.

HR-SEM and AFM micrographs of the CdS films deposited from the solutions with 0.1 mM and 0.5 mM of H_2SeO_3 were analyzed and compared to the reference film obtained from the Se-free solution (Fig. 6). The average thickness of the CdS films is in the range of 70 – 100 nm. The film deposited from the initial Se-free solution consists of grains and covers the ITO/glass substrate uncontinuously (Fig. 6(a)). On the other hand, the CdS films deposited from the initial solution with H_2SeO_3 microadditive are denser with smaller grains uniformly distributed on the substrate surface (Fig. 6(b) and (c)). Improved density of CdS films deposited from Se-containing solution may be explained by larger number of initial nucleation centers generated by the H_2SeO_3 microadditive.

The AFM 3D topographical images (Fig. 7) taken over the area of $2 \times 2 \mu\text{m}^2$ have a good correlation with the HR-SEM images (Fig. 6). The average surface roughness and grain size values were analyzed using the Nanoscope software with corresponding two dimensional images. The analysis was performed at different places. It can be seen from the AFM images that the surface of the CdS deposited from the Se-free solution covers the substrate unevenly

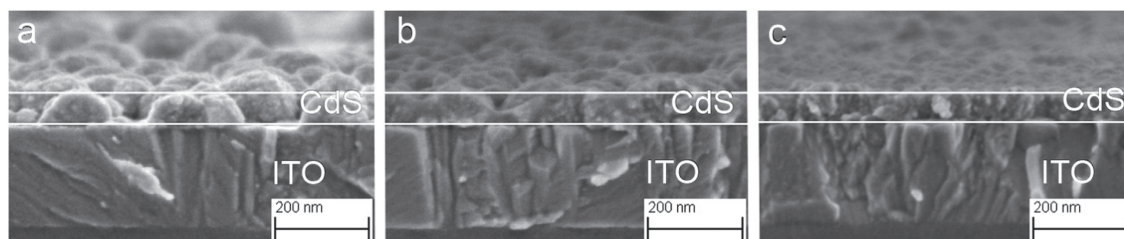


Fig. 6. HR-SEM cross-sectional images of CdS films electrodeposited at 50 °C, pH 3.5 for 30 min from initial solutions: a) Se-free, b) with 0.1 mM of H_2SeO_3 , c) with 0.5 mM of H_2SeO_3 .

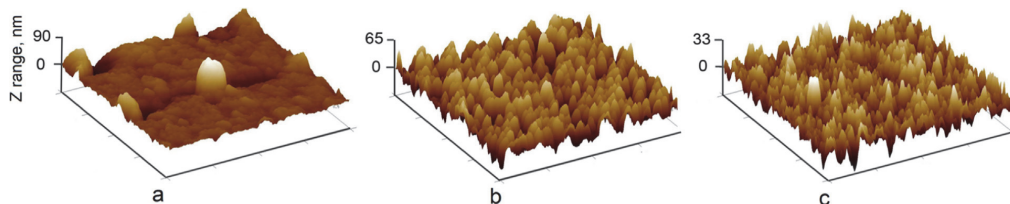


Fig. 7. AFM topography of CdS thin films electrodeposited at 50 °C, at pH 3.5 for 30 min from initial solutions: a) Se-free, H₂SeO₃, b) with 0.1 mM of H₂SeO₃, c) with 0.5 mM of H₂SeO₃.

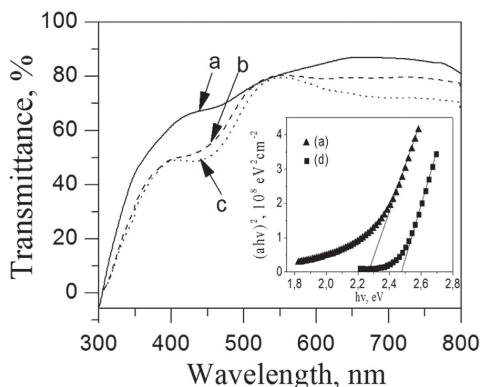


Fig. 8. UV-vis transmittance spectra of CdS films deposited at 50 °C, pH 3.5, –1.2 V vs. SSE for 30 min from initial solution: a) Se-free, b) with 0.05 mM of H₂SeO₃, c) with 0.5 mM of H₂SeO₃. In the inset: extrapolation of $(\alpha h\nu)^2$ versus $h\nu$ plot for CdS films deposited from initial solution: Se-free (a) and with 0.5 mM of H₂SeO₃ (c).

with distinctly smaller grains that are loosely packed, and at particular regions grow as agglomerated islands, thus z-scale is higher (Fig. 7(a)) than for the CdS thin films deposited in the presence of Se (Fig. 7(b) and (c)). The average surface roughness was 11, 17 and 9 nm for the CdS films deposited at the H₂SeO₃ concentrations of 0, 0.1 and 0.5 mM, respectively. The reported average roughness values are relatively dependent on the thickness of the film. With increase of the H₂SeO₃ concentration in the solution, the average grain size decreases from 77 nm to 46 nm in the electrodeposited CdS films.

Changes in CdS density are reflected in the optical properties as well. The optical transmittance (Fig. 8) of the CdS thin films decreases from 81% to 75% with addition of H₂SeO₃ microadditive into the initial solution, the optical band gap value slightly increased from 2.3 eV to 2.5 eV (Fig. 8-inset), and the red shift of the absorption edge is observed. The decrease in the transmittance may be due to the scattering effects, deviations in composition stoichiometry and/or changes in thickness. The second slope at ~400 nm may be attributed to the presence of oxides or/and to the size confinement effect in nanocrystalline CdS films [31,32], which can be responsible for the formation of localized states in band gap. The increase of sub-band gap with addition of H₂SeO₃ can be explained by the decrease of the average crystallite size. Generally, nano-size particles have higher surface area due to increase of band bending at grain boundaries, and also the changes in stacking order of the structure results in the sub-band gap states as per the quantum mechanical considerations [33,34]. The obtained band gap results are consistent with our XRD analysis.

4. Conclusions

We investigated the influence of H₂SeO₃ microadditive on the

properties of the CdS thin films deposited electrochemically from the acidic medium at different pH and temperatures. Thickness of the obtained CdS thin films is in the range of 70–100 nm. Nearly stoichiometric CdS thin films with sulfur content of 52 at% were deposited from Se-containing solution at the lower temperature of 50 °C at the pH 3.5, while the most appropriate temperature for the electrodeposition of CdS from Se-free solution is ≥ 80 °C. Addition of micromolar concentration of H₂SeO₃ into the working solution influences the mechanism of CdS formation promoting the transformation of the mixed-phase crystalline structure to a more hexagonal.

In addition, it promotes the decrease of the average grain size and surface roughness from 77 nm to 46 nm and from 11 nm to 9 nm, respectively. Resulted CdS thin films deposited from Se-containing solution are denser and cover uniformly the underlying substrate. With addition of 0.5 mM H₂SeO₃ the band gap value increases from 2.3 eV to 2.5 eV.

Although no Se-containing phases were detected by Raman or XRD analyses in the electrodeposited CdS films from Se-containing solutions. The main XRD peak C(001)/H(002) at around 26.5° is shifted towards the 2 θ value corresponding to the pure hexagonal structure, the lattice parameter is slightly increased from 4.13 Å to 4.14 Å. All these changes indicate to the inclusion of Se into the CdS lattice. The reason of Se inclusion into CdS may be CdSe nuclei formation during the electrodeposition process, where Se did not exchange to S.

Acknowledgements

This research was supported by the institutional research funding IUT19-28 and IUT19-4 of the Estonian Ministry of Education and Research, the European Union through the European Regional Development Fund, Project TK141, by ERA.NET RUS PLUS Project Flexapp (ETAG15028), and by University Base finance B54.

References

- [1] V. Rejo'n, I. Riech, J.L. Pen-a, Study of CdS/CdTe solar cells activated with an oxygen-CHClF₂ gas mixture, *Sol. Energy* 95 (2013) 319–324, <http://dx.doi.org/10.1016/j.solener.2013.06.026>.
- [2] P. Qi, D. Zhang, Y. Zeng, Y. Wana, Biosynthesis of CdS nanoparticles: a fluorescent sensor for sulfate-reducing bacteria detection, *Talanta* 147 (2016) 142–146, <http://dx.doi.org/10.1016/j.talanta.2015.09.046>.
- [3] X. Li, Q. Yang, H. Hua, L. Chen, X. He, C. Hu, Y. Xi, CdS/CdSe core/shell nanowall arrays for high sensitive photoelectrochemical sensors, *J. Alloy. Compd.* 630 (2015) 94–99, <http://dx.doi.org/10.1016/j.jallcom.2015.01.020>.
- [4] S. Adachi, *Properties of Group-IV, III-V and II-VI Semiconductors*, John Wiley & Sons, Chichester, 2005.
- [5] H. Uda, H. Yonezawa, Y. Ohtsubo, M. Kosaka, H. Sonomura, Thin CdS films prepared by metalorganic chemical vapor deposition, *Sol. Energy Mater. Sol. Cells* 75 (2003) 219–226, [http://dx.doi.org/10.1016/S0927-0248\(02\)00163-0](http://dx.doi.org/10.1016/S0927-0248(02)00163-0).
- [6] N. Maticiuc, J. Hiie, V. Mikli, T. Potlog, V. Valdna, Structural and optical properties of cadmium sulfide thin films modified by hydrogen annealing, *Mater. Sci. Semicond. Process.* 26 (2014) 169–174, <http://dx.doi.org/10.1016/j.mssp.2014.04.031>.

- [7] K. Ravichandran, P. Philominathan, Investigations on microstructural and optical properties of CdS films fabricated by a low-cost simplified spray technique using perfume atomizer for solar cell applications, *Sol. Energy* 82 (2008) 1062–1066, <http://dx.doi.org/10.1016/j.solener.2008.04.012>.
- [8] F. Lisco, P.M. Kaminski, A. Abbas, K. Bass, J.W. Bowers, G. Claudio, M. Losurdo, J. M. Walls, The structural properties of CdS deposited by chemical bath deposition and pulsed direct current magnetron sputtering, *Thin Solid Films* 582 (2015) 323–327, <http://dx.doi.org/10.1016/j.tsf.2014.11.062>.
- [9] A. Izgorodin, O. Winther-Jensen, B. Winther-Jensen, D.R. MacFarlane, CdS thin-film electrodeposition from a phosphonium ionic liquid, *Phys. Chem. Chem. Phys.* 11 (2009) 8532–8537, <http://dx.doi.org/10.1039/B906995J>.
- [10] K. Zarebska, M. Skompska, Electrodeposition of CdS from acidic aqueous thiosulfate solution—Investigation of the mechanism by electrochemical quartz microbalance technique, *Electrochim. Acta* 56 (2011) 5731–5739, <http://dx.doi.org/10.1016/j.electacta.2011.04.046>.
- [11] K. Premaratne, S.N. Akurathilaka, I.M. Dharmadasa, A.P. Samantilleka, Electrodeposition using non-aqueous solutions at 170 °C and characterisation of CdS, Cd₂Se_(1-x) and CdSe compounds for use in graded band gap solar cells, *Renew. Energy* 29 (2003) 549–557, <http://dx.doi.org/10.1016/j.renene.2003.08.002>.
- [12] A. Baral, C.K. Sarangi, B.C. Tripathy, I.N. Bhattacharya, T. Subbaiah, Copper electrodeposition from sulfate solutions—effects of seleniUm, *Hydro-metallurgy* 146 (2014) 8–14, <http://dx.doi.org/10.1016/j.hydromet.2014.03.001>.
- [13] P. Radhakrishnamurthy, A.K.N. Reddy, Mechanism of action of selenic acid in the electrodeposition of manganese, *J. Appl. Electrochem.* 7 (1977) 113–117, <http://dx.doi.org/10.1007/bf00611032>.
- [14] L.L. Shreir, J.W. Smith, Effects of addition agents on the cathode polarization potential during the electrodeposition of copper, *Trans. Faraday Soc.* 50 (1954) 393–403, <http://dx.doi.org/10.1039/TF9545000393>.
- [15] F. Kadirgan, D. Mao, W. Song, T. Ohno, B. McCandless, Properties of electrodeposited cadmium sulfide films for photovoltaic devices with comparison to CdS films prepared by other methods, *Turk. J. Chem.* 24 (2000) 21–33.
- [16] J.M. Nel, H.L. Gaigher, F.D. Auret, Microstructures of electrodeposited CdS layers, *Thin Solid Films* 436 (2003) 186–195, [http://dx.doi.org/10.1016/S0040-6090\(03\)00570-4](http://dx.doi.org/10.1016/S0040-6090(03)00570-4).
- [17] R. Das, S. Pandey, Comparison of optical properties of bulk and nano crystalline thin films of CdS using different precursors, *Int. J. Mater. Sci.* 1 (1s 1) (2011) 35–40 (<http://dx.doi.org/>).
- [18] K. Anuar, Z. Zulkarnain, N. Saravanan, M. Nazri, R. Sharin, Effects of electrodeposition periods and solution temperatures towards the properties of CdS thin films prepared in the presence of sodium tartrate, *Mater. Sci.* 11 (2) (2005) 101–104 (<http://dx.doi.org/>).
- [19] J. Nishino, S. Chatani, Y. Uotani, Y. Nosaka, Electrodeposition method for controlled formation of CdS films from aqueous solutions, *J. Electroanal. Chem.* 473 (1999) 217–222 (<http://dx.doi.org/>).
- [20] A.V. Kozyskiy, O.L. Stroyuk, S.Ya Kuchmiy, A.V. Mazanik, S.K. Poznyak, EA Streltsov, A.I. Kulak, O.V. Korolik, V.M. Dzhagan, Photoelectrochemical and Raman characterization of nanocrystalline CdS grown on ZnO by successive ionic layer adsorption and reaction method, *Thin Solid Films* 562 (2014) 56–62, <http://dx.doi.org/10.1016/j.tsf.2014.03.070>.
- [21] C.S. Venkateswaran, The Raman spectra of sulphur and phosphorus, *Proc. Ind. Acad. Sci. USA* 4 (1936) 414–418.
- [22] A.T. Ward, *Raman Spectroscopy of Sulfur, Sulfur-Selenium, and Sulfur Arsenic Mixtures*, Irerex Research Laboratories, Rochester, New York, 1968.
- [23] S.N. Yannopoulos, K.S. Andrikopoulos, Raman scattering study on structural and dynamical features of noncrystalline selenium, *J. Chem. Phys.* 121 (10) (2004) 4747–4758, <http://dx.doi.org/10.1063/1.1780151>.
- [24] V.V. Ison, A. Ranga Rao, V. Dutta, P.K. Kulriya, D.K. Avasthi, S.K. Tripathi, Swift heavy ion induced structural changes in CdS thin films possessing different microstructures: a comparative study, *J. Appl. Phys.* 106 (2009) 023508, <http://dx.doi.org/10.1063/1.3173180>.
- [25] ICDD file no: 01-089-0440, Bibl.: D. Rodic, V. Spasojevic, A. Bajorek, P.J. Onnerud, *Magn. Mater.*, vol. 152, 1996, p. 159.
- [26] ICDD file no: 01-074-9663, Bibl.: H. Sowa, *Solid State Sci.*, vol. 7, 2005, p. 73.
- [27] P.N. Gibsom, M.E. Ozzan, D. Lincot, P. Cowache, D. Summa, Modelling of the structure of CdS thin films, *Thin Solid Films* 361–362 (2000) 34–40, [http://dx.doi.org/10.1016/S0040-6090\(99\)00833-0](http://dx.doi.org/10.1016/S0040-6090(99)00833-0).
- [28] D. Lincot, B. Mokili, M. Froment, R. Cortes, M.C. Bernard, C. Witz, J. Lafait, Phase transition and related phenomena in chemically deposited polycrystalline cadmium sulfide thin films, *J. Phys. Chem.* 101 (1997) 2174–2181, <http://dx.doi.org/10.1021/jp962399c>.
- [29] R. Henríquez, A. Badán, P. Greza, E. Mu-noz, J. Vera, E.A. Dalchiale, R. E. Marotti, H. Gómez, Electrodeposition of nanocrystalline CdSe thin films from dimethyl sulfoxide solution: nucleation and growth mechanism, structural and optical studies, *Electrochim. Acta* 56 (2011) 4895–4901, <http://dx.doi.org/10.1016/j.electacta.2011.02.113>.
- [30] S.A. Gawali, C.H. Bhosale, Structural and optical properties of nanocrystalline CdSe and Al:CdSe thin films for photoelectrochemical application, *Mater. Chem. Phys.* 129 (2011) 751–755, <http://dx.doi.org/10.1016/j.matchemphys.2011.04.059>.
- [31] L.V. Azaroff, M.J. Buerger, *The Powder Method in X-Ray Crystallography*, McGraw-Hill, New York, 1958.
- [32] M.A. Islam, F. Haque, K.S. Rahman, N. Dhar, M.S. Hossain, Y. Sulaiman, N. Amin, Effect of oxidation on structural, optical and electrical properties of CdS thin films grown by sputtering, *Optik* 126 (2015) 3177–3180, <http://dx.doi.org/10.1016/j.ijleo.2015.07.078>.
- [33] J.D. Dow, D. Redfield, Toward a unified theory of Urbach's Rule and exponential absorption edges, *Phys. Rev. B* 5 (1972) 594, <http://dx.doi.org/10.1103/PhysRevB.5.594>.
- [34] V. Srikanth, D.R. Clarke, Optical absorption edge of ZnO thin films: the effect of substrate, *J. Appl. Phys.* 81 (1997) 6357, <http://dx.doi.org/10.1063/1.364393>.

Paper V

J. Maricheva, S. Bereznev, N. Maticiuc, O. Volobujeva, and J. Kois, Influence of selenous acid microadditive on electrochemical formation of CdS thin films, *Electrochim. Acta* 242 (2017) 280–286.



Influence of selenous acid microadditive on electrochemical formation of CdS thin films



Jelena Maricheva*, Sergei Bereznev, Natalia Maticiuc, Olga Volobujeva, Julia Kois

Department of Materials and Environmental Technology, Tallinn University of Technology, Ehitajate tee 5, 19086 Tallinn, Estonia

ARTICLE INFO

Article history:

Received 31 October 2016

Received in revised form 5 May 2017

Accepted 7 May 2017

Available online 8 May 2017

Keywords:

CdS
electrodeposition
formation
H₂SeO₃ microadditive
electrolyte

ABSTRACT

Electrodeposition of CdS in the presence of H₂SeO₃ microadditive at 50 °C in an aqueous solution was studied. Addition of H₂SeO₃ affects the growth of CdS thin films and improves structure ordering, coverage, and stoichiometry. The effect of H₂SeO₃ is advantageous as allows simultaneously improve the coverage and decrease the thickness of the CdS film during the electrodeposition process. Elemental Se detected in the as-deposited CdS films can be easily removed by a vacuum thermal treatment. The reported approach allows the electrodeposition of uniform polycrystalline photosensitive CdS thin films at reduced temperature. The optimal concentration of the microadditive at given conditions is reported.

© 2017 Elsevier Ltd. All rights reserved.

1. Introduction

CdS thin films have been intended for various applications such as photocatalytic devices [1], sensors [2], light-emitting diodes [3] or solar cells (SC) [4] due to unique electrical and optical properties. Low-cost chemical methods such as chemical bath deposition (CBD) [5], electrodeposition (ED) [6] and chemical spray pyrolysis [7] are usually applied for the CdS synthesis. The most efficient SC structures with a CdS buffer layer are based on CdTe [8], CZTS [9], CIGS [8] absorbers with laboratory efficiencies of 21.5%, 12.6%, 21.7%, respectively. Nowadays, the industry of the CIGS and CZTS SCs uses mainly the CBD CdS buffer [10], however, ED was also shown to be an effective method for CdS in a large-scale production [11]. Interest towards the ED method was brought back by the possibility to fabricate self-assembled nanostructures [12] with a high level of material utilization.

A general problem of the electrodeposited films is a deviation from stoichiometry, and required post-deposition thermal treatment of amorphous films. Improvement of the ED process can be achieved by changing external, electrical and solution variables of a system [13]. Yamaguchi et al. showed that too high cathodic potential over -0.75 V (SCE) increases deposition of metallic Cd, thus leading to the CdS and metallic Cd mixed phase formation [14]. Using of a deposition potential value lower than Cd reduction potential helps to achieve desired composition and crystalline

structure. Decrease of pH from 4.6 to 1.6 accelerated the film growth due to the improved cathodic current of a proton reduction without disordering of the crystalline structure [14]. Another possibility is to use complexing agents such as trisodium citrate, ethylenediamine tetraacetic acid (Edta), or tartaric acid in the solution, which shift the reduction potential and, hence, help to control the elemental composition, morphology, crystalline structure and electrical properties of deposits [15–17]. The use of a microadditive such as selenous acid (H₂SeO₃) was previously shown for the ED of metals and metal alloys [18,19], as it shifts the reduction potential, influences the polarization of the electrode, affecting the current efficiency and energy consumption of the ED process. In a previous work [20] we showed that addition of 0.05 mM of H₂SeO₃ promotes growth of nearly stoichiometric CdS films with improved coverage, and found appropriate pH of 3.5 and temperature of 50 °C for the ED.

In this work we prepare CdS films by the ED at fixed pH and temperature in order to study the CdS formation steps in the presence of H₂SeO₃ microadditive. In addition, we investigate structural and electrical properties of ED films and compare to CBD CdS films. Also we highlight advantageous effect of using H₂SeO₃ microadditive and report its optimal concentration.

2. Experimental

Electrochemical and photoelectrochemical (PEC) experiments were performed using a potentiostat Voltalab PGZ100 in a conventional three-electrode cell with an ITO/glass or CdS/ITO/

* Corresponding author.

E-mail address: jelena.maricheva@ttu.ee (J. Maricheva).

glass working electrode (WE), a platinum-wire counter electrode and a reference electrode.

CdS thin films were electrodeposited potentiostatically on ITO/glass substrates ($15 \Omega \text{ sq}^{-1}$). An aqueous working solution contained reagent grade 0.01 M CdCl_2 (99.0%, Alfa-Aesar), 0.02 M Na_2Edta (Sigma-Aldrich), 0.05 M $\text{Na}_2\text{S}_2\text{O}_3$ ($\text{Na}_2\text{S}_2\text{O}_3 \cdot 5\text{H}_2\text{O}$, >99.0%, Alfa-Aesar), and $0\text{--}10^{-4}$ M H_2SeO_3 (from SeO_2 , 99.4%, Alfa-Aesar) microadditive. In comparison to our previous work [20] we used lower H_2SeO_3 concentrations as the deposition time was increased up to 1.5 h. The ED was carried out at -1.2 V vs. mercury-mercurous sulfate ($\text{Hg}/\text{Hg}_2\text{SO}_4/\text{SO}_4^{2-}$) reference electrode (-0.8 V, $\text{Hg}/\text{Hg}_2\text{Cl}_2/\text{Cl}^-$ (SCE)) at 50°C and the pH 3.5 adjusted by 0.1 M HCl. The behavior of electrochemical systems was studied stepwise by cyclic voltammetry (CV) in order to understand the CdS formation steps in the presence of H_2SeO_3 . The CV experiments were held at the same conditions as for the ED on the ITO/glass WE in the potential range from -0.2 V to -1 V and from 0.6 V to -1 V vs. SCE scanning to the negative direction at the scan rate of 20 mV s^{-1} . In order to remove secondary phases ED CdS films were annealed in vacuum (10^{-5} Pa) at 120°C for 1 h.

We compared our ED CdS films with CBD CdS films, as the industry of CIGS and CZTS SCs uses CdS buffer layers deposited mainly by CBD [8,9]. CBD CdS thin films were obtained at 85°C and the pH 9.5 on ITO/glass substrates ($15 \Omega \text{ sq}^{-1}$) [21]. The thickness of CBD CdS thin film is in the range of 40–60 nm.

PEC measurements were performed as a comparative qualitative study of as-electrodeposited CdS/ITO/glass electrodes in aqueous background electrolyte of 0.1 M Na_2SO_4 (pH 7) under chopped white light illumination of 100 mW cm^{-2} under linearly increasing bias (from -0.5 V to $+0.5$ V). Morphology and thickness

of the CdS films were characterized by high-resolution scanning electron microscopy (HR-SEM, Zeiss Merlin). Elemental composition of the CdS films was determined by energy-dispersive full range X-ray microanalysis (EDX) system (Bruker Xflash6/30 detector) at an operating voltage of 7 kV. Quantification of EDX results was performed by means of interactive PB-ZAF standard less mode. X-ray diffraction (Rigaku Ultima IV diffractometer with $\text{Cu-K}\alpha$ radiation) was applied to analyze phase composition and crystalline structure of the deposited films. Surface potential and photoresponse of the obtained layers were measured by means of Kelvin probe (KP) method (KP Technology Scanning Kelvin Probe system 5050 equipped with a red laser of 5 mW cm^{-2} light beam intensity) with the method error of $\pm 5 \text{ mV}$.

3. Results and discussion

3.1. Cyclic voltammetry study of initial electrochemical system

An initial electrochemical system for the CdS formation on the ITO/glass substrate in the acidic aqueous electrolyte was studied by the CV (Fig. 1). For a blank solution (0.02 M Na_2Edta) two cathodic processes labeled as C1 and C2 starting at ca. -0.57 V were detected (Fig. 1a). The C1 slope can be described as an adsorption of the protonated Edta anions [21] on the surface of ITO. This slope is observed for all the solutions containing Na_2Edta , and for other electrochemical systems is labeled as C1' and C1'' (Fig. 1b, d). The cathodic peak C2 with onset at -0.83 V appears due to the reduction of ITO by the following reaction:

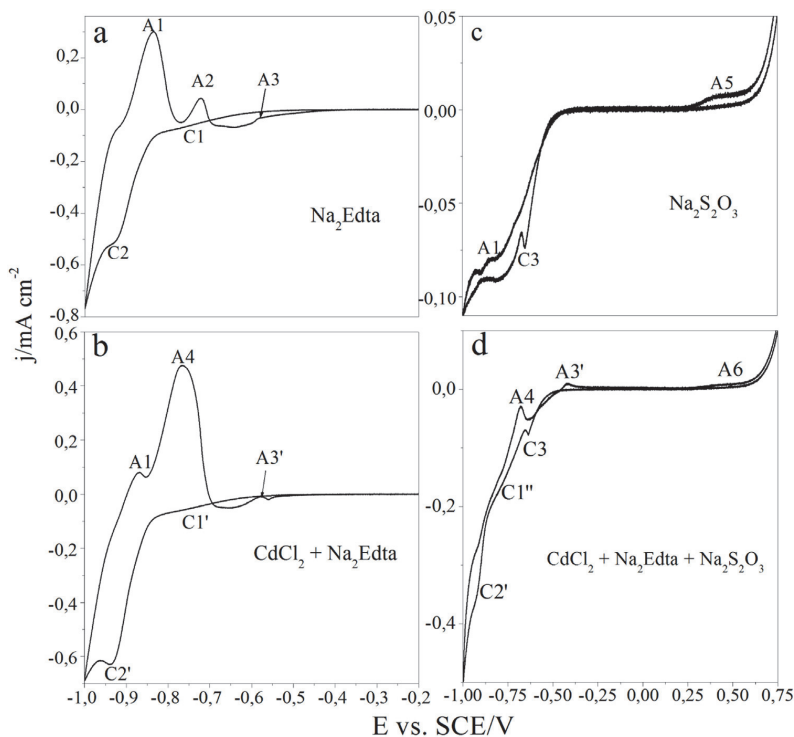


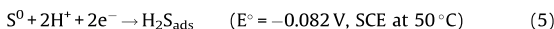
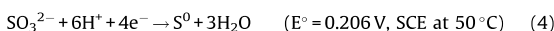
Fig. 1. Cyclic voltammograms obtained on ITO/glass in aqueous solutions containing (a) 0.02 M Na_2Edta , (b) 0.01 M CdCl_2 + 0.02 M Na_2Edta , (c) 0.05 M $\text{Na}_2\text{S}_2\text{O}_3$, and (d) 0.01 M CdCl_2 + 0.02 M Na_2Edta + 0.05 M $\text{Na}_2\text{S}_2\text{O}_3$ at pH 3.5 and 50°C at the scan rate 20 mV s^{-1} .

At the reverse scan peaks A1 and A2 with onsets at ca. -0.91 V and ca. -0.76 V corresponding to the oxidation reactions of In to In⁺ and In³⁺. The A3 peak may be attributed to the reactions of desorption of protonated Edta from ITO.

Fig. 1b shows the electrochemical behavior of the system with addition of 0.01 M CdCl₂ into the blank solution. The C2' cathodic peak indicates the reduction of Cd ions to Cd⁰ (reaction 2) and concurrent with the reduction peak of ITO. The A4 anodic peak corresponds to the oxidation of Cd reduced on the surface of ITO and is close to the oxidation A1 peak of In⁰. The potential value of the Cd reduction is shifted towards a more negative region due to the presence of Edta in the solution.



An electrochemical behavior of the system containing 0.05 M Na₂S₂O₃ is shown in Fig. 1c. According to Zarebska et. al [22] S₂O₃²⁻ anions disproportionate by the reaction (3) to S and sulfite anions. Under cathodic polarization products of the disproportionation reaction could be reduced to S⁰ (reaction 4), and finally to H₂S (reaction 5).



The peak of the reduction of SO₃²⁻ (reaction 4) was not detected at positive potentials during the cathodic sweep (Fig. 1c), due to slow rate of the reaction, and additional passivation of the cathode by the formed insulating S layer. The C3 slope with onset at -0.48 V corresponds to the reduction of S to H₂S on the surface of the electrode (reaction 5). Considering the presence of elemental sulfur in the solution formation of polysulfide anions may take place (reaction 6). Thus, the peak C3 may also indicate chemisorption of polysulfide anions to ITO, which may cause passivation represented by the decrease of the current density at -0.67 V [23].



The oxidation of S (reaction 7) may be responsible for the anodic peak A5 with onset at 0.27 V. Further, the same peak labeled as A5' arises for the solution containing CdCl₂, Na₂S₂O₃, Na₂Edta (Fig. 1d).



Cathodic processes of the solution containing 0.01 M CdCl₂, 0.05 M Na₂S₂O₃, 0.02 M Na₂Edta are depicted in Fig. 1d. The C1'' slope in the range of 0.66–0.86 V is attributed to the adsorption of H₂S (reaction 5). A chemical reaction between Cd cations and H₂S results in the CdS formation (reaction 8). Onset of the reduction of Cd²⁺ is at -0.86 V and labeled as C2' (reaction 2), further increase in the current density may be explained by the hydrogen reduction.



The anodic peak A6 with onset at 0.28 V indicates oxidation of S and may be attributed to the oxidative dissolution of CdS by the following reaction:



3.2. Study of CdS formation in the presence of H₂SeO₃ microadditive

When micromolar concentration of H₂SeO₃ is involved into the deposition process of CdS the electrochemical formation seems to

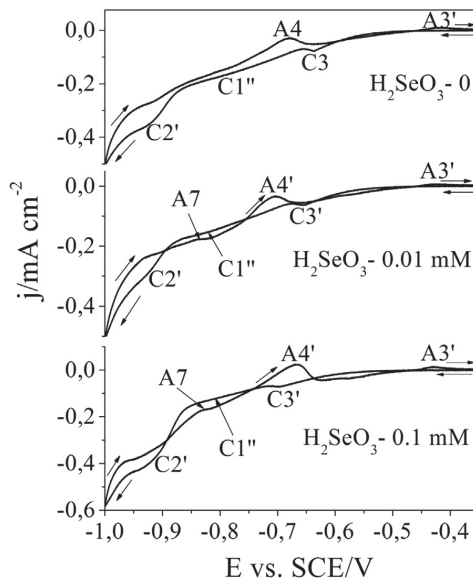
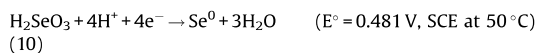


Fig. 2. Cyclic voltammograms obtained on ITO/glass in the solution containing 0.01 M CdCl₂, 0.05 M Na₂S₂O₃, 0.02 M Na₂Edta in the presence of various concentrations of H₂SeO₃ at pH 3.5 and 50 °C.

occur differently (Fig. 2). In acidic medium Se⁰ appears as a product of the H₂SeO₃ reduction by the following reaction:



Then elemental Se reduces to H₂Se on the surface of ITO (reaction 11) under a cathodic potential [24].



With addition of H₂SeO₃ the C3 peak is shifted (Fig. 2) towards lower potentials due to additional Se reduction reaction. The shifted peak labeled as C3' was identified at -0.66 V and -0.69 V for the films deposited with addition of 0.01 mM and 0.1 mM of H₂SeO₃, respectively, and is attributed to the simultaneous reduction of S (reaction 5) and Se (reaction 11) as well as chemisorption of polysulfide anions (reaction 6). The decrease of a valley following the C3' peak indicates deposition of a more conductive film. The onset of C1'' shifts from -0.65 V to -0.67 V and -0.72 V with addition of 10⁻⁵ M and 10⁻⁴ M of H₂SeO₃, respectively. This shift indicates a higher rate of CdS formation (reaction 8), which is represented by the decrease of the current density, and indicates more organized thin film formation. With addition of H₂SeO₃ into the working solution the slope C2', which is attributed to the reduction of Cd²⁺, shifts to more negative potential values, and a new peak A7 appears, corresponding to the reduction of Se phases.

A crossover of the cathodic and anodic branches of the CV appearing at about -0.89 V (Fig. 2) is typical to nucleation and surface phase formed on the electrode in the solution containing H₂SeO₃ [25].

On the basis of the CV study of the electrochemical systems discussed in Sections 3.1 and 3.2, as well as thermodynamic analysis of the reactions we propose an order of steps in the CdS electrochemical formation (Fig. 3). Fig. 3a shows a schematic representation of steps in the CdS thin film formation without H₂SeO₃. Firstly, S₂O₃²⁻ reduction (reaction 4) occurs on the surface

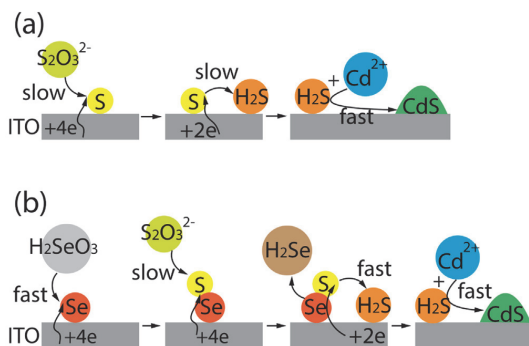


Fig. 3. Schematic representation of steps in CdS electrochemical formation (a) without and (b) in the presence of H_2SeO_3 .

of the ITO/glass substrate, which is followed by the S nuclei formation. This part of the process is slow as it requires 4 electrons to proceed, and defines the further CdS thin film formation. Gaining electrons S reduces (reaction 5) to H_2S adsorbed to the surface of the cathode. H_2S rapidly reacts with Cd^{2+} (reaction 8), and CdS forms. Fig. 3b shows the steps in electrochemical CdS formation in the presence of H_2SeO_3 . A more positive reduction potential of Se and more negative Gibbs free energy (ΔG) of the reaction promote its faster electrochemical reduction (reaction 10) which initiates Se nucleation prior to S nucleation. The growth of Se nuclei is limited due to low diffusion rate of H_2SeO_3 to the WE, although the reduction reaction of $\text{S}_2\text{O}_3^{2-}$ may occur on the surface of Se nucleus. In this case the reactions taking place on the cathode occur faster due to higher electrical conductivity of Se in comparison to S. The reactions of Se (reaction 10), S (reaction 4), H_2S (reaction 5) and CdS (8) formation are spontaneous ($\Delta G < 0$), but the reaction of H_2SeO_3 reduction (10) occurs first as it is characterized by the most negative ΔG value. Se itself may also reduce to H_2Se according to the reaction 11 and overcome into the liquid form. Although this reaction (reaction 11) is endergonic, it will take place under the applied potential of -0.8 V vs. SCE which is much higher than the standard reduction potential. Although, there is a theoretical probability of the CdSe formation on the surface of the WE none of our previous results [20] neither Raman nor XRD confirmed this phase presence in the CdS films in the range of sensitivity of these methods. Se species may provide a higher number of more conductive nucleation centers and, therefore, contribute to a faster formation of the CdS thin film with improved surface coverage.

In situ monitoring of the current density during the potentiostatic ED provides further analysis of the CdS thin film growth, and confirms the influence of the H_2SeO_3 on the process (Fig. 4). The first 4–8 s is an induction time corresponding to the incubation time for nucleation, and no dependence on the concentration of H_2SeO_3 in the solution is observed (Fig. 4-inset) [26]. However, further stages of the film growth are H_2SeO_3 dependent. Noteworthy that a number of nuclei may increase with time that agrees with a heterogeneous precipitation process present in the reduction-precipitation mechanism [26]. As the electrical conductivity of CdS ($10^{-8}\ \Omega^{-1}\ \text{sq}^{-1}$) is much lower than of ITO, further steps of the film growth may be indicated by the decrease of the current density. In the case of CdS electrodeposited from Se-free solution the deposition curve represents a descending monotonous slope with the increasing current density, which indicates a steady-state growth. The shape of the transient in the Se-free solution may be attributed to the growth of islands instead of a

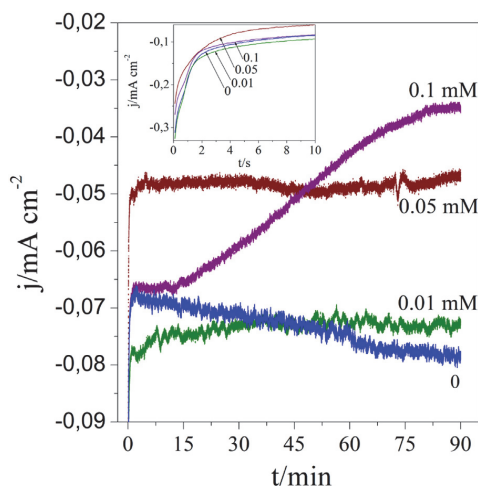


Fig. 4. j vs t transients obtained during ED of CdS thin film onto the ITO/glass substrate at -0.79 V vs. SCE for 1.5 h at $50\text{ }^\circ\text{C}$ from solution containing various concentrations of H_2SeO_3 .

continuous film [27]. Addition of 10^{-5} M and $5 \times 10^{-5}\text{ M}$ of H_2SeO_3 changes the transients' shape, which suggests increased amount of nucleation centres with time and further growth of a more compact CdS film. Addition of maximal concentration of 10^{-4} M H_2SeO_3 intensifies the growth of the CdS thin film (Fig. 4).

The growth of the CdS thin film can be divided into several stages (Fig. 5) considering previous discussion of the ED transients. When no H_2SeO_3 is added into the working solution, there are two main stages: S nuclei formation and slow growth of CdS islands. Inclusion of H_2SeO_3 into the process generates additional stages and makes the process of CdS formation more complex. In this case the initial stage is Se nuclei formation is followed by the adsorption of S on the surface of the cathode. Further, adsorbed S takes part in the growth of CdS islands. In addition, a secondary nucleation of Se may allow to achieve a continuous CdS thin film. It seems that at optimal H_2SeO_3 concentration a uniform, compact and well organized CdS thin film will form.

3.3. Characterization of electrodeposited CdS thin films

The morphology of the electrodeposited CdS films is influenced by the H_2SeO_3 concentration (Fig. 6). CdS thin film deposited without H_2SeO_3 represents a nonuniform layer with an

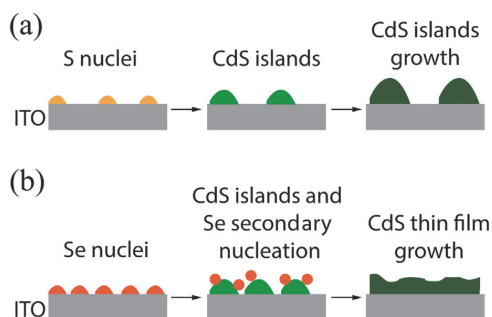


Fig. 5. The schematic representation of CdS thin film growth (a) without and (b) with H_2SeO_3 .

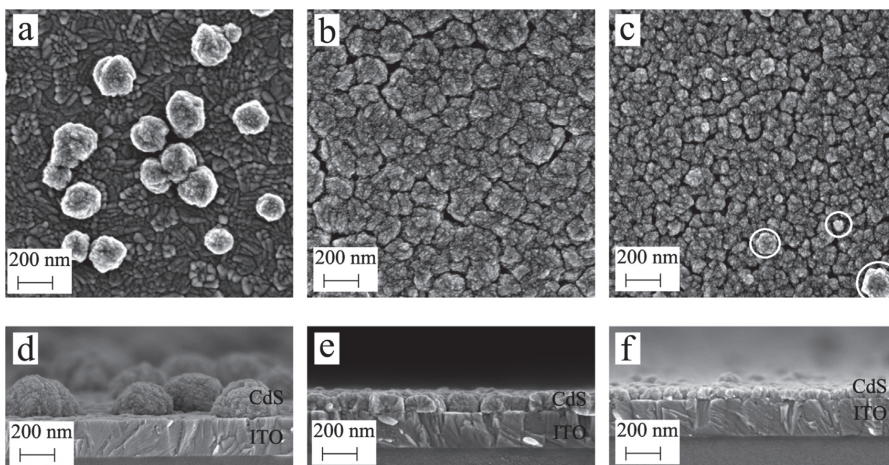


Fig. 6. HR-SEM surface and cross-sectional images of CdS films as-electrodeposited in the presence of (a, d) 0, (b, e) 5×10^{-5} M and (c, f) 10^{-4} M of H_2SeO_3 .

incontinuous island structure (Fig. 6a, d). The average island height is ca. 200 nm, and diameter is in the range of 200–300 nm. One can also observe a thin intermediate layer of several nanometres on the surface of ITO between islands (Fig. 6d). Addition of 5×10^{-5} M of H_2SeO_3 into the solution promotes formation of a continuous uniform polycrystalline CdS film with a thickness of ca. 103 nm, however some pinholes are observed. Such a changed microstructure of the CdS thin film confirms the impact of H_2SeO_3 on the ED of CdS (Fig. 3). Higher concentration of 10^{-4} M of H_2SeO_3 involved into the ED process leads to the decrease of the thickness to ca. 64 nm due to decrease of the islands size. In addition, there are some adherent secondary particles (marked with circles) on the surface of this film (Fig. 6c). Higher concentration of H_2SeO_3 contributes to the films thinning and improved coverage of the substrate.

In order to clarify the elemental composition of the CdS films and the adherent particles the EDX analysis was applied. Firstly, the increase of H_2SeO_3 concentration in the working solution shifts stoichiometry of as-deposited CdS (Table 1). Secondly, Se inclusion of 1.3 at.% and 4.7 at.% was detected in the CdS films deposited at 5×10^{-5} M and 10^{-4} M of H_2SeO_3 , respectively. The latter concentration of H_2SeO_3 in the solution led to the formation of Se-rich particles on the CdS surface (Fig. 6c). The detected Se seems to be a surface contamination, as it was easily removed by the vacuum treatment (Table 1). However, 1 at.% of Se remained in the treated CdS film deposited at 10^{-4} M of H_2SeO_3 . It seems that the applied vacuum treatment at $120^\circ C$ for 1 h is not sufficient for a complete removal of 4.7 at.% of Se.

The presence of Se in the as-deposited CdS films synthesized with H_2SeO_3 was confirmed also by the XRD analysis. CdS films obtained from the Se-free solution exhibit hexagonal and cubic structure corresponding to (100), (002), (101) (Fig. 7b-inset) and (311) (Fig. 7b) planes, respectively [28,29], similarly to our previous

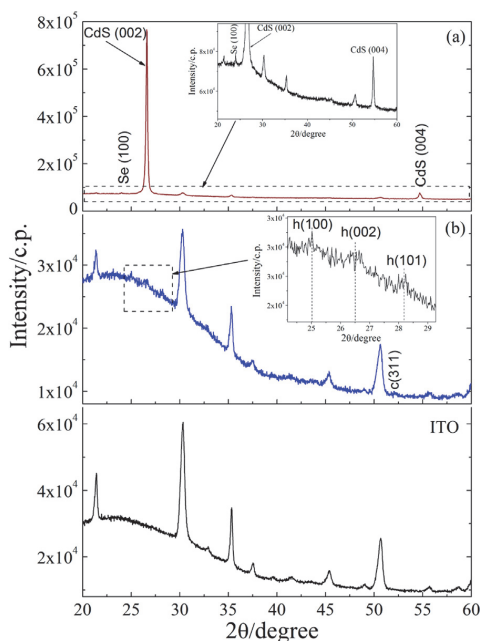


Fig. 7. XRD spectra of as-deposited CdS films electrodeposited at $50^\circ C$, pH 3.5 for 1.5 h from solutions containing CdCl₂, Na₂Edta, Na₂S₂O₃ and H_2SeO_3 of (a) 5×10^{-5} M and (b) without.

Table 1
Composition of ED CdS thin films as-deposited and thermally treated.

C_M H_2SeO_3 , mM	Cd, at.%		S, at.%		Se, at.%	
	As-dep.	Treated	As-dep.	Treated	As-dep.	Treated
0	50.0	50.3	50.0	49.7	0.0	0.0
0.05	52.4	50.4	46.3	49.6	1.3	0.0
0.1	51.5	50.6	43.8	48.4	4.7	1.0

results [20]. Other CdS peaks are suppressed by the ITO peaks that indicates poor coverage of the substrate. Addition of 0.05 mM of H_2SeO_3 into the solution promotes growth of CdS hexagonal crystalline structure with (002) and (004) planes [29,30]. This change can be caused by nucleation initiating Se identified at 24.0° exhibiting hexagonal structure with a (100) plane (Fig. 7a-inset) [31]. The improved intensity of the (002) CdS peak (Fig. 7a) indicates a better signal collected due to improved coverage of the CdS film deposited with the Se-containing microadditive which

modified the growth in terms of surface and interface energy (Section 3.2.). Due to improved ordering of the structure the thickness of the CdS films decreases (Fig. 6e, f) with a higher concentration of H_2SeO_3 that is in agreement with our previous results [20]. Concentration of $5 \cdot 10^{-5} \text{ M}$ of H_2SeO_3 seems to be optimal for the ED of CdS with improved coverage and stable hexagonal structure.

PEC measurements of CdS were carried out in 0.1 M Na_2SO_4 background solution at the pH 7 (Fig. 8). Photocurrent was observed for all the analyzed CdS films as a result of semiconductor photodecomposition with participation of minority charge carriers (holes) generated in the CdS films indicating an n-type photoconducting behavior [32]. CdS films electrodeposited in the presence of H_2SeO_3 show improved PEC performance similar to CBD CdS and may be explained by the differences caused by the microadditive in the structural, morphological, compositional properties of the films. Also enhanced photocurrent densities indicate the delay of the electron-hole pair recombination [33].

With addition of H_2SeO_3 the surface potential of CdS in dark increases from ca. -0.34 V to ca. -0.53 V , which is comparable to the value of stoichiometric CBD CdS (Fig. 9). This increase may be caused by incorporation of Se atoms into the surface (Table 1) causing the shift of the Fermi level. The photoresponse of CdS deposited with H_2SeO_3 appears due to trapped Se which is photosensitive under red light [34] or imperfect stoichiometry of the films. The photoresponse of ED CdS without Se may appear due to secondary phases present in the film.

4. Conclusions

This study showed that inclusion of the H_2SeO_3 microadditive into the electrochemical system has impact on the CdS ED process and modifies the growth of a film. The CdS thin film deposited

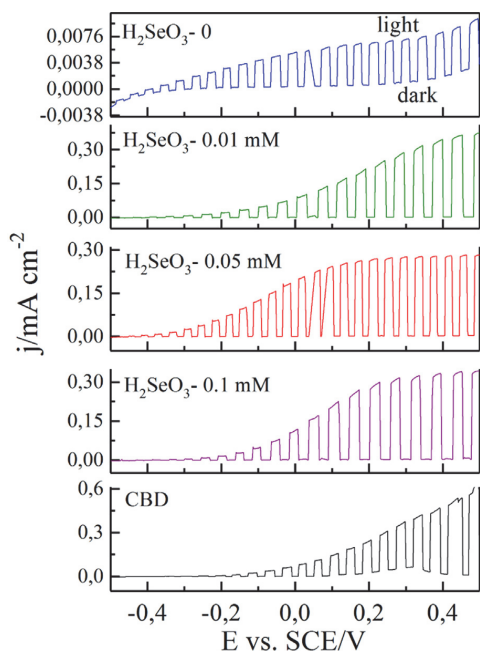


Fig. 8. Current vs potential curves of as-deposited CdS/ITO/glass electrodes in 0.1 M Na_2SO_4 background electrolyte for CdS deposited by ED at various H_2SeO_3 concentrations and by CBD.

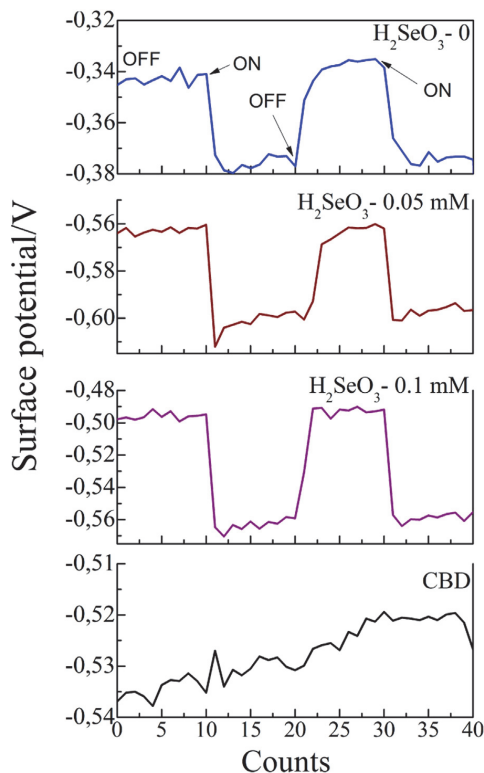


Fig. 9. KP measurements of as-deposited CdS films ED with and without H_2SeO_3 and CBD CdS film vs. gold-coated vibrating tip with a diameter of 2 mm under chopped red laser with a beam irradiation intensity of 5 mW cm^{-2} .

without H_2SeO_3 represents a nonuniform layer with an island structure, whereas continuous and uniform films were obtained with addition of H_2SeO_3 . Using $5 \cdot 10^{-5} \text{ M}$ H_2SeO_3 in the working solution causes formation of a more stable hexagonal CdS instead of the mixed-phase structure. Micromolar concentration of H_2SeO_3 in the solution is beneficial as it allows simultaneously improve the coverage and decrease the thickness of the CdS film during the ED. In addition, CdS films electrodeposited in the presence of H_2SeO_3 have enhanced PEC performance.

Secondary phases of Se not exceeding 4.7 at.% can be easily removed by vacuum treatment at 120°C . The H_2SeO_3 concentration of $5 \cdot 10^{-5} \text{ M}$ seems to be the optimal one for the ED of a continuous and compact CdS thin films at lower deposition temperature of 50°C .

Acknowledgements

This research was supported by the institutional research funding IUT19-28 and IUT19-4 of the Estonian Ministry of Education and Research, the European Union through the European Regional Development Fund, Project TK141, by University Base finance B54, PUT1495 Project and by ERA.NET RUS PLUS Project Flexapp (ETAG15028).

References

- [1] M.E. Khan, M.M. Khan, M.H. Cho, CdS-graphene nanocomposite for efficient visible-light-driven photocatalytic and photoelectrochemical applications, *J. Colloid Interface Sci.* 482 (2016) 221–232, doi:http://dx.doi.org/10.1016/j.jcis.2016.07.070.
- [2] Y. Wang, C. Gao, S. Ge, J. Yu, M. Yan, Plate like WO₃ sensitized with CdS quantum dots heterostructures for photoelectrochemical dynamic sensing of H₂O₂ based on enzymatic etching, *Biosens. Bioelectron.* 85 (2016) 205–211, doi:http://dx.doi.org/10.1016/j.bios.2016.05.015.
- [3] M. Molaie, M. Marandi, E. Saeivar-Iranizad, N. Taghavinia, B. Liu, H.D. Sun, X.W. Sun, Near-white emitting QD-LED based on hydrophilic CdS nanocrystals, *J. Lumin.* 132 (2012) 467–473, doi:http://dx.doi.org/10.1016/j.jlumin.2011.08.038.
- [4] H. Dang, V.P. Singh, S. Guduru, J.T. Hastings, Embedded nanowire window layers for enhanced quantum efficiency in window-absorber type solar cells like CdS/CdTe, *Sol. Energy Mater. Sol. Cells* 144 (2016) 641–651, doi:http://dx.doi.org/10.1016/j.solmat.2015.09.044.
- [5] S.M. Pawar, B.S. Pawar, J.H. Kim, Oh-Shim Joo, C.D. Lokhande, Recent status of chemical bath deposited metal chalcogenide and metal oxide thin films, *Curr. Appl. Phys.* 11 (2011) 117–161, doi:http://dx.doi.org/10.1016/j.cap.2010.07.007.
- [6] K. Schlesinger, N.R. Rajeshwar, in: M. Schlesinger, M. Paunovic (Eds.), *Electrodeposition of semiconductors, Modern Electroplating, Fifth Edition*, John Wiley & Sons, Inc, 2010.
- [7] A.A. Yadav, M.A. Barote, E.U. Mazumdar, Studies on nanocrystalline cadmium sulphide (CdS) thin films deposited by spray pyrolysis, *Solid state sci* 12 (2010) 1173–1177, doi:http://dx.doi.org/10.1016/j.solidstaterci.2010.04.001.
- [8] M.A. Green, K. Emery, Y. Hishikawa, W. Warta, E.D. Dunlop, Solar cell efficiency tables (version 47), *Prog. Photovolt: Res. Appl.* 24 (2016) 3–11, doi:http://dx.doi.org/10.1002/pip.2728.
- [9] W. Wang, M.T. Winkler, O. Gunawan, T. Gokmen, T.K. Todorov, Y. Zhu, D.B. Mitzi, Device characteristics of CZTSSe thin film solar cells with 12.6% efficiency, *Adv. Energy Mater.* 4 (2013) 1301465, doi:http://dx.doi.org/10.1002/aenm.201301465.
- [10] H. Ilchuk, P. Shapoval, V. Kusnez, Chemical surface deposition of CdS Ultra thin films from aqueous solutions, in: L.A. Kosyachenko (Ed.), *Solar Cells –Thin-film technologies*, InTech, 2011 ISBN: 978-953-307-570-9, available from: <http://www.intechopen.com/books/solar-cells-thin-film-technologies/chemical-surface-deposition-of-cds-ultra-thin-films-from-aqueous-solutions>.
- [11] I.M. Dharmadasa, P.A. Bingham, O.K. Echendu, H.I. Salim, T. Druffel, R. Dharmadasa, G.U. Sumanasekera, R.R. Dharmasena, M.B. Dergacheva, K.A. Mit, K.A. Urazov, L. Bowen, M. Walls, A. Abbas, Fabrication of CdS/CdTe-based Thin Film Solar Cells Using an Electrochemical Technique, *Coatings* 4 (2014) 380–415, doi:http://dx.doi.org/10.3390/coatings4030380.
- [12] H. Karami, A. Kaboli, Pulsed Current Electrochemical Synthesis of Cadmium Sulfide Nanofibers, *Int. J. Electrochem. Sci.* 5 (2010) 706–719 https://www.researchgate.net/publication/260364216_Pulsed_Current_Electrochemical_Synthesis_of_Cadmium_Sulfide_Nanofibers.
- [13] A.J. Bard, L.R. Faulkner, in: D. Harris, E. Swain, C. Robey, E. Aiello (Eds.), *Electrochemical methods: Fundamentals and applications*, 2nd edition, John Wiley & Sons, Inc., New York, 2001, pp. 9–23.
- [14] K. Yamaguchi, T. Yoshida, T. Sugiura, H. Minoura, A Novel Approach for CdS Thin-Film Deposition: Electrochemically Induced Atom-by-Atom Growth of CdS Thin Films from Acidic Chemical Bath, *J. Phys. Chem. B* 102 (1998) 9677–9686, doi:http://dx.doi.org/10.1021/jp9824757.
- [15] E.M. Mkawi, K. Ibrahim, M.K.M. Ali, M.A. Farrukh, A.S. Mohamed, N.K. Allam, Effect of complexing agents on the electrodeposition of Cu-Zn-Sn metal precursors and corresponding Cu₂ZnSnS₄-based solar cells, *J. Electroanal. Chem.* 735 (2014) 129–135, doi:http://dx.doi.org/10.1016/j.jelechem.2014.10.021.
- [16] L. Liu, S. Yellinek, I. Valding, A. Donval, D. Mandler, Important implications of the electrochemical reduction of ITO, *Electrochim. Acta* 176 (2015) 1374–1381, doi:http://dx.doi.org/10.1016/j.electacta.2015.07.129.
- [17] A. Ghazali, Z. Zainal, M.Z. Hussein, A. Kassim, Cathodic electrodeposition of SnS in the presence of EDTA in aqueous media, *Sol. Energy Mater. Sol. Cells* 55 (1998) 237–249, doi:http://dx.doi.org/10.1016/S0927-0248(98)00106-8.
- [18] P. Radhakrishnu, A.K.N. Reddy, Mechanism of action of selenious acid in the electrodeposition of manganese, *J. Appl. Electrochem.* 7 (1977) 113–117, doi:http://dx.doi.org/10.1007/BF00611032.
- [19] L.L. Shreir, J.W. Smith, Effects of addition agents on the cathode polarization potential during the electrodeposition of copper, *Trans. Faraday Soc.* 50 (1954) 393–403, doi:http://dx.doi.org/10.1039/TF9545000393.
- [20] J. Maricheva, S. Bereznev, R. Naidu, N. Maticic, V. Mikli, J. Kois, Improved electrodeposition of CdS layers in presence of activating H₂SeO₃ microadditive, *Mater. Sci. Semicond. Process.* 54 (2016) 14–19, doi:http://dx.doi.org/10.1016/j.mssp.2016.06.013.
- [21] N. Maticic, J. Hiie, V. Mikli, T. Potlog, V. Valdna, Structural and optical properties of cadmium sulfide thin films modified by hydrogen annealing, *Mater. Sci. Semicond. Process.* 26 (2014) 169–174, doi:http://dx.doi.org/10.1016/j.mssp.2014.04.031.
- [22] K. Zarebska, M. Skompska, Electrodeposition of CdS from acidic aqueous thiosulfate solution- investigation of the mechanism by electrochemical quartz microbalance technique, *Electrochim. Acta* 56 (2011) 5731–5739, doi:http://dx.doi.org/10.1016/j.electacta.2011.04.046.
- [23] E. Fatas, P. Herrasti, Voltammetric study of the electrodeposition of CdS films from propylene carbonate solutions, *Electrochim. Acta* 33 (1988) 959–965, doi:http://dx.doi.org/10.1016/0013-4686(88)80095-1.
- [24] M. Bouroushian, *Electrochemistry of Metal Chalcogenides, Monographs in Electrochem*, Springer-Verlag, Berlin/Heidelberg, 2010, doi:http://dx.doi.org/10.1007/978-3-642-03967-6_2.
- [25] D. Grujicic, B. Pesic, Electrodeposition of copper: the nucleation mechanisms, *Electrochim. Acta* 47 (2002) 2901–2912, doi:http://dx.doi.org/10.1016/S0013-4686(02)00161-5.
- [26] F. Lai, J. Liu, Z. Li, Y. Zhang, Nucleation and growth of selenium electrodeposition onto tin oxide electrode, *J. Electroanal. Chem.* 639 (2010) 187–192, doi:http://dx.doi.org/10.1016/j.jelechem.2009.11.026.
- [27] H. Majidi, J.B. Baxter, Electrodeposition of CdSe coatings on ZnO nanowire arrays for extremely thin absorber solar cells, *Electrochim. Acta* 56 (2011) 2703–2711, doi:http://dx.doi.org/10.1016/j.electacta.2010.12.044.
- [28] M.A. Barote, A.A. Yadav, E.U. Masumdar, Synthesis, characterization and photoelectrochemical properties of n-CdS thin films, *E. U. Physica B* 406 (2011) 1865–1871, doi:http://dx.doi.org/10.1016/j.physb.2011.02.044.
- [29] H. Sowa, On the mechanism of the pressure-induced wurtzite- to NaCl-type phase transition in CdS: an X-ray diffraction study, *Solid State Sci.* 7 (2005) 73–78, doi:http://dx.doi.org/10.1016/j.solidstaterci.2004.10.011.
- [30] T. Torimoto, N. Tsumura, H. Nakamura, S. Kuwabata, T. Sakata, H. Mori, H. Yoneyama, Photoelectrochemical properties of size-quantized semiconductor photoelectrodes prepared by two-dimensional cross-linking of monodisperse CdS nanoparticles, *Electrochim. Acta* 45 (2000) 3269–3276 PII: S0013-4686(00)00443-6.
- [31] D.R. McCann, L.J. Cartz, Bond distances and chain angle of hexagonal selenium at high pressure, *J. Appl. Phys.* 43 (1972) 4473, doi:http://dx.doi.org/10.1063/1.1660946.
- [32] H. Gerischer, Photoassisted interfacial electron transfer, *Surf. Sci.* 101 (1980) 518–530, doi:http://dx.doi.org/10.1016/0039-6028(80)90646-9.
- [33] C. Liu, J. Chen, H. Che, K. Huang, P.A. Charpentier, W.Z. Xu, W. Shi, H.J. Dong, Construction and enhanced photocatalytic activities of a hydrogenated TiO₂ nanobelt coated with CdS/MoS₂ nanosheets, *RSC Adv.* 7 (2017) 8429–8442, doi:http://dx.doi.org/10.1039/C6RA28479E.
- [34] K.J. Siemsen, H.D. Riccius, Infrared photoconductivity of polycrystalline selenium, *Solid State Commun.* 11 (1972) 1379–1383, doi:http://dx.doi.org/10.1016/0038-1098(72)90547-9.

Paper VI

J. Gurevits, J. Kois, S. Bereznev, E. Mellikov, A. Öpik, Electrochemical Synthesis of CdSe/CdTe Nanowires for Hybrid Photovoltaic Structures. *MRS Proceedings* 3 (2014) 1707.

Electrochemical synthesis of CdSe/CdTe nanowires for hybrid photovoltaic structures

Jelena Gurevits, Sergei Bereznev, Valdek Mikli, Revathi Naidu, Enn Mellikov, Julia Kois
Tallinn University of Technology, Department of Materials Science, Ehitajate tee 5, 19086
Tallinn, Estonia

ABSTRACT

Advanced electrochemical technique was elaborated to fabricate self-organized CdSe nanowire structures from aqueous electrolytes on ITO coated glass substrates. We have recently been demonstrated successful electrochemical formation of free-assistent CdSe nanowire structures with diameter around 30 nm. This work has extended our previous research of electrodeposition of Cd chalcogenide (CdSe, CdS) nanowires to formation of core-shell CdSe/CdTe photosensitive nanowire structures. CdSe nanowire structures were synthesized potentiostatically from an acidic solution of H_2SeO_3 and CdCl_2 at room temperature. Then the CdSe (core) nanowires were further passivated with CdTe (shell) thin film by method of electrochemical deposition from acidic solution of H_2TeO_3 and CdCl_2 . The effect of interfacial passivation with CdTe layer on the performance of the prepared photovoltaic structures was investigated and special account was paid to the morphology, composition and photovoltaic properties of obtained CdSe/CdTe nano-layers. It should be noted, that electrically conductive polymer photoabsorbers (poly (3-octylthiophene) etc.) were applied successfully for preparation of high work-function ohmic contact-sensitizer layer to CdTe shells. The electrodeposition and spin-casting techniques were applied step-by-step to prepare complete hybrid photovoltaic structures.

INTRODUCTION

In recent years, studies of hybrid nanostructures have attracted a great interest in the field of solar cell application, [1]. Various nanosized semiconductors have been studied, based on CdS [2], CdSe [3], CdTe [4] and Sb_2S_3 [5], in the fabrication of optoelectronic devices. Among these materials, CdSe and CdTe are promising candidates for hybrid solar cell structures, due to its optical energy band gap of about 1.70 eV and 1.45 eV respectively, which have a strong absorption in solar spectrum.

Different aqueous and nonaqueous methods have been applied for the synthesis of CdSe nanostructures e.g. chemical bath deposition, dip-coating, ionic layer adsorption, molecular beam epitaxy and chemical vapour deposition [6, 7]. As an alternative, electrodeposition is a commercially important process because of its simplicity, low cost as well as possibility for large-scale production. A method for electrochemical deposition of various self organized CdSe structures (nanofibers, nonotubes and pearl-chain structures) was developed in our laboratory [8].

In this work we used electrodeposited CdSe nanowire core and CdTe shell with a covered conductive polymer layer to fabricate hybrid PV structures.

EXPERIMENTAL DETAILS

Hybrid PV glass/ITO/CdSe/CdTe/polymer composite nanowire structures were fabricated in three main steps: (i) electrochemical deposition of CdSe nanowires on glass/ITO substrate, (ii) electrodeposition of CdTe thin layer on CdSe nanowires and (iii) coating of fabricated CdSe/CdTe structure with conductive polymer contact-sensitizer layer.

Preparation of CdSe nanowires. CdSe nanowires were electrodeposited in a standard three-electrode electrochemical cell (EC). Saturated calomel electrode (SCE) was used as reference electrode, platinum wire was used as counter electrode and glass/ITO substrate was used as working electrode (WE). Potentiostat/galvanostat Voltalab PGZ100 was applied for the electrodeposition. CdSe nanowires were electrodeposited from aqueous electrolyte of H_2SeO_3 and CdCl_2 with concentration of 10 mM and 25 mM respectively. The pH of the solution was around 2.4 adjusted with 0.1 M hydrochloric acid. The deposition was performed potentiostatically under cathodic potential value of -750mV vs. SCE during 20 min at room temperature. As-grown CdSe nanowires were annealed on a precision graphite hot-plate in air at 350 °C for 30 min.

Preparation of CdSe/CdTe structure. CdTe layer was formed by the photo-assisted electrodeposition on the annealed CdSe nanowire structure. During deposition glass/ITO/CdSe WE was illuminated through the solution with a white light of 100 mW/cm² intensity to facilitate formation of CdTe layer onto photoactive CdSe nanostructure and improve quality of obtained structure. Photo-assisted electrodeposition was performed potentiostatically at -600 mV vs. SCE during 30 min at room temperature in the aqueous solution of H_2TeO_3 and CdCl_2 with concentrations of 1 mM and 50 mM respectively. The pH value of 1.8 was adjusted with 0.1 M hydrochloric acid. Obtained ITO/CdSe/CdTe structures were secondary annealed on a precision graphite hot-plate in air at 200 °C for 30 min.

Preparation of conductive polymer contact-sensitizer layer. Part of prepared glass/ITO/CdSe/CdTe PV structures was completed with a conductive polymer contact-sensitizer layer. Two types of conductive polymer photoabsorbers (i) well-known poly(3-octylthiophene) (P3OT) and (ii) the “last generation” poly[N-9'-heptadecanyl-2,7-carbazole-alt-5,5-(4',7'-di-2-thienyl-2',1',3'-benzothiadiazole)] (PCDTBT) (Aldrich) were deposited. Both polymers were deposited in form of composite with electron acceptor of substituted fullerene phenyl-C61-butyric acid methyl ester (PCBM) (Aldrich). The solutions for spin-casting were prepared in the following concentrations: 1.5% P3OT/1.5% PCBM and 1.5% PCDTBT/1.5% PCBM in chlorobenzene. The solutions were prepared using Vortex Genie 2 shaker for 24 h with following ultrasonic treatment in VWR Ultrasonic bath for 2 h. Double-speed spin-casting technique (800 rpm for 9 sec/ 3000 rpm for 60 sec) was applied for the deposition of the composite layers. Then, glass/ITO/CdSe/CdTe/composite structures were annealed on a hot-plate in pure argon atmosphere at 150 °C for 10 min in Omni Lab glove box. Finally, graphite suspension dot contacts (Alfa Aesar) were painted on the investigated structures and dried for 1 h in an oven at 60 °C.

Characterization of the structures. The morphology of prepared structures was characterized by high-resolution scanning electron microscopy (HR-SEM) (Zeiss Ultra 55 microscope). Composition of CdSe nanowires was determined by energy dispersive X-ray (EDX) analysis (Zeiss ULTRA 55 HRSEM microscope equipped with Röntec EDX Xflash 3001 detector). Surface composition of electrodeposited layers was determined by Micro Raman spectroscopy (Horiba's LabRam high-resolution spectrometer). PV parameters of prepared glass/ITO/CdSe/CdTe and glass/ITO/CdSe/CdTe/composite structures were measured using po-

tentiostat/galvanostat Autolab PGSTAT 30. A calibrated halogen lamp was used for the I–V measurements under white-light illumination at an intensity of 100 mW/cm².

RESULTS AND DISCUSSION

Preparation and investigation of the CdSe/CdTe shell-core nanowire structures.

EDX analysis of as-deposited CdSe nanowires showed stoichiometric composition, where Cd and Se ratio is 1:1, this is in a good agreement with our previous results. Figure 1 shows the surface and cross-sectional HR-SEM images of as-deposited and annealed ITO/CdSe structures. The average diameter of CdSe nanowires is about 30 nm (Figure 1a), whereas the length of the nanowires is approximately 1 μ m. Cross-sectional image (Figure 1b) of as-deposited CdSe structure shows a bottom dense nanocrystalline-amorphous [9] part with a thickness of about 400 nm, whereas the thickness of the full CdSe layer is about 600 nm.

Figure 1c and Figure 1d show the surface of CdSe and cross-sectional view of ITO/CdSe annealed in air at 350 $^{\circ}$ C for 30 min, respectively. After annealing CdSe nanowires demonstrate a pearl-chain structure with pearls diameter of about 40-60 nm and length up to 1 μ m (Figure 1c). Cross-sectional image of annealed CdSe layer (Figure 1d) shows that the thickness of the layer did not change (\sim 600 nm). Bottom part of CdSe layer shows growth of grains with a grain size of about 50-100 nm and demonstrates more visible grain boundaries in comparison with non-annealed layer (Figure 1b).

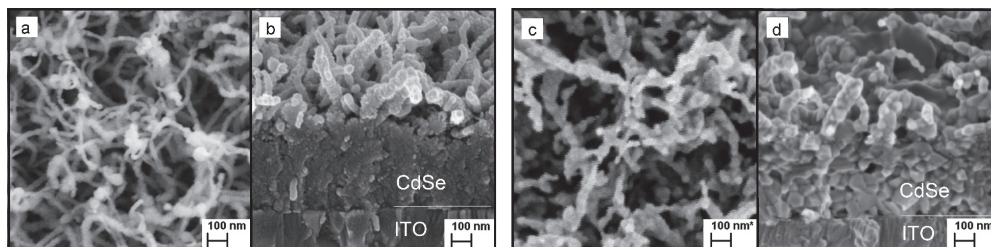


Figure 1. HR-SEM images of as-deposited ITO/CdSe: (a) surface and (b) cross-section; annealed ITO/CdSe: (c) surface and (d) cross-section.

To improve PV properties of obtained CdSe nanostructures thin CdTe layers were electrodeposited onto annealed glass/ITO/CdSe structures under white light illumination with following thermal annealing in air at 200 $^{\circ}$ C for 30 min. Surface and cross-sectional HR-SEM images of the obtained CdSe/CdTe structure are shown in Figure 2 (a, b). Fabricated CdSe/CdTe nanowires have a diameter of about 80-100 nm (Figure 2a) vs. 30 nm for initial CdSe nanowires (Figure 1a) i.e. CdSe core nanowires are covered with a thin CdTe layer with the CdTe grains size of about 10-20 nm. It can be seen, that round-shaped thickenings (caps) with a diameter from 100 to 200 nm cover the tops of CdSe/CdTe nanowires. Overall CdSe/CdTe structure thickness is about 700 nm (Figure 2b). Observed morphology of prepared CdSe/CdTe nanostructures confirms preferable CdTe grains-growth along to the CdSe nanowires direction as an “extension” of CdSe nanowires on the basis of the similar mechanism of CdTe nucleation as for CdSe [10, 11].

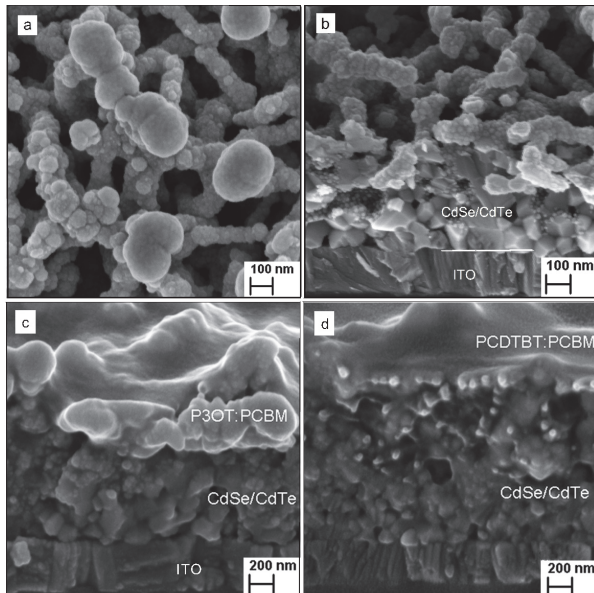


Figure 2. HR-SEM images of annealed glass/ITO/CdSe/CdTe structure: (a) CdTe surface and (b) cross-section; and glass/ITO/CdSe/CdTe structures coated with (c) P3OT:PCBM and (d) PCDTBT:PCBM composite layers.

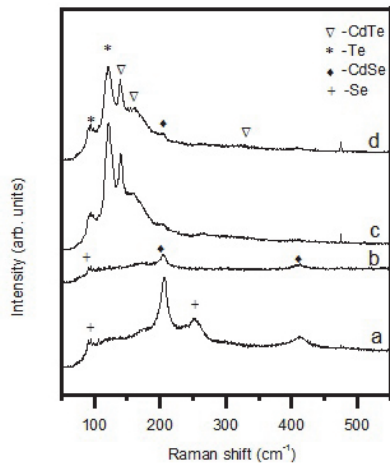


Figure 3. Raman spectra of the surface of CdSe: (a) as-deposited, (b) annealed; and CdSe/CdTe: (c) as-deposited, (d) annealed.

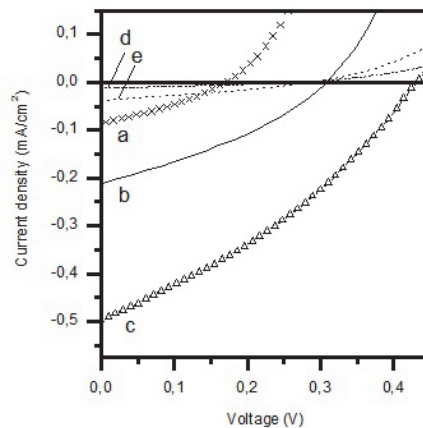


Figure 4. I-V characteristics of complete PV structures under irradiance of 100 mW/cm² intensity: (a) annealed ITO/CdSe/CdTe; ITO/CdSe/CdTe/P3OT:PCBM (b) as-deposited, (c) annealed; ITO/CdSe/CdTe/PCDTBT:PCBM (d) as-deposited, (e) annealed.

Figure 3 shows the Raman spectra of the surface of as-deposited and annealed glass/ITO/CdSe and glass/ITO/CdSe/CdTe structures. The spectra (a, b) show the peaks at around 204 cm^{-1} , 411 cm^{-1} attributable to presence of CdSe [12, 13] and Se (peaks at around 100 cm^{-1} , 250 cm^{-1} [14] bands) in as-deposited glass/ITO/CdSe structure (Figure 3a). For annealed glass/ITO/CdSe structure (Figure 3b) mainly CdSe peaks are observed. Figure 3c shows the Raman spectra of the surface of as-deposited glass/ITO/CdSe/CdTe structure, where peaks at around 140 cm^{-1} , 163 cm^{-1} and 330 cm^{-1} belong to CdTe [15] and Te band is at 94 cm^{-1} , 120 cm^{-1} [16]. After annealing of the glass/ITO/CdSe/CdTe structure in air at $200\text{ }^{\circ}\text{C}$ for 30 min Te peak's intensity decreases (Figure 3d). For both as-deposited and annealed glass/ITO/CdSe/CdTe structures CdSe low-intensity peak at 206 cm^{-1} is observed.

Preparation and investigation of the hybrid structure. Cross-sectional micrographs of complete glass/ITO/CdSe/CdTe structures with composite contact-sensitizer layers of P3OT:PCBM and PCDTBT:PCBM are represented in Figure 2c and 2d respectively. From the micrographs it can be seen that composite layers cover CdSe/CdTe nanolayer uniformly with good adhesion, without cracks and holes. It should be noted, that P3OT:PCBM layer (Figure 2c) penetrates into the porous layer of CdSe/CdTe more deeply in comparison with the PCDTBT:PCBM composite layer (Figure 2d) (probably due to the difference in the viscosity of the solutions for spin-casting). In further work we plan to use different concentrations of PCDTBT:PCBM to obtain deeper penetration of the polymer composite layer into the structure comparable with the diffusion of P3OT:PCBM. The overall thickness of the prepared CdSe/CdTe/composite structures was about $1.2\text{ }\mu\text{m}$.

I-V characterisation of the complete PV structures. I-V characteristics of glass/ITO/CdSe/CdTe and glass/ITO/CdSe/CdTe/composite structures are represented in Figure 4. It can be seen that prepared glass/ITO/CdSe/CdTe structure (Figure 4a) is photosensitive (open circuit voltage (V_{oc}) around 200 mV) and PV parameters are seriously improved as the result of the P3OT:PCBM composite layer deposition (Figure 4b and 4c).

It should be noted, that the glass/ITO/CdSe/CdTe structure coated with PCDTBT:PCBM has a short circuit current density (I_{sc}) value lower than uncovered structure. On the other hand, the structure coated with PCDTBT:PCBM demonstrates V_{oc} value of about 0.26 V , that is higher than V_{oc} of uncovered structure. It can be seen, that thermal treatment of the glass/ITO/CdSe/CdTe/PCDTBT:PCBM structures improves its PV properties (V_{oc} increased up to 0.29 V). FF of the structures coated with PCDTBT:PCBM was about 30%.

More promising results were achieved so far by coating of the glass/ITO/CdSe/CdTe structure with P3OT:PCBM layer. As deposited ITO/CdSe/CdTe/P3OT:PCBM structure (Figure 4b) has V_{oc} of about 0.3 V and the short circuit current density is about 0.2 mA/cm^2 . Annealing of the glass/ITO/CdSe/CdTe/P3OT:PCBM structure in argon at $150\text{ }^{\circ}\text{C}$ for 10 min improves current-voltage characteristics, where V_{oc} increases up to 0.43 V and I_{sc} value was about 0.5 mA/cm^2 (Figure 4c). FF value of the structures coated with P3OT:PCBM was about 33%.

It should be noted, that PV performance of prepared CdSe/CdTe nanostructures is relatively low so far. On the other hand, conductive polymer composite layer improves significantly PV parameters of complete structures i.e. on the basis of improving of the initial CdSe/CdTe nanolayers the overall efficiency of complete hybrid structures can be improved also. Moreover, the door is open to increase quality of PCDTBT:PCBM layers e.g. varying the concentration of the solution for spin-casting.

CONCLUSIONS

CdSe/CdTe shell-core nanowire structures were successfully synthesized by electrochemical technique. EDX analysis of as-deposited CdSe nanowires showed stoichiometric composition with Cd and Se ratio of 1:1. The as-deposited CdSe structures showed nanowire morphology, whereas the pearl-chain structure is established for annealed structures at 350 °C for 30 min. CdSe shell nanowires were covered electrochemically with a thin CdTe layer with a grain size of about 10 - 20 nm and CdTe caps on the tops. It was found, that the deposition of P3OT:PCBM and PCDTBT:PCBM established a contact-sensitizer layer with glass/ITO/CdSe/CdTe structures. The best structure was formed with the presence of P3OT:PCBM composite layer so far showed an open circuit voltage of 430 mV and a short circuit current density of about 0.5 mA/cm² under white light illumination of 100 mW/cm² intensity.

ACKNOWLEDGEMENTS

This work was supported by institutional research funding IUT19-28 of the Estonian Ministry of Education and Research and European Social Fund's Doctoral Studies and Internationalisation Programme DoRa, which is carried out by Foundation Archimedes.

REFERENCES

1. E. Maiera, T. Rath, W. Haas, O. Werzer, R. Saf, F. Hofer, D. Meissner, O. Volobujeva, S. Bereznev, E. Mellikov, H. Amenitsch, R. Resel and G. Trimmel, *Solar Energy Materials and Solar Cells* **95**, 1354–1361 (2011)
2. I.S. Kim, Y. Kang, H. Lee and D. Kim, *Solid State Phenom.* **124-126**, 967-970 (2007)
3. Y. Chen, L. Wei, G. Zhang and J. Jiao, *Nanoscale Res. Lett.* **7**, 516 (2012)
4. V. Corregidor, L.C. Alves, N. Franco, M.A. Barreiros, N.V. Sochinskii and E. Alves, *Nucl. Instrum. Meth. B.* **306**, 218-221 (2013)
5. J.H. Heo, S.H. Im, H.-J. Kim, P.P. Boix, S.J. Lee, S.I. Seok, I.M. Sero and J. Bisquert, *J. Phys. Chem. C.* **116**, 20717-20721 (2012)
6. Y. Choi, M. Seol, W. Kim and K. Yong, *J. Phys. Chem. C.* **118**(11), 5664-5670 (2014)
7. H. Lee, M. Wang, P. Chen, D.R. Gamelin, S.M. Zakeeruddin, M. Gratzel and M.K. Nazeeruddin, *Nano Lett.* **9**(12), 4221-4227 (2009)
8. J. Kois, S. Bereznev, O. Volobujeva, J. Gurevits and E. Mellikov, *J. Cryst. Growth.* **320**, 9-12 (2011)
9. J. Kois, S. Bereznev, J. Gurevits, O. Volobujeva, *Mater. Lett.* **95**, 110-113 (2012)
10. J. Kois, J. Gurevits, S. Bereznev, O. Volobujeva, A. Öpik, E. Mellikov, *Appl. Surf. Sci.* **283**, 982-985 (2013)
11. Q. Li, L. Tian, K. Chi, H. Yang, M. Sun, W. Fu, *Appl. Surf. Sci.* **270**, 707-711 (2013)
12. R. Ionov and T. Dudev, *Appl. Phys. A* **55**, 203-206 (1992)
13. A.M. Kelley, Q. Dai, Z. Jiang, J.A. Baker, D.F. Kelley, *Chem. Phys.* **422**, 272-276 (2013)
14. I.L. Li, S.C. Ruan, Z.M. Li, J.P. Zhai and Z.K. Tang, *Appl. Phys. Lett.* **87**, 071920 (2005)
15. S.C. Ray and K. Mallick, *Int. J. Chem. Eng. Appl.* Vol. **4**, No. 4 (2013)
16. M.J. Soares and M.C. do Carmo, *P. SPIE*, **4469** (1) (2001)

APPENDIX B

Curriculum Vitae

1. Personal data

Name: Jelena Maricheva
Date and place of birth: 12.12.1988, Tallinn, Estonia
E-mail address: jelena.maricheva@ttu.ee

2. Education

Educational institution	Graduation year	Education (field of study/degree)
Tallinn university of technology	2013	Master
Tallinn university of technology	2011	Bachelor
Tallinn high school of humanities	2008	Secondary education

1. Language competence/skills (fluent, average, basic skills)

Language	Level
Russian	Mother tongue
Estonian	Average
English	Average
German	Basic skills

2. Special courses

Period	Educational or other organisation
February 2017	FMTDK doktorantide esinemisokuste 1+1 koolitus
27 November–2 December 2016	MRS Fall Meeting & Exhibit
15–17 June 2016	6th Baltic Electrochemistry Conference
16–18 September 2015	Baltic polymer symposium 2015
11–16 May 2015	E-MRS Spring Meeting and Exhibit 2015
24–26 September 2014	Baltic polymer symposium 2014

21–25 April 2014	MRS 2014 Spring Meeting & Exhibit
18–21 September 2013	Baltic Polymer Symposium- BPS 2013

3. Professional employment

Period	Organisation	Position
2015–...	Tallinn university of technology	Engineer
2009–2014	Tallinn university of technology	Other staff

4. Research activity, including thesis supervised

Projects

- 1.01.2014–
31.12.2019 IUT19-28 "New materials and technologies for solar energetics";
- 1.04.2016–
31.12.2018 B54 "SnS thin films for solar cells";
- 1.10.2015–
31.12.2017 ETAG15028 "ERA.NET RUS PLUS Project Flexapp "Flexible hybrid heterojunction nanostructures for optoelectronic";
- 1.01.2013–
31.12.2016 PUT265 "CZTS (Kesterite) Monograin Membranes for Photoelectrochemical Water Splitting";
- 1.01.2011–
31.12.2013 ETF8655 "Photoactive nanostructures formed by of chalcogenide semiconductors".

Co-supervision

- 01.01.2015–
31.05.2017 Denisa Dosenovicova, Master's thesis „Hybrid solar cells prepared by selective photoelectrochemical deposition of polypyrrole onto hydrogenated amorphous silicon“, Tallinna Tehnikaülikool.

Defended dissertations

- 2013 Master's thesis „Frozen ice glazed *Pangasius hypophthalmus* thawing method development“, Tallinn university of technology, supervisor Raivo Vokk.

List of publications

1. Kois, J.; Bereznev, S.; **Maricheva, J.**; Naidu, R. (2017). Electrochemical and photoelectrochemical characterization of SnS photoabsorber films. *Materials Science in Semiconductor Processing*, 58, 76–81.
2. **Maricheva, J.**; Bereznev, S.; Maticiu, N.; Volobujeva, O.; Kois, J. (2017). Influence of selenous acid microadditive on electrochemical formation of CdS thin films. *Electrochimica Acta*, 242, 280–286.
3. Dosenovicova D.; **Maricheva J.**; Neumüller A.; Sergeev O.; Volobujeva O.; Nasibulin A.; Kois J.; Öpik A.; Bereznev S. (2017). Selective photoelectrochemical deposition of PPy onto hydrogenated a-Si for optoelectronic applications. *Materials Science in Semiconductor Processing* 68, 1–5.
4. **Maricheva, J.**; Bereznev, S.; Naidu, R.; Maticiu, N.; Mikli, V.; Kois, J. (2016). Improved electrodeposition of CdS layers in presence of activating H₂SeO₃ microadditive. *Materials Science in Semiconductor Processing*, 54, 14–19.
5. Revathi, N.; Bereznev, S.; Loorits, M.; Raudoja, J.; Lehner, J.; **Gurevits, J.**; Traksmäa, R.; Mikli, V.; Mellikov, E.; Volobujeva, O. (2014). Annealing effect for SnS thin films prepared by high-vacuum evaporation. *Journal of Vacuum Science & Technology A-Vacuum Surfaces and Films*, 32 (6), 061506-1.
6. Kois, J.; **Gurevits, J.**; Bereznev, S.; Volobujeva, O.; Öpik, A.; Mellikov, E. (2013). CdSe nanofiber and nanohorn structures on ITO substrates fabricated by electrochemical deposition. *Applied Surface Science*, 283, 982–985.
7. Kois, J.; Bereznev, S.; **Gurevits, J.**; Volobujeva, O. (2013). Electrochemically synthesised CdSe nanofibers and pearl-chain nanostructures for photovoltaic applications. *Materials Letters*, 95, 110–113.
8. Kois, J.; Bereznev, S.; Volobujeva, O.; **Gurevits, J.**; Mellikov, E. (2011). Electrocrystallization of CdSe from aqueous electrolytes: Structural arrangement from thin films to self-assembled nanowires. *Journal of Crystal Growth*, 320 (1), 9–12.

Elulookirjeldus

1. Isikuandmed

Ees- ja perekonnanimi: Jelena Maricheva

Sünniaeg ja -koht: 12.12.1988, Tallinn, Eesti

Kodakondsus: Eesti

E-posti aadress: jelena.maricheva@ttu.ee

2. Hariduskäik

Õppeasutus (nimetus lõpetamise ajal)	Lõpetamise aeg	Haridus (eriala/kraad)
Tallinna Tehnikaülikool	2013	Magistrikraad
Tallinna Tehnikaülikool	2011	Bakalaureusekraad
Tallinna Humanitaargümnaasium	2008	Keskharidus

3. Keelteoskus (alg-, kesk- või kõrgtase)

Keel	Tase
Vene	Emakeel
Eesti	Kesk-tase
Inglise	Kesk-tase
Saksa	Algtase

4. Täiendusõppe

Õppimise aeg	Täiendusõppe korraldaja nimetus
Veebruar 2017	FMTDK doktorantide esinemisosekuste 1+1 koolitus
27 November–2 Detsember 2016	MRS Fall Meeting & Exhibit
15–17 Juuni 2016	6th Baltic Electrochemistry Conference
16–18 September 2015	Baltic polymer symposium 2015
11–16 Mai 2015	E-MRS Spring Meeting and Exhibit 2015
24–26 September 2014	Baltic polymer symposium 2014
21–25 Aprill 2014	MRS 2014 Spring Meeting & Exhibit

18–21 September 2013	Baltic Polymer Symposium- BPS 2013
----------------------	------------------------------------

5. Teenistuskäik

Töötamise aeg	Tööandja nimetus	Ametikoht
2015–...	Tallinna Tehnikaülikool	Insener
2009–2014	Tallinna Tehnikaülikool	Tehniline töötaja

6. Teadustegevus, sh juhendatud lõputööd

Projektid

- 1.01.2014–
31.12.2019 IUT19-28 "Uued materjalid ja tehnoloogiad päikeseenergeetikale;
- 1.04.2016–
31.12.2018 B54 "SnS thin films for solar cells";
- 1.10.2015–
31.12.2017 ETAG15028 "ERA.NET RUS PLUS Project Flexapp "Flexible hybrid heterojunction nanostructures for optoelectronic applications;
- 1.01.2013–
31.12.2016 PUT265 "CZTS (Kesterite) monoterakihtid kui võimalus vee elektrokeemiliseks lagundamiseks";
- 1.01.2011–
31.12.2013 ETF8655 "Nanostruktuursete kalkogeniid-pooljuhtide süntees elektrokeemilise sadestamise meetodil".

Kaasjuhendamine

- 01.01.2015–
31.05.2017 Denisa Dosenovicova, Master's thesis „Hybrid solar cells prepared by selective photoelectrochemical deposition of polypyrrole onto hydrogenated amorphous silicon“, Tallinna Tehnikaülikool.

Kaitstud lõputööd

- 2013 Master's thesis „Frozen ice glazed Pangasius hypophthalmus thawing method development“, Tallinn university of technology, supervisor Raivo Vokk.

Publikatsioonid

1. Kois, J.; Bereznev, S.; **Maricheva, J.**; Naidu, R. (2017). Electrochemical and photoelectrochemical characterization of SnS photoabsorber films. *Materials Science in Semiconductor Processing*, 58, 76–81.
2. **Maricheva, J.**; Bereznev, S.; Maticiuc, N.; Volobujeva, O.; Kois, J. (2017). Influence of selenous acid microadditive on electrochemical formation of CdS thin films. *Electrochimica Acta*, 242, 280–286.
3. Dosenovicova D.; **Maricheva J.**; Neumüller A.; Sergeev O.; Volobujeva O.; Nasibulin A.; Kois J.; Öpik A.; Bereznev S. (2017). Selective photoelectrochemical deposition of PPy onto hydrogenated a-Si for optoelectronic applications. *Materials Science in Semiconductor Processing* 68, 1–5.
4. **Maricheva, J.**; Bereznev, S.; Naidu, R.; Maticiuc, N.; Mikli, V.; Kois, J. (2016). Improved electrodeposition of CdS layers in presence of activating H₂SeO₃ microadditive. *Materials Science in Semiconductor Processing*, 54, 14–19.
5. Revathi, N.; Bereznev, S.; Loorits, M.; Raudoja, J.; Lehner, J.; **Gurevits, J.**; Traksmäa, R.; Mikli, V.; Mellikov, E.; Volobujeva, O. (2014). Annealing effect for SnS thin films prepared by high-vacuum evaporation. *Journal of Vacuum Science & Technology A-Vacuum Surfaces and Films*, 32 (6), 061506-1.
6. Kois, J.; **Gurevits, J.**; Bereznev, S.; Volobujeva, O.; Öpik, A.; Mellikov, E. (2013). CdSe nanofiber and nanohorn structures on ITO substrates fabricated by electrochemical deposition. *Applied Surface Science*, 283, 982–985.
7. Kois, J.; Bereznev, S.; **Gurevits, J.**; Volobujeva, O. (2013). Electrochemically synthesised CdSe nanofibers and pearl-chain nanostructures for photovoltaic applications. *Materials Letters*, 95, 110–113.
8. Kois, J.; Bereznev, S.; Volobujeva, O.; **Gurevits, J.**; Mellikov, E. (2011). Electrocrystallization of CdSe from aqueous electrolytes: Structural arrangement from thin films to self-assembled nanowires. *Journal of Crystal Growth*, 320 (1), 9–12.

**DISSERTATIONS DEFENDED AT
TALLINN UNIVERSITY OF TECHNOLOGY ON
NATURAL AND EXACT SCIENCES**

1. **Olav Kongas**. Nonlinear Dynamics in Modeling Cardiac Arrhythmias. 1998.
2. **Kalju Vanatalu**. Optimization of Processes of Microbial Biosynthesis of Isotopically Labeled Biomolecules and Their Complexes. 1999.
3. **Ahto Buldas**. An Algebraic Approach to the Structure of Graphs. 1999.
4. **Monika Drews**. A Metabolic Study of Insect Cells in Batch and Continuous Culture: Application of Chemostat and Turbidostat to the Production of Recombinant Proteins. 1999.
5. **Eola Valdre**. Endothelial-Specific Regulation of Vessel Formation: Role of Receptor Tyrosine Kinases. 2000.
6. **Kalju Lott**. Doping and Defect Thermodynamic Equilibrium in ZnS. 2000.
7. **Reet Koljak**. Novel Fatty Acid Dioxygenases from the Corals *Plexaura homomalla* and *Gersemia fruticosa*. 2001.
8. **Anne Paju**. Asymmetric oxidation of Prochiral and Racemic Ketones by Using Sharpless Catalyst. 2001.
9. **Marko Vendelin**. Cardiac Mechanoenergetics *in silico*. 2001.
10. **Pearu Peterson**. Multi-Soliton Interactions and the Inverse Problem of Wave Crest. 2001.
11. **Anne Menert**. Microcalorimetry of Anaerobic Digestion. 2001.
12. **Toomas Tiivel**. The Role of the Mitochondrial Outer Membrane in *in vivo* Regulation of Respiration in Normal Heart and Skeletal Muscle Cell. 2002.
13. **Olle Hints**. Ordovician Scolecodonts of Estonia and Neighbouring Areas: Taxonomy, Distribution, Palaeoecology, and Application. 2002.
14. **Jaak Nõlvak**. Chitinozoan Biostratigraphy in the Ordovician of Baltoscandia. 2002.
15. **Liivi Kluge**. On Algebraic Structure of Pre-Operad. 2002.
16. **Jaanus Lass**. Biosignal Interpretation: Study of Cardiac Arrhythmias and Electromagnetic Field Effects on Human Nervous System. 2002.
17. **Janek Peterson**. Synthesis, Structural Characterization and Modification of PAMAM Dendrimers. 2002.
18. **Merike Vaher**. Room Temperature Ionic Liquids as Background Electrolyte Additives in Capillary Electrophoresis. 2002.
19. **Valdek Mikli**. Electron Microscopy and Image Analysis Study of Powdered Hardmetal Materials and Optoelectronic Thin Films. 2003.
20. **Mart Viljus**. The Microstructure and Properties of Fine-Grained Cermets. 2003.
21. **Signe Kask**. Identification and Characterization of Dairy-Related *Lactobacillus*. 2003.
22. **Tiiu-Mai Laht**. Influence of Microstructure of the Curd on Enzymatic and Microbiological Processes in Swiss-Type Cheese. 2003.
23. **Anne Kuusksalu**. 2–5A Synthetase in the Marine Sponge *Geodia cydonium*. 2003.

24. **Sergei Bereznev.** Solar Cells Based on Polycrystalline Copper-Indium Chalcogenides and Conductive Polymers. 2003.
25. **Kadri Kriis.** Asymmetric Synthesis of C₂-Symmetric Bimorpholines and Their Application as Chiral Ligands in the Transfer Hydrogenation of Aromatic Ketones. 2004.
26. **Jekaterina Reut.** Polypyrrole Coatings on Conducting and Insulating Substrates. 2004.
27. **Sven Nõmm.** Realization and Identification of Discrete-Time Nonlinear Systems. 2004.
28. **Olga Kijatkina.** Deposition of Copper Indium Disulphide Films by Chemical Spray Pyrolysis. 2004.
29. **Gert Tamberg.** On Sampling Operators Defined by Rogosinski, Hann and Blackman Windows. 2004.
30. **Monika Übner.** Interaction of Humic Substances with Metal Cations. 2004.
31. **Kaarel Adamberg.** Growth Characteristics of Non-Starter Lactic Acid Bacteria from Cheese. 2004.
32. **Imre Vallikivi.** Lipase-Catalysed Reactions of Prostaglandins. 2004.
33. **Merike Peld.** Substituted Apatites as Sorbents for Heavy Metals. 2005.
34. **Vitali Syritski.** Study of Synthesis and Redox Switching of Polypyrrole and Poly(3,4-ethylenedioxythiophene) by Using *in-situ* Techniques. 2004.
35. **Lee Põllumaa.** Evaluation of Ecotoxicological Effects Related to Oil Shale Industry. 2004.
36. **Riina Aav.** Synthesis of 9,11-Secosterols Intermediates. 2005.
37. **Andres Braunbrück.** Wave Interaction in Weakly Inhomogeneous Materials. 2005.
38. **Robert Kitt.** Generalised Scale-Invariance in Financial Time Series. 2005.
39. **Juss Pavelson.** Mesoscale Physical Processes and the Related Impact on the Summer Nutrient Fields and Phytoplankton Blooms in the Western Gulf of Finland. 2005.
40. **Olari Ilison.** Solitons and Solitary Waves in Media with Higher Order Dispersive and Nonlinear Effects. 2005.
41. **Maksim Säkki.** Intermittency and Long-Range Structurization of Heart Rate. 2005.
42. **Enli Kiipli.** Modelling Seawater Chemistry of the East Baltic Basin in the Late Ordovician–Early Silurian. 2005.
43. **Igor Golovtsov.** Modification of Conductive Properties and Processability of Polyparaphenylene, Polypyrrole and polyaniline. 2005.
44. **Katrin Laos.** Interaction Between Furcellaran and the Globular Proteins (Bovine Serum Albumin β -Lactoglobulin). 2005.
45. **Arvo Mere.** Structural and Electrical Properties of Spray Deposited Copper Indium Disulphide Films for Solar Cells. 2006.
46. **Sille Ehala.** Development and Application of Various On- and Off-Line Analytical Methods for the Analysis of Bioactive Compounds. 2006.
47. **Maria Kulp.** Capillary Electrophoretic Monitoring of Biochemical Reaction Kinetics. 2006.

48. **Anu Aaspõllu.** Proteinases from *Vipera lebetina* Snake Venom Affecting Hemostasis. 2006.
49. **Lyudmila Chekulayeva.** Photosensitized Inactivation of Tumor Cells by Porphyrins and Chlorins. 2006.
50. **Merle Uudsemaa.** Quantum-Chemical Modeling of Solvated First Row Transition Metal Ions. 2006.
51. **Tagli Pitsi.** Nutrition Situation of Pre-School Children in Estonia from 1995 to 2004. 2006.
52. **Angela Ivask.** Luminescent Recombinant Sensor Bacteria for the Analysis of Bioavailable Heavy Metals. 2006.
53. **Tiina Lõugas.** Study on Physico-Chemical Properties and Some Bioactive Compounds of Sea Buckthorn (*Hippophae rhamnoides* L.). 2006.
54. **Kaja Kasemets.** Effect of Changing Environmental Conditions on the Fermentative Growth of *Saccharomyces cerevisiae* S288C: Auxo-accelerostat Study. 2006.
55. **Ildar Nisamedtinov.** Application of ^{13}C and Fluorescence Labeling in Metabolic Studies of *Saccharomyces* spp. 2006.
56. **Alar Leibak.** On Additive Generalisation of Voronoï's Theory of Perfect Forms over Algebraic Number Fields. 2006.
57. **Andri Jagomägi.** Photoluminescence of Chalcopyrite Tellurides. 2006.
58. **Tõnu Martma.** Application of Carbon Isotopes to the Study of the Ordovician and Silurian of the Baltic. 2006.
59. **Marit Kauk.** Chemical Composition of CuInSe₂ Monograin Powders for Solar Cell Application. 2006.
60. **Julia Kois.** Electrochemical Deposition of CuInSe₂ Thin Films for Photovoltaic Applications. 2006.
61. **Ilona Oja Ačik.** Sol-Gel Deposition of Titanium Dioxide Films. 2007.
62. **Tiia Anmann.** Integrated and Organized Cellular Bioenergetic Systems in Heart and Brain. 2007.
63. **Katrin Trummal.** Purification, Characterization and Specificity Studies of Metalloproteinases from *Vipera lebetina* Snake Venom. 2007.
64. **Gennadi Lessin.** Biochemical Definition of Coastal Zone Using Numerical Modeling and Measurement Data. 2007.
65. **Enno Pais.** Inverse problems to determine non-homogeneous degenerate memory kernels in heat flow. 2007.
66. **Maria Borissova.** Capillary Electrophoresis on Alkylimidazolium Salts. 2007.
67. **Karin Valmsen.** Prostaglandin Synthesis in the Coral *Plexaura homomalla*: Control of Prostaglandin Stereochemistry at Carbon 15 by Cyclooxygenases. 2007.
68. **Kristjan Piirimäe.** Long-Term Changes of Nutrient Fluxes in the Drainage Basin of the Gulf of Finland – Application of the PolFlow Model. 2007.
69. **Tatjana Dedova.** Chemical Spray Pyrolysis Deposition of Zinc Sulfide Thin Films and Zinc Oxide Nanostructured Layers. 2007.

70. **Katrin Tomson.** Production of Labelled Recombinant Proteins in Fed-Batch Systems in *Escherichia coli*. 2007.
71. **Cecilia Sarmiento.** Suppressors of RNA Silencing in Plants. 2008.
72. **Vilja Mardla.** Inhibition of Platelet Aggregation with Combination of Antiplatelet Agents. 2008.
73. **Maie Bachmann.** Effect of Modulated Microwave Radiation on Human Resting Electroencephalographic Signal. 2008.
74. **Dan Hüvonen.** Terahertz Spectroscopy of Low-Dimensional Spin Systems. 2008.
75. **Ly Villo.** Stereoselective Chemoenzymatic Synthesis of Deoxy Sugar Esters Involving *Candida antarctica* Lipase B. 2008.
76. **Johan Anton.** Technology of Integrated Photoelasticity for Residual Stress Measurement in Glass Articles of Axisymmetric Shape. 2008.
77. **Olga Volobujeva.** SEM Study of Selenization of Different Thin Metallic Films. 2008.
78. **Artur Jõgi.** Synthesis of 4'-Substituted 2,3'-dideoxynucleoside Analogues. 2008.
79. **Mario Kadastik.** Doubly Charged Higgs Boson Decays and Implications on Neutrino Physics. 2008.
80. **Fernando Pérez-Caballero.** Carbon Aerogels from 5-Methylresorcinol-Formaldehyde Gels. 2008.
81. **Sirje Vaask.** The Comparability, Reproducibility and Validity of Estonian Food Consumption Surveys. 2008.
82. **Anna Menaker.** Electrosynthesized Conducting Polymers, Polypyrrole and Poly(3,4-ethylenedioxythiophene), for Molecular Imprinting. 2009.
83. **Lauri Ilison.** Solitons and Solitary Waves in Hierarchical Korteweg-de Vries Type Systems. 2009.
84. **Kaia Ernits.** Study of In₂S₃ and ZnS Thin Films Deposited by Ultrasonic Spray Pyrolysis and Chemical Deposition. 2009.
85. **Veljo Sinivee.** Portable Spectrometer for Ionizing Radiation "Gammamapper". 2009.
86. **Jüri Virkepu.** On Lagrange Formalism for Lie Theory and Operadic Harmonic Oscillator in Low Dimensions. 2009.
87. **Marko Piirsoo.** Deciphering Molecular Basis of Schwann Cell Development. 2009.
88. **Kati Helmja.** Determination of Phenolic Compounds and Their Antioxidative Capability in Plant Extracts. 2010.
89. **Merike Sõmera.** Sobemoviruses: Genomic Organization, Potential for Recombination and Necessity of P1 in Systemic Infection. 2010.
90. **Kristjan Laes.** Preparation and Impedance Spectroscopy of Hybrid Structures Based on CuIn₃Se₅ Photoabsorber. 2010.
91. **Kristin Lippur.** Asymmetric Synthesis of 2,2'-Bimorpholine and its 5,5'-Substituted Derivatives. 2010.
92. **Merike Luman.** Dialysis Dose and Nutrition Assessment by an Optical Method. 2010.

93. **Mihhail Berezovski.** Numerical Simulation of Wave Propagation in Heterogeneous and Microstructured Materials. 2010.
94. **Tamara Aid-Pavlidis.** Structure and Regulation of BDNF Gene. 2010.
95. **Olga Bragina.** The Role of Sonic Hedgehog Pathway in Neuro- and Tumorigenesis. 2010.
96. **Merle Randrüüt.** Wave Propagation in Microstructured Solids: Solitary and Periodic Waves. 2010.
97. **Marju Laars.** Asymmetric Organocatalytic Michael and Aldol Reactions Mediated by Cyclic Amines. 2010.
98. **Maarja Grossberg.** Optical Properties of Multinary Semiconductor Compounds for Photovoltaic Applications. 2010.
99. **Alla Maloverjan.** Vertebrate Homologues of Drosophila Fused Kinase and Their Role in Sonic Hedgehog Signalling Pathway. 2010.
100. **Priit Pruunsild.** Neuronal Activity-Dependent Transcription Factors and Regulation of Human *BDNF* Gene. 2010.
101. **Tatjana Knjazeva.** New Approaches in Capillary Electrophoresis for Separation and Study of Proteins. 2011.
102. **Atanas Katerski.** Chemical Composition of Sprayed Copper Indium Disulfide Films for Nanostructured Solar Cells. 2011.
103. **Kristi Timmo.** Formation of Properties of CuInSe_2 and $\text{Cu}_2\text{ZnSn}(\text{S},\text{Se})_4$ Monograin Powders Synthesized in Molten KI. 2011.
104. **Kert Tamm.** Wave Propagation and Interaction in Mindlin-Type Microstructured Solids: Numerical Simulation. 2011.
105. **Adrian Popp.** Ordovician Proetid Trilobites in Baltoscandia and Germany. 2011.
106. **Ove Pärn.** Sea Ice Deformation Events in the Gulf of Finland and This Impact on Shipping. 2011.
107. **Germo Väli.** Numerical Experiments on Matter Transport in the Baltic Sea. 2011.
108. **Andrus Seiman.** Point-of-Care Analyser Based on Capillary Electrophoresis. 2011.
109. **Olga Katargina.** Tick-Borne Pathogens Circulating in Estonia (Tick-Borne Encephalitis Virus, *Anaplasma phagocytophilum*, *Babesia* Species): Their Prevalence and Genetic Characterization. 2011.
110. **Ingrid Sumeri.** The Study of Probiotic Bacteria in Human Gastrointestinal Tract Simulator. 2011.
111. **Kairit Zovo.** Functional Characterization of Cellular Copper Proteome. 2011.
112. **Natalja Makarytsheva.** Analysis of Organic Species in Sediments and Soil by High Performance Separation Methods. 2011.
113. **Monika Mortimer.** Evaluation of the Biological Effects of Engineered Nanoparticles on Unicellular Pro- and Eukaryotic Organisms. 2011.
114. **Kersti Tepp.** Molecular System Bioenergetics of Cardiac Cells: Quantitative Analysis of Structure-Function Relationship. 2011.

115. **Anna-Liisa Peikolainen.** Organic Aerogels Based on 5-Methylresorcinol. 2011.
116. **Leeli Amon.** Palaeoecological Reconstruction of Late-Glacial Vegetation Dynamics in Eastern Baltic Area: A View Based on Plant Macrofossil Analysis. 2011.
117. **Tanel Peets.** Dispersion Analysis of Wave Motion in Microstructured Solids. 2011.
118. **Liina Kaupmees.** Selenization of Molybdenum as Contact Material in Solar Cells. 2011.
119. **Allan Olsper.** Properties of VPg and Coat Protein of Sobemoviruses. 2011.
120. **Kadri Koppel.** Food Category Appraisal Using Sensory Methods. 2011.
121. **Jelena Gorbatšova.** Development of Methods for CE Analysis of Plant Phenolics and Vitamins. 2011.
122. **Karin Viipsi.** Impact of EDTA and Humic Substances on the Removal of Cd and Zn from Aqueous Solutions by Apatite. 2012.
123. **David Schryer.** Metabolic Flux Analysis of Compartmentalized Systems Using Dynamic Isotopologue Modeling. 2012.
124. **Ardo Illaste.** Analysis of Molecular Movements in Cardiac Myocytes. 2012.
125. **Indrek Reile.** 3-Alkylcyclopentane-1,2-Diones in Asymmetric Oxidation and Alkylation Reactions. 2012.
126. **Tatjana Tamberg.** Some Classes of Finite 2-Groups and Their Endomorphism Semigroups. 2012.
127. **Taavi Liblik.** Variability of Thermohaline Structure in the Gulf of Finland in Summer. 2012.
128. **Priidik Lagemaa.** Operational Forecasting in Estonian Marine Waters. 2012.
129. **Andrei Errapart.** Photoelastic Tomography in Linear and Non-linear Approximation. 2012.
130. **Külliki Krabbi.** Biochemical Diagnosis of Classical Galactosemia and Mucopolysaccharidoses in Estonia. 2012.
131. **Kristel Kaseleht.** Identification of Aroma Compounds in Food using SPME-GC/MS and GC-Olfactometry. 2012.
132. **Kristel Kodar.** Immunoglobulin G Glycosylation Profiling in Patients with Gastric Cancer. 2012.
133. **Kai Rosin.** Solar Radiation and Wind as Agents of the Formation of the Radiation Regime in Water Bodies. 2012.
134. **Ann Tiiman.** Interactions of Alzheimer's Amyloid-Beta Peptides with Zn(II) and Cu(II) Ions. 2012.
135. **Olga Gavrilova.** Application and Elaboration of Accounting Approaches for Sustainable Development. 2012.
136. **Olesja Bondarenko.** Development of Bacterial Biosensors and Human Stem Cell-Based *In Vitro* Assays for the Toxicological Profiling of Synthetic Nanoparticles. 2012.

137. **Katri Muska.** Study of Composition and Thermal Treatments of Quaternary Compounds for Monograin Layer Solar Cells. 2012.
138. **Ranno Nahku.** Validation of Critical Factors for the Quantitative Characterization of Bacterial Physiology in Accelerostat Cultures. 2012.
139. **Petri-Jaan Lahtvee.** Quantitative Omics-level Analysis of Growth Rate Dependent Energy Metabolism in *Lactococcus lactis*. 2012.
140. **Kerti Orumets.** Molecular Mechanisms Controlling Intracellular Glutathione Levels in Baker's Yeast *Saccharomyces cerevisiae* and its Random Mutagenized Glutathione Over-Accumulating Isolate. 2012.
141. **Loreida Timberg.** Spice-Cured Sprats Ripening, Sensory Parameters Development, and Quality Indicators. 2012.
142. **Anna Mihhalevski.** Rye Sourdough Fermentation and Bread Stability. 2012.
143. **Liisa Arike.** Quantitative Proteomics of *Escherichia coli*: From Relative to Absolute Scale. 2012.
144. **Kairi Otto.** Deposition of In₂S₃ Thin Films by Chemical Spray Pyrolysis. 2012.
145. **Mari Sepp.** Functions of the Basic Helix-Loop-Helix Transcription Factor TCF4 in Health and Disease. 2012.
146. **Anna Suhhova.** Detection of the Effect of Weak Stressors on Human Resting Electroencephalographic Signal. 2012.
147. **Aram Kazarjan.** Development and Production of Extruded Food and Feed Products Containing Probiotic Microorganisms. 2012.
148. **Rivo Uiboupin.** Application of Remote Sensing Methods for the Investigation of Spatio-Temporal Variability of Sea Surface Temperature and Chlorophyll Fields in the Gulf of Finland. 2013.
149. **Tiina Kriščiunaite.** A Study of Milk Coagulability. 2013.
150. **Tuuli Levandi.** Comparative Study of Cereal Varieties by Analytical Separation Methods and Chemometrics. 2013.
151. **Natalja Kabanova.** Development of a Microcalorimetric Method for the Study of Fermentation Processes. 2013.
152. **Himani Khanduri.** Magnetic Properties of Functional Oxides. 2013.
153. **Julia Smirnova.** Investigation of Properties and Reaction Mechanisms of Redox-Active Proteins by ESI MS. 2013.
154. **Mervi Sepp.** Estimation of Diffusion Restrictions in Cardiomyocytes Using Kinetic Measurements. 2013.
155. **Kersti Jääger.** Differentiation and Heterogeneity of Mesenchymal Stem Cells. 2013.
156. **Victor Alari.** Multi-Scale Wind Wave Modeling in the Baltic Sea. 2013.
157. **Taavi Päll.** Studies of CD44 Hyaluronan Binding Domain as Novel Angiogenesis Inhibitor. 2013.
158. **Allan Niidu.** Synthesis of Cyclopentane and Tetrahydrofuran Derivatives. 2013.
159. **Julia Geller.** Detection and Genetic Characterization of *Borrelia* Species Circulating in Tick Population in Estonia. 2013.

160. **Irina Stulova**. The Effects of Milk Composition and Treatment on the Growth of Lactic Acid Bacteria. 2013.
161. **Jana Holmar**. Optical Method for Uric Acid Removal Assessment During Dialysis. 2013.
162. **Kerti Ausmees**. Synthesis of Heterobicyclo[3.2.0]heptane Derivatives *via* Multicomponent Cascade Reaction. 2013.
163. **Minna Varikmaa**. Structural and Functional Studies of Mitochondrial Respiration Regulation in Muscle Cells. 2013.
164. **Indrek Koppel**. Transcriptional Mechanisms of BDNF Gene Regulation. 2014.
165. **Kristjan Pilt**. Optical Pulse Wave Signal Analysis for Determination of Early Arterial Ageing in Diabetic Patients. 2014.
166. **Andres Anier**. Estimation of the Complexity of the Electroencephalogram for Brain Monitoring in Intensive Care. 2014.
167. **Toivo Kallaste**. Pyroclastic Sanidine in the Lower Palaeozoic Bentonites – A Tool for Regional Geological Correlations. 2014.
168. **Erki Kärber**. Properties of ZnO-nanorod/In₂S₃/CuInS₂ Solar Cell and the Constituent Layers Deposited by Chemical Spray Method. 2014.
169. **Julia Lehner**. Formation of Cu₂ZnSnS₄ and Cu₂ZnSnSe₄ by Chalcogenisation of Electrochemically Deposited Precursor Layers. 2014.
170. **Peep Pitk**. Protein- and Lipid-rich Solid Slaughterhouse Waste Anaerobic Co-digestion: Resource Analysis and Process Optimization. 2014.
171. **Kaspar Valgepea**. Absolute Quantitative Multi-omics Characterization of Specific Growth Rate-dependent Metabolism of *Escherichia coli*. 2014.
172. **Artur Noole**. Asymmetric Organocatalytic Synthesis of 3,3'-Disubstituted Oxindoles. 2014.
173. **Robert Tsanev**. Identification and Structure-Functional Characterisation of the Gene Transcriptional Repressor Domain of Human Gli Proteins. 2014.
174. **Dmitri Kartofelev**. Nonlinear Sound Generation Mechanisms in Musical Acoustic. 2014.
175. **Sigrid Hade**. GIS Applications in the Studies of the Palaeozoic Graptolite Argillite and Landscape Change. 2014.
176. **Agne Velthut-Meikas**. Ovarian Follicle as the Environment of Oocyte Maturation: The Role of Granulosa Cells and Follicular Fluid at Pre-Ovulatory Development. 2014.
177. **Kristel Hälvin**. Determination of B-group Vitamins in Food Using an LC-MS Stable Isotope Dilution Assay. 2014.
178. **Mailis Pärri**. Characterization of the Oligoadenylate Synthetase Subgroup from Phylum Porifera. 2014.
179. **Jekaterina Kazantseva**. Alternative Splicing of *TAF4*: A Dynamic Switch between Distinct Cell Functions. 2014.
180. **Jaanus Suurväli**. Regulator of G Protein Signalling 16 (RGS16): Functions in Immunity and Genomic Location in an Ancient MHC-Related Evolutionarily Conserved Synteny Group. 2014.

181. **Ene Viiard.** Diversity and Stability of Lactic Acid Bacteria During Rye Sourdough Propagation. 2014.
182. **Kristella Hansen.** Prostaglandin Synthesis in Marine Arthropods and Red Algae. 2014.
183. **Helike Lõhelaid.** Allene Oxide Synthase-lipoxygenase Pathway in Coral Stress Response. 2015.
184. **Normunds Stivriņš.** Postglacial Environmental Conditions, Vegetation Succession and Human Impact in Latvia. 2015.
185. **Mary-Liis Kütt.** Identification and Characterization of Bioactive Peptides with Antimicrobial and Immunoregulating Properties Derived from Bovine Colostrum and Milk. 2015.
186. **Kazbulat Šogenov.** Petrophysical Models of the CO₂ Plume at Prospective Storage Sites in the Baltic Basin. 2015.
187. **Taavi Raadik.** Application of Modulation Spectroscopy Methods in Photovoltaic Materials Research. 2015.
188. **Reio Pöder.** Study of Oxygen Vacancy Dynamics in Sc-doped Ceria with NMR Techniques. 2015.
189. **Sven Siir.** Internal Geochemical Stratification of Bentonites (Altered Volcanic Ash Beds) and its Interpretation. 2015.
190. **Kaur Jaanson.** Novel Transgenic Models Based on Bacterial Artificial Chromosomes for Studying BDNF Gene Regulation. 2015.
191. **Niina Karro.** Analysis of ADP Compartmentation in Cardiomyocytes and Its Role in Protection Against Mitochondrial Permeability Transition Pore Opening. 2015.
192. **Piret Laht.** B-plexins Regulate the Maturation of Neurons Through Microtubule Dynamics. 2015.
193. **Sergei Žari.** Organocatalytic Asymmetric Addition to Unsaturated 1,4-Dicarbonyl Compounds. 2015.
194. **Natalja Buhhalko.** Processes Influencing the Spatio-temporal Dynamics of Nutrients and Phytoplankton in Summer in the Gulf of Finland, Baltic Sea. 2015.
195. **Natalia Maticiuc.** Mechanism of Changes in the Properties of Chemically Deposited CdS Thin Films Induced by Thermal Annealing. 2015.
196. **Mario Öeren.** Computational Study of Cyclohexylhemicucurbiturils. 2015.
197. **Mari Kalda.** Mechanoenergetics of a Single Cardiomyocyte. 2015.
198. **Ieva Grudzinska.** Diatom Stratigraphy and Relative Sea Level Changes of the Eastern Baltic Sea over the Holocene. 2015.
199. **Anna Kazantseva.** Alternative Splicing in Health and Disease. 2015.
200. **Jana Kazarjan.** Investigation of Endogenous Antioxidants and Their Synthetic Analogues by Capillary Electrophoresis. 2016.
201. **Maria Safonova.** SnS Thin Films Deposition by Chemical Solution Method and Characterization. 2016.
202. **Jekaterina Mazina.** Detection of Psycho- and Bioactive Drugs in Different Sample Matrices by Fluorescence Spectroscopy and Capillary Electrophoresis. 2016.

203. **Karin Rosenstein.** Genes Regulated by Estrogen and Progesterone in Human Endometrium. 2016.
204. **Aleksei Tretjakov.** A Macromolecular Imprinting Approach to Design Synthetic Receptors for Label-Free Biosensing Applications. 2016.
205. **Mati Danilson.** Temperature Dependent Electrical Properties of Kesterite Monograin Layer Solar Cells. 2016.
206. **Kaspar Kevvai.** Applications of ^{15}N -labeled Yeast Hydrolysates in Metabolic Studies of *Lactococcus lactis* and *Saccharomyces Cerevisiae*. 2016.
207. **Kadri Aller.** Development and Applications of Chemically Defined Media for Lactic Acid Bacteria. 2016.
208. **Gert Preegel.** Cyclopentane-1,2-dione and Cyclopent-2-en-1-one in Asymmetric Organocatalytic Reactions. 2016.
209. **Jekaterina Služenikina.** Applications of Marine Scatterometer Winds and Quality Aspects of their Assimilation into Numerical Weather Prediction Model HIRLAM. 2016.
210. **Erkki Kask.** Study of Kesterite Solar Cell Absorbers by Capacitance Spectroscopy Methods. 2016.
211. **Jürgen Arund.** Major Chromophores and Fluorophores in the Spent Dialysate as Cornerstones for Optical Monitoring of Kidney Replacement Therapy. 2016.
212. **Andrej Šamarin.** Hybrid PET/MR Imaging of Bone Metabolism and Morphology. 2016.
213. **Kairi Kasemets.** Inverse Problems for Parabolic Integro-Differential Equations with Instant and Integral Conditions. 2016.
214. **Edith Soosaar.** An Evolution of Freshwater Bulge in Laboratory Scale Experiments and Natural Conditions. 2016.
215. **Peeter Laas.** Spatiotemporal Niche-Partitioning of Bacterioplankton Community across Environmental Gradients in the Baltic Sea. 2016.
216. **Margus Voolma.** Geochemistry of Organic-Rich Metalliferous Oil Shale/Black Shale of Jordan and Estonia. 2016.
217. **Karin Ojamäe.** The Ecology and Photobiology of Mixotrophic Alveolates in the Baltic Sea. 2016.
218. **Anne Pink.** The Role of CD44 in the Control of Endothelial Cell Proliferation and Angiogenesis. 2016.
219. **Kristiina Kreek.** Metal-Doped Aerogels Based on Resorcinol Derivatives. 2016.
220. **Kaia Kukk.** Expression of Human Prostaglandin H Synthases in the Yeast *Pichia pastoris*. 2016.
221. **Martin Laasmaa.** Revealing Aspects of Cardiac Function from Fluorescence and Electrophysiological Recordings. 2016.
222. **Eeva-Gerda Kobrin.** Development of Point of Care Applications for Capillary Electrophoresis. 2016.
223. **Villu Kikas.** Physical Processes Controlling the Surface Layer Dynamics in the Stratified Gulf of Finland: An Application of Ferrybox Technology. 2016.

224. **Maris Skudra**. Features of Thermohaline Structure and Circulation in the Gulf of Riga. 2017.
225. **Sirje Sildever**. Influence of Physical-Chemical Factors on Community and Populations of the Baltic Sea Spring Bloom Microalgae. 2017.
226. **Nicolae Spalatu**. Development of CdTe Absorber Layer for Thin-Film Solar Cells. 2017.
227. **Kristi Luberg**. Human Tropomyosin-Related Kinase A and B: from Transcript Diversity to Novel Inhibitors. 2017.
228. **Andrus Kaldma**. Metabolic Remodeling of Human Colorectal Cancer: Alterations in Energy Fluxes. 2017.
229. **Irina Osadchuk**. Structures and Catalytic Properties of Titanium and Iridium Based Complexes. 2017.
230. **Roman Boroznjak**. A Computational Approach for Rational Monomer Selection in Molecularly Imprinted Polymer Synthesis. 2017.
231. **Sten Erm**. Use of Mother-Daughter Multi-Bioreactor Systems for Studies of Steady State Microbial Growth Space. 2017.
232. **Merike Kriisa**. Study of ZnO:In, Zn(O,S) and Sb₂S₃ Thin Films Deposited by Aerosol Methods. 2017.
233. **Marianna Surženko**. Selection of Functional Starter Bacteria for Type I Sourdough Process. 2017.
234. **Nkwusi God'swill Chimezie**. Formation and Growth of Cu₂ZnSnS₄ Monograin Powder in Molten CdI₂. 2017.
235. **Ruth Tomson**. Urea- and Creatinine-Based Parameters in the Optical Monitoring of Dialysis: The Case of Lean Body Mass and Urea Rebound Assessment. 2017.
236. **Natalja Jepihhina**. Heterogeneity of Diffusion Restrictions in Cardiomyocytes. 2017.
237. **Sophie Maria Teresa Marinucci de Reguardati**. High-Accuracy Reference Standards for Quantitative Two-Photon Absorption Spectroscopy. 2017.
238. **Martin Lints**. Optimised Signal Processing for Nonlinear Ultrasonic Nondestructive testing of Complex Materials and Biological Tissues. 2017.
239. **Maris Pilvet**. Study of Cu₂(Zn,Cd)SnS₄ Absorber Materials for Monograin Layer Solar Cells. 2017.

